LA-3202-MS

LOS ALAMOS SCIENTIFIC LABORATORY
OF THE UNIVERSITY OF CALIFORNIA ○ LOS ALAMOS   NEW MEXICO

SEMIANNUAL STATUS REPORT OF THE LASL

CONTROLLED THERMONUCLEAR RESEARCH PROGRAM

FOR PERIOD ENDING OCTOBER 20, 1964

LEGAL NOTICE

LOS ALAMOS SCIENTIFIC LABORATORY
OF THE UNIVERSITY OF CALIFORNIA   LOS ALAMOS   NEW MEXICO

SEMIANNUAL STATUS REPORT OF THE LASL

CONTROLLED THERMONUCLEAR RESEARCH PROGRAM

FOR PERIOD ENDING OCTOBER 20, 1964

INTRODUCTION

(J. L. Tuck)[*]

The broad strategy of our Sherwood activity at Los Alamos was stated in the introduction to the last semiannual report.

Briefly, we are interested in pulsed confinement; we have had some success with pulsed open systems. We feel that the time has come to study pulsed closed systems and, more specifically, flute stable closed systems. Pulsed systems imply sudden plasma creation; auxiliary activities, such as E x B heating, hydromagnetic plasma trapping thus provide support for the pulsed concept.

In May, just as the last report went to press, Scylla IV, operating at 470 kJ, suffered a short circuit between the collector plates. The accident has taken approximately half a year of intense labor to repair. Within a few days, cautious electric testing will commence, but with Scylla IV now brought up to the full design, by completion of the 3 MJ power crowbar.

Scylla I resists retirement to the Smithsonian Institution by continuing to be useful - e.g., providing comparison spectra for identifying solar corona lines taken on recent rocket flights.

For another division (GMX) we have been concerned in the design of magnetic θ-pinch coils for explosive after-compression. Explosive compression can provide the equivalent of many megajoules

---

[*] This section has been reproduced exactly as submitted without any editorial changes.

of electromagnetic compression. There can be little doubt, that if the presently achieved[1] explosive compressions could be piled on top of an appropriately chosen intermediate stage in the presently achieved Scylla electromagnetic compression, very strong thermonuclear reactions would result. The final fields already achieved in such systems (but without plasma) are 1 MG with glass walls and 10 MG without any such inert material inside the compression conductor. These should be contrasted with the 90 kG of Scylla IV. There are, however, special problems associated with the explosive method - the electrical coils must be light to allow efficient acceleration by the high explosive. This makes them mechanically too weak to withstand the electromagnetic forces for more than one full power discharge. Thus full scale plasma tests before the explosive destruction of the coil are not possible. The present experiments[2] have been plagued by asymmetrical electromagnetic compressions for rather trivial reasons - the normal side feed of the Scylla type coil interferes with the explosive. The current was therefore brought in at each end of the coil; this however, introduced completely unacceptable electromagnetic perturbations.

There are several ways to design an end fed coil where the currents are constrained to take a helical path to one end and back, which compensates the magnetic field of the axial current component. Electrical checks of this arrangement though scarcely necessary, have confirmed that highly symmetrical magnetic fields can be produced, and the coil of Fig. 3 has given a 10-fold field amplification by explosive compression. End fed coils are probably superior to the old established side fed Scylla coil arrangement, and might have supplanted them in electromagnetic θ-pinches
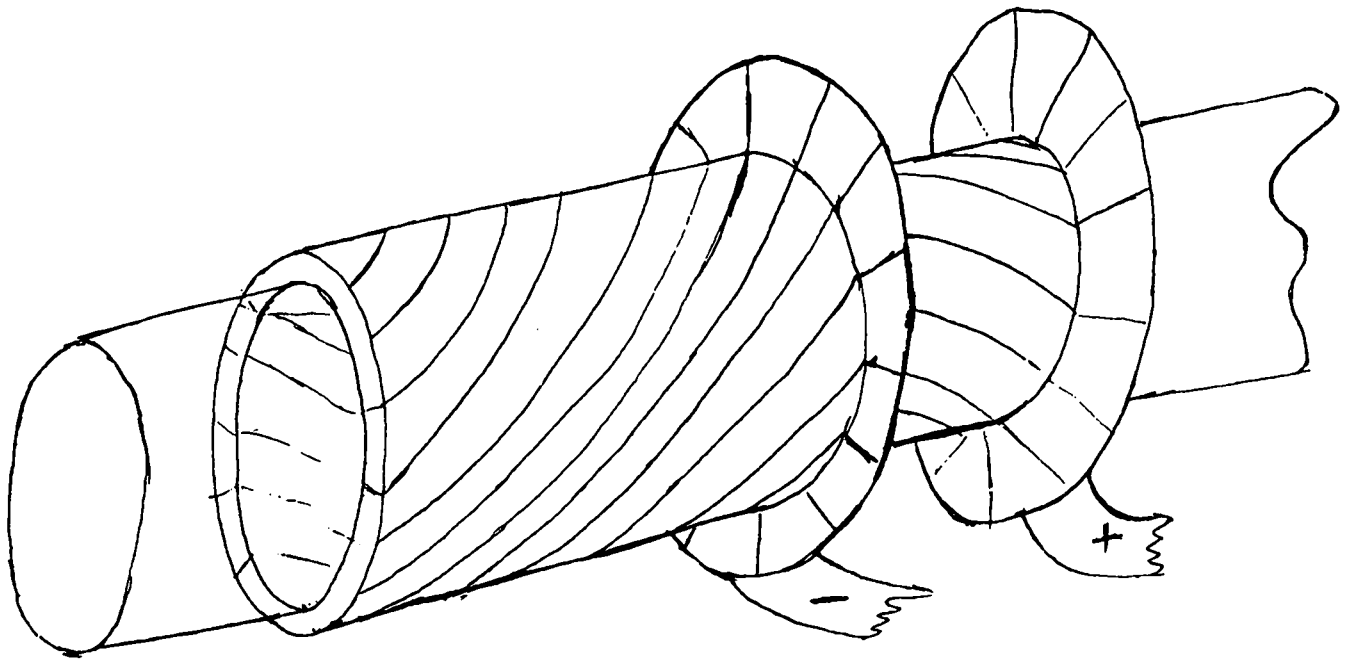
Figure 1.   End fed coil arrangements for producing symmetrical
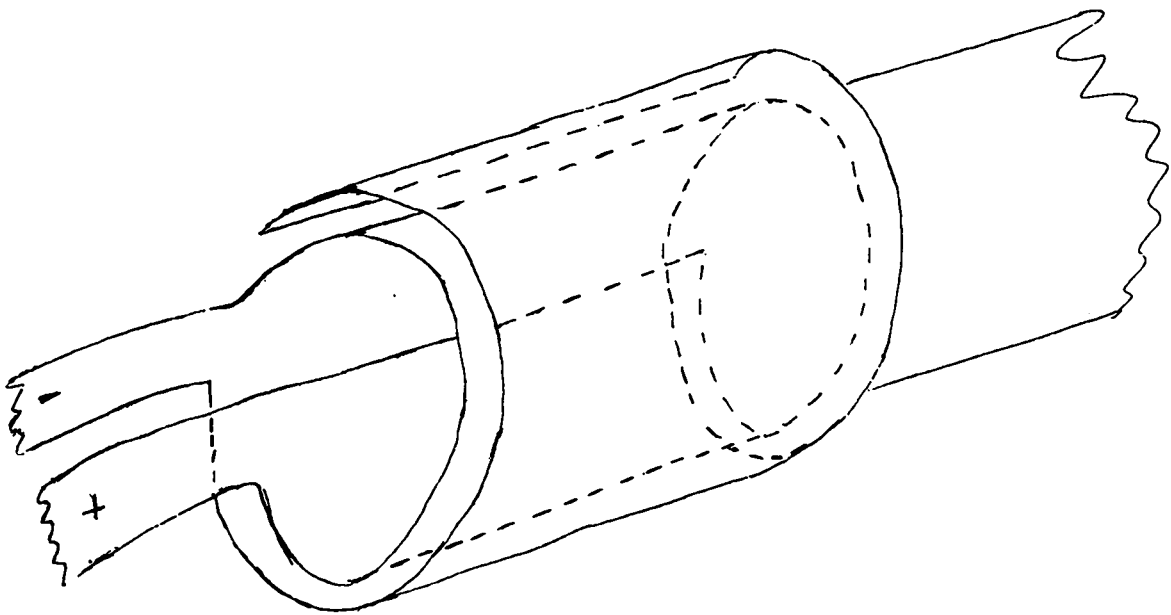   longitudinal magnetic fields.

Figure 2.   In this type, the unbalanced radial magnetic field is made
             small by making l, the path length of the line integral $\int B \cdot dl$
             round the current, through the feed point, large.

except for the fact that they are mechanically weak and it is probably not possible to make coils strong enough to last more than one electromagnetic shot. Thus the outlook for achieving a very strong thermonuclear reaction by explosive compression looks good.

Turning now to the closed flute stable magnetic bottle program (caulked cusp). A criterion of merit for such systems is not entirely obvious. In a flute stable system, there exists some range of magnetic surfaces, moving from the inside of the machine to the wall, over which $\left| \int \frac{dl}{B} \right|$ is decreasing.

For reasons of magnetic energy economy, one places the wall at the last magnetic surface before $\int \frac{dl}{B}$ turns unfavorable. The thickness of this flute stable magnetic wall, measured in cyclotron radii defines the quality of the wall. We then require to express this quality in terms of the effort needed to produce it. One way to express this effort might be the mean magnetic field strength in the wall. Another more searching method proposed in the text, is to express it in terms of the number of megajoules required to establish the whole bottle.

So far most progress has been made on the multifilar type of bottle, with two levitated conductors. Its competitor, the helixion, is very complicated to calculate. For a zero approximation to the helixion, we have calculated the $\int \frac{dl}{B}$ stability regions for a series of 14 rings spaced around a torus, encircling the minor axis. This proved to have extensive $\int \frac{dl}{B}$ stable regions and be the most economical magnetic field distribution we have yet seen. But this is not a practical construction. In the next approximation, we extend the array of rings into a continuous helix. So far, this has been shown to give quite controllable field

Fig. 3. Photograph of the Tuck-Marshall Coil

minima. But only a few of the extremely complicated magnetic field lines has, with our current use of computer time, been computed.

Another consideration also rises: Closed flute stable systems necessarily rely on averaging along the field lines. The unpleasant possibility exists that particles in an unfavorable region may drift to an unacceptable extent, before they ever reach the region where the compensating drift is to be made. Thus it is advantageous to have the positive and negative compensating regions spaced closely along the field lines. This problem is being studied quantitatively. However, it is clear by inspection that the multipolar caulked cusp is inferior to the helixion in this respect.

The caulked cusp program is going more slowly than expected. For one thing, it is taking a different shape than expected. Certain design possibilities have come to be appreciated in good time before building anything; for example, low voltage operation, with conducting liner and no feed point; magnetic energy storage, for safety at high stored energies.

In conclusion, on an unconnected subject: The dense plasma focus (reported within) has achieved the surprising yield of more than 10^{11} neutrons from a few mm^3 of plasma, in a time of $\sim 10^{-7}$ sec. Mach-Zehnder interferograms, as obtained for Scylla IV, should do much to elucidate this interesting plasma formation.

REFERENCES

1. C. M. Fowler, W. B. Garn, R. S. Caird, J. App. Phys. <u>31</u>, 588 (1960).

2. C. M. Fowler, D. B. Thompson, R. S. Caird and W. B. Garn, San Diego meeting, Plasma Physics Division, A.P.S., November 1963, Paper Nos. E-1, E-2.

TOROIDAL CAULKED CUSP

(John Marshall)

Acknowledgment

Introduction

The study of high-density, closed-field geometry reactors has not received much attention in the Sherwood program, probably because of engineering difficulties. The Caulked Picket Fence or Caulked Cusp offers in principle the possibility of a magnetic bottle for such a reactor. It combines the extreme hydromagnetic stability of a quadrupole field null with bridged field lines between cusps, so as to stop the excessive plasma leakage inherent in the nonadiabatic behavior of particles in the region of a field null. The bridged field lines between cusps should take care of the leakage of scattered particles from a dense plasma, which of course would be there even in the absence of nonadiabatic behavior.

Pioneering work has been done in the experimental realization of the Caulked Cusp concept by Kerst and by Ohkawa both of whom are working with toroidal octupole machines. In their machines the cusp lines are bridged around four conducting rings inductively driven by currents in the walls of the toroidal outer vessel of square cross section. These currents originate in a capacitor bank, and both Kerst and Ohkawa use rather modest stored energies.

This of course simplifies the engineering of the machines, but it limits the particle energies which can be contained. As a result, the plasma energies are quite low, and this makes it possible to hang the ring conductors on supports. In addition, because of reduced charge exchange cross sections, as well as smaller particle velocities accompanying the low plasma temperatures, the vacuum requirements are quite modest. On the other hand, since the low plasma temperatures and energy content are low, there are a number of important diagnostic methods which cannot be applied.

It is felt at LASL that there is a need for carrying the Caulked Cusp type of confinement to high plasma energies and temperatures. It is realized that great difficulties will have to be overcome, but it is possible that more information will be obtainable than at low energies. The major difficulties are that large field energies will be required, that the machine will be of large dimensions, and that the internal conductors will have to be truly levitated. Mechanical supports are not permissible because of contamination difficulties arising from their bombardment by the plasma.

The coaxial guns in use at LASL appear to be capable of supplying usable quantities of D plasma of approximately 10 keV average D energy, and of injecting this plasma across a field. Design figures are being based on gun performance and on cross field injection experiments of Baker and Hammel. The indications are that the high-density, relatively slow plasma, which follows the fast plasma from a coaxial gun, can be rejected by appropriate depolarization conductors while the fast plasma can still penetrate the field. On the other hand, no significant amount of plasma appears to be capable of passing through a quadrupole null if the field lines from the cusps on the two sides of the null are bridged in vacuum so as to allow the plasma to depolarize itself.

Magnetic Field Requirements

In order to be satisfactory, the magnetic field must satisfy a number of conditions. These can be enumerated as follows:

1. The field must have enough strength and distance between the plasma and the wall to contain 10-keV D's. Somewhat incomplete experimental data indicate that this requirement implies, in quantitative terms, that there should be a blanket of approximately 5 gyro radii between the separatrix and any wall. The separatrix is the flux surface connecting to the field null.

2. The internal conductors must be levitated. In other words, there must be no mechanical supports crossing from conductors to walls, since these would necessarily intersect the separatrix, where there is expected to be energetic plasma. Levitation requires that there be no large impulse delivered by the field to the conductors during the time of the experiment; since the field energies are so large, the motion due to a large impulse would probably be destructive.

3. The field must be capable of stable hydromagnetic confinement of plasma. The best information at present is that this implies that $\int \frac{d\ell}{B}$, taken along a closed magnetic field line, must decrease as the line chosen as the path of integration is taken farther and farther from the plasma.

4. The field should be reasonably constant in magnitude and shape for at least a number of milliseconds after plasma is injected. In addition, there should be the minimum possible electric fields in the containment region, so that $\frac{\vec{E} \times \vec{B}}{B^2}$ plasma drifts will not be excessively large.

5. The magnetic field strength must be sufficiently low to permit a reasonable mechanical structure to support the forces.

6. The injection region should have a field at the wall small enough to make cross field injection possible. As a rough guide, a limit of 10 kG has been taken in preliminary planning.

Quadrufilar Field Configuration

The simplest field which appears to be capable of satisfying these requirements is a bridged cusp toroidal quadrupole or quadrufile. The word quadrupole strictly applies to the field at large distances from two magnetic dipoles arranged so that their dipole moments cancel each other. Quadrufile or quadrufilar is used here to denote the field near the origin which is produced by four wires at a long distance arranged symmetrically so that the total field is zero at the origin. Such a field can be generated by the arrangement shown at A in the diagram below; the form of

A

the magnetic field is depicted at B on the following page. A field null appears at a point approximately midway between the levitated conducting rings. The current in the rings has to be driven inductively since no material object can be allowed to intercept the plasma.

The major reason for choosing the toroidal quadrufilar configuration in place of some other multifile is that it alone is free of net translational force on the levitated conductors. The inner ring is subject

SEPARATRIX

INDUCTIVELY
DRIVEN
INNER
CONDUCTOR

QUADRUFILAR FIELD NULL

OUTER PRIMARY CONDUCTOR

MAJOR AXIS OF TOROID

B

to outward forces which amount to a hoop stress, while the outer ring is compressed magnetically inward toward the null. In the case of the octufile with rings in the four corners of a square, two above the median plane and two below, there is in addition a net translational force driving the rings toward the median plane. If the rings were superconducting and thus capable of carrying steady currents, it would be possible to support them magnetically at the expense of some field symmetry, but for the moment this is not practical.

Unfortunately it appears to be somewhat more difficult to achieve a large region of hydromagnetically stable confinement in a quadrufile than in an octufile. In this connection it must be remembered that mechanical equilibrium does not require that the field resemble that of a pure quadrufile at all. The essential requirement is that there should be only two levitated rings, one on the inside and one on the outside of the toroidal null.

Stability and Field Shape

As is stated above, the criterion for stability of a containment field against hydromagnetic fluting is taken to be that $\int \frac{d\ell}{B}$ decreases as the closed field line, along which the line integral is taken, is chosen farther from the plasma containment region. Inspection of the field plot in Fig. 4 shows that there are regions in which the variation of the integral is favorable and regions in which it is unfavorable. The favorable regions are those in which the field lines are convex inward, and the unfavorable where they are convex outward. In the favorable regions the length of the path is smaller and the field strength is larger farther out. Both effects produce a favorable variation of the integral. It is immediately obvious that stability can be enhanced by making the field large in the unfavorable regions and small in the favorable regions. Since B is in the denominator, the value of the integral is strongly increased as the path is taken close to the field null, and in such a field configuration there is always some flux surface outside of the separatrix inside of which the containment is stable.

To achieve the desired blanket of 5 gyro radii between separatrix and wall, any realizable field shape can be taken and the field strength multiplied by a factor such that it does not exceed limits set by practicability. The linear dimensions are then multiplied by whatever factor is necessary to realize the desired blanket. In practice, it will be found that the amount of energy required will then depend on the details of the field shape. Since the most expensive part of the machine is likely to be the energy storage system, and since, even if it were not expensive, the handling of large amounts of energy presents serious problems, a reasonable criterion as to the excellence of a given field configuration is the amount of energy required to create the field subject to the constraints: (a) That the field near the wall adjacent to the field null shall not exceed 10 kG; this figure is chosen to assure that cross field injection will be possible. (b) That enough area be clear of hardware in the hole in the doughnut so that an iron core can be put through it to handle the necessary flux. The latter is

Fig. 4. Field lines for various values of $\int \frac{d\ell}{B}$

the flux between primary current conductor and the inner levitated ring
including the amount soaked into the conductors. (c) That the maximum
field in the bridges between cusps not exceed an amount dictated by
strength of materials; 50 kG might be a reasonable figure to start with.

At present, the process of searching for an optimum field shape has
barely commenced. The computer code developed by R. A. Dory for use in
designing the toroidal octufile at the University of Wisconsin has just
been adapted to computation of these particular field shapes on LASL
computers, and only test problems have been run. However, some calculations
by another method (see report of Baker and Mann below) indicate that a
satisfactory field can probably be designed which will use between
5 and 10 MJ of energy. The field shape will be roughly as indicated below.

AXIS OF TOROID

The back side of each of the levitated rings is hollowed out to reduce the field in the middle of the bridge, to decrease the net stability against fluting toward the rings, and to increase the stability against outward loss of plasma by adding a region of favorable curvature with a somewhat lower field strength.

Magnet and Vacuum Envelope Construction

The diagrams given above have been made on the assumption that the outer primary current is carried on a one-turn conducting doughnut, the surface of the doughnut becoming a flux surface of the field through the skin effect. This is a very convenient way of designing a pulsed magnet and the current conductor can do double duty as the vacuum envelope. It is a method which lends itself to very accurate field shaping through machining of the surface but it also has some difficulties.

The major problem is that, because of the rings, the doughnut must be split so as to come apart into an upper and a lower half like a clam shell, and that it must also be interrupted in at least one place around its circumference, to permit current to be fed to it. The vacuum seal must then have a T joint and the insulator at the current feed has to link the rings; it must thus be split and reassembled. If the primary conductor actually forms the wall of the vacuum chamber, a serious difficulty can arise from voltages appearing across the feed points. The electric fields resulting from these voltages will, in general, be normal to the magnetic field, and will result in plasma drift with velocity $\vec{v} = \frac{\vec{E} \times \vec{B}}{B^2}$. This velocity is parallel to the Poynting vector and hence, if there is an energy sink in the machine, plasma will drift toward it. If energy is allowed to leave the machine through its terminals, plasma will drift to the insulator, and there is a good chance that a short circuit might develop which would have to dissipate a large fraction of the field energy. Thus, to prevent serious damage to the machine, a nearly perfect crowbar would have to be put across its terminals. Such a crowbar is beyond the present normal state of the art.

18

A way of avoiding the problem of plasma drifting against the insulator is the use of a resistive metal liner to the doughnut. The energy dissipated by eddy currents in the liner can be made arbitrarily small by making the time constant of the rise of the field long compared to the L/R time of the liner. In the machine considered at LASL, a stainless steel liner 1/32-in. thick would have an L/R time of roughly 500 μsec. Thus the field would probably have to rise with about a 10-msec time constant, and about 5% of the total field energy would be dissipated in the liner. At first this seemed prohibitively long because of the additional energy which would have to be supplied to provide the energy of the field soaked into the conductors. Then it became apparent that if long containment times should actually be achieved, it would be convenient to have a nearly constant field shape during the containment time, and that the farther the field has soaked into the conductor, the more slowly does the additional field soak in. Furthermore, if the field has soaked a large distance into a conductor, current has too and, since the current is carried in a larger area of Cu, the resistive voltage drop is smaller. This reduces plasma drift toward the conductors since it reduces the Poynting flux.

With long rise times, the skin effect determination of flux surfaces becomes less attractive, and more serious consideration can be given to the determination of the field by placing current carrying conductors in calculated positions. In any event, in order to match normal energy storage devices, it becomes convenient to have a large number of turns in the primary winding of the machine. The result is that at the present time the device is seen as essentially a fiberglass and epoxy plus copper coil structure built up on a thin stainless steel liner. The liner could be fabricated from units the size of an automobile fender, welded together along radial seams, each half making what would look like an enormous somewhat distorted angel food cake pan. Two viton O-rings would be used to make the seals in the equatorial plane.

The inductance of a one-turn doughnut with two secondary rings is likely to be ~ 1 μH. In order to achieve a 10-msec rise time with 10 kV on the windings, it would be more convenient to have ~ 1 mH of inductance. This implies that the machine should have about 30 turns in its primary winding. These turns could be laid on top of a solid metal doughnut, which could be used for shaping the field, and this would relax considerably the precision required in applying the 30 turns. More Cu (or Al) would be required here since the current, in effect, would have to be carried around the doughnut three times in the primary winding: once in the 30 turns, once in the image current on the outside of the doughnut under the 30 turns, and once on the inside of the doughnut to generate the containment field. This point will have to be studied carefully before final design.

Magnetic Core

The current in the levitated rings has to be driven inductively. A simple way of looking at the system is that the primary is a single turn doughnut of high conductivity, of such a thickness that field does not soak through it completely. The current on the inside of the doughnut is then exactly equal and opposite to the current on the two conducting rings. This follows since, as the field in the doughnut wall is zero, $\int$ H.dℓ linking the rings in the metal of the wall is zero also, and therefore the net current inside is zero. The exterior surface of the doughnut, however, can carry current too. It represents a parasitic inductive load across the load which has to be driven. In order of magnitude, the inductance of this load will also be ~ 1 μH, and thus it would absorb half of the energy from the source. In order to avoid this, the simplest approach is to thread a ferromagnetic circuit through the hole in the doughnut to increase the inductance of the parasitic current path. This amounts to an ordinary transformer core.

If the inner levitated ring is assumed to have effectively zero resistance, the flux through it will not be able to change with time.

Thus all flux in the inner bridge between cusps must be compensated during
a shot by an equal and opposite flux linking the hole in the doughnut.
Stacked transformer Fe normally cannot be magnetized at all efficiently
beyond about 15,000 G, so this puts a lower limit on the area of the hole
in the doughnut for a given field configuration. There is still too little
known about the optimum field configuration to be able to specify the hole
area, but it appears that a 1-m diam clear hole would almost certainly be
adequate. In selecting this area, allowance has been made for flux biasing
the Fe. If before a shot the Fe core is already magnetized in the reverse
direction by a dc winding, twice the flux change is obviously available from
a given area of Fe. The only difficulty is that the changing flux in the
core during a shot induces a large emf in the dc winding; operation of the
machine would then be impossible if the emf is allowed to drive the current
it normally would through the power supply connections or through a short
across the winding terminals. According to Lenz's law, the emf is in the
direction to maintain the original flux in the core. The ordinary way of
taking care of this problem is to insert a choke coil between the power
supply and the bias winding. The trouble is that this choke turns out to
have twice as much Fe in it as the core linking the doughnut. For the
machine under consideration, the situation is saved by the long time constant
of the conducting rings around the core (of the order of 20 sec). If the
flux bias winding is opened, first by a switch with a resistor across it,
and then completely, the bias current is transferred to the rings; no
choke is necessary since the bias winding is open.

Energy Storage I, Capacitor Bank

Of the order of 10 MJ of energy will have to be stored to produce
the containment field of the machine. The conventional method of storing
energy for such purposes is in capacitor banks, and this can readily be
done at LASL. Because of the availability of capacitors capable of slow
energy storage and costing 2 cents per joule, it should be possible to assemble
the necessary stored energy for about $3 x 10^5. There would undoubtedly be
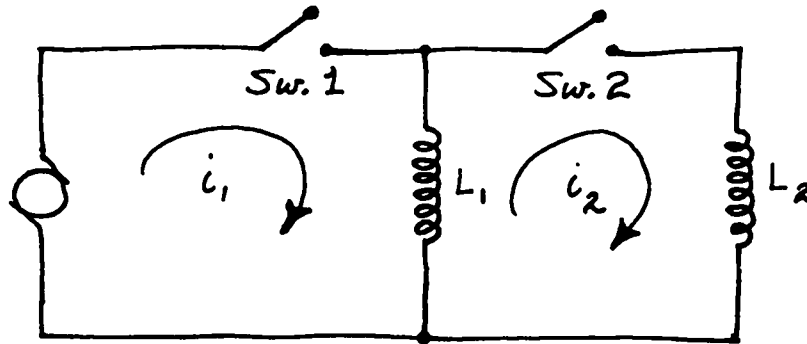
frequent capacitor failures, and it would probably be necessary to provide clearing fuses which would isolate a failed capacitor; the machine could then be fired even after one or two loud explosions during the charge phase. These capacitors are said to be operable only if they are crowbarred to prevent voltage reversal. The bank would be provided with ignitrons for this purpose, but in addition a mechanical crowbar of very low resistance would be applied across the machine terminals. This switch should have a resistance of the order of 10^{-4} Ω and be operable with a jitter of less than 1 msec; this is based on the assumption that the crowbar would be applied to the 30-turn, 1-mH machine primary. The switch would have to close a circuit carrying about 1.5×10^5 A.

Energy Storage II, Inductive Energy Storage

Although approximately 10 MJ of capacitive energy storage is installed at LASL, nothing approaching this quantity has ever been connected to one load, and very few capacitor banks are ever run at full rated voltage. A considerable amount of maintenance would probably be required if a bank as large as this one is used. The most likely fault to occur is a short circuit across the bank; such a fault always results in an explosion and frequently there is damage from blast or from resulting shrapnel. Consequently, alternatives to a 10-MJ capacitor bank should be considered.

The current through a short circuit across a load fed from a storage inductor can never exceed the current stored in the inductor. To deliver a large amount of energy suddenly to a fault in such a circuit, the fault must approach an opened circuit, and the only real problem in inductive energy storage in the past has been the opening of circuits. The worst danger is likely to be fires from arcs in broken circuits, and this should be no worse than with dc magnet circuits.

Consider an inductive energy storage system driving an inductive load; the most obvious way of drawing the circuit is shown on the following page. To begin with, switch 1 would be closed and the generator

would be operated to build up a current $i_1 = I_s$ in the storage circuit.
At some time, switch 2 would be closed and switch 1 would be opened.
Breaking the current in inductor L_1 produces a large voltage across the
terminals of L_2 and transfers energy to it. However, the circuit cannot
and does not work this way because the instantaneous opening of an inductive
circuit would produce an infinite voltage. Actually the switch would arc,
and this might be considered as a resistance that varies in a complicated way
with time. Analysis of circuits containing resistances of varying time
dependence shows that the efficiency of energy transfer from L_1 to L_2 is
the same whether the resistance varies as a step function from zero to a
constant value, increases linearly with time after $t = 0$, or increases
quadratically with time. The efficiency in each case is

$$\eta = \frac{\frac{1}{2} L_2 \, i_2(t = \infty)}{\frac{1}{2} L_1 \, I_s} = \frac{L_1 \, L_2}{(L_1 + L_2)^2} \quad .$$

It has been found (H. R. Lewis, LASL) that the energy transfer
efficiency is the same for an arbitrary dependence of resistance on time,
so long as the resistance varies in such a way as to bring I_1 to zero at
large times. In the case of a step function from zero to R (a switch opened
across a resistor R), the current in the load varies as

$$i_2 = -I_s \, \frac{L_1}{(L_1 + L_2)} \left(1 - e^{\frac{-R(L_1 + L_2)t}{L_1 \, L_2}} \right).$$

The maximum energy transfer efficiency is 1/4, and is achieved with $L_1 = L_2$.

At first sight an energy transfer efficiency less than 1/4 appears very poor. It must be remembered, however, that for an occasional shot the cost of energy itself is small, and that only the initial cost and maintenance of the installation should be considered. For this reason a more careful look has been taken at the problems involved.

Resistor

It is important to remember that half of the stored energy is dissipated in the resistor, even if the resistor is the arc across an opened switch. Obviously the resistor must have a capacity for soaking up energy rarely met with in practice. It happens that in actual fact this is the easiest and cheapest component of the system to build. The resistor would be electrolytic, and would consist of $\sim 1 \, m^3$ of a salt solution, the salt concentration being adjusted to produce an appropriate resistance. The electrodes would be large stainless steel sheets interleaved and hanging in the electrolyte like the plates of a storage battery. The inductance of such a configuration can be made negligible, and only the outside plates are subject to magnetic forces. The dissipation of 20 MJ in $1 \, m^3$ of water would raise the temperature about 5° C. A test cell has been operated successfully with a 15° C rise in a much shorter time. The only problem was that the rapid thermal expansion of the electrolyte threw water upward from the surface of the cell. Electrolytic resistors with smaller temperature rises are in routine operation in the laboratory.

Switch

With a low inductance resistor across it, the switch has to break the full storage current, but never has to stand off voltage greater than RI_s. A reasonable arrangement might be a combination of a mechanical switch capable of carrying the storage current ($\sim 3 \times 10^5$ A) and a fuse, preferably of very low inductance, which will open ~ 1 msec after the switch opens. There may be suitable commercial fuses, but if not, a foil type under high pressure, such as has been tested by H. Early at the University of Michigan, could be used.
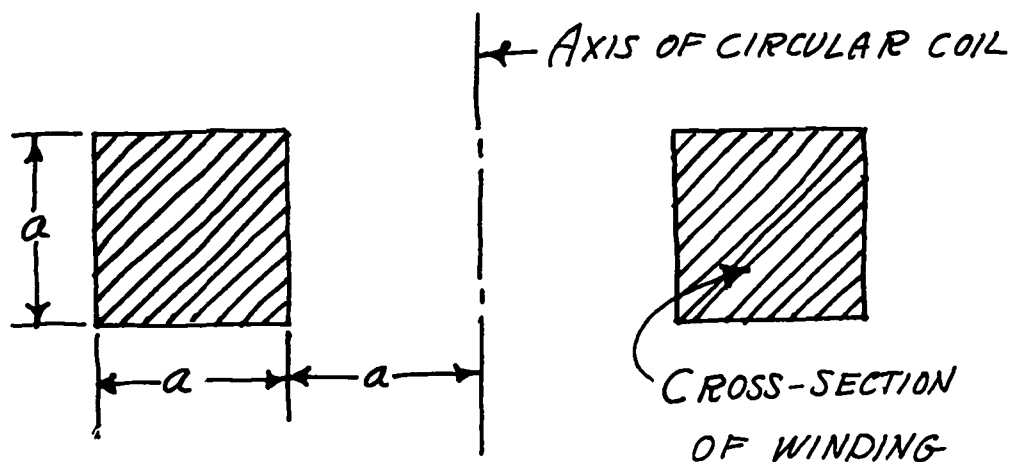
Storage Inductor

The storage inductor is probably the most difficult part of the system to construct, simply because of its large size. It must store ~ 40 MJ and, for reasons of economy, should be chargeable with an existing power supply. It can be shown that the maximum amount of energy, U, which can be stored in an inductor, is related to the maximum power output, w, of the charging supply by the formula

$$U = \tfrac{1}{2} w\tau,$$

where τ is the L/R time constant of the storage inductor circuit, and w is the maximum power output of the supply when it is connected to this particular load. There is available at LASL a power supply capable of delivering 2.5 MW at 72 kA and 35 V. The storage inductor then should have a time constant of at least 32 sec.

An examination of Fe core inductors shows that it is probably easier and cheaper if there is little or no Fe; furthermore, calculations are certainly simpler if a pure air core inductance is used. The reason is that for completely unsaturated Fe, an air gap of 50 m^3 would be required to store the energy at 14,000 G. An enormous amount of transformer Fe would be required, as well as a large amount of Cu. The most efficient use of conducting material without Fe is made by a coil having approximately the "Brooks" shape, as indicated in the following sketch.

AXIS OF CIRCULAR COIL

CROSS-SECTION OF WINDING

The inductance of the coil is $L = 0.0255aN^2$ µH, where a is in cm and N is the total number of turns. The resistance is $R = \frac{3\pi}{af}\rho N^2$, where ρ is the resistivity of the winding material and f is the space factor (fraction of winding volume filled by conductor). For Cu, $\rho = 1.7 \times 10^{-6}$ Ω-cm, and for Al it is 2.83×10^{-6}, at 20°C. Using the foregoing expressions for L and R, setting L/R = 32 sec, and assuming a space factor of 0.8, suitable inductors are found to have the following characteristics:

Material	Dimension, a(cm)	Outside Diameter	Mass of Material (tons)
Cu	158.7	633 cm (21 ft)	268
Al	204.5	818 cm (27 ft)	174

Assuming that Al and Cu cost the same per pound, it would be more economical to make the inductor from the former.

It was assumed in the section on Magnet and Vacuum Envelope Construction that, to match to a 10-kV capacitor bank with about a 10-msec rise time, the machine winding would have an inductance of ~ 1 mH. This winding would require 1.4×10^5 A for a 10-MJ energy content. A storage inductor would then have to start with 2.8×10^5 A to deliver the current to the load. In order to charge the inductor considered above with the existing power supply, which has only one fourth of this current capacity, the inductance should be 16 mH; the rise time of 10 msec would then imply a 40-kV terminal voltage. The optimum arrangement for matching power supply, storage inductor, and switch will have to be determined, if it is decided to use magnetic energy storage.

One consideration favoring higher voltage and lower current is the formidable bus bars required for these currents, and the necessity of locating the inductor at some distance from working areas because of stray field. The latter will be about 5 G at 30 m, and will fall off inversely as the cube of the distance. It might be possible to reduce the stray field considerably by a certain amount of Fe in the return flux path. This would also improve the inductor somewhat.

The inductor would have a small number of turns for an inductance
of 1 mH or 16 mH, e.g., 14 or 56 turns, respectively, for Al. On
the other hand, the individual strands would need to have a small cross
section so as to minimize skin effect. These rather contradictory
requirements can be satisfied by the use of a large number of leads in
parallel. The coil would be assembled from a number of pancakes, for
example with 30 pancakes, each pancake consisting of 100 leads in parallel,
each lead making a half turn from inside to out. The lead to lead voltage
inside a pancake would be very small so that insulation would be quite easy,
but the coil would require some mechanical strength because of the high
magnetic field and large dimensions. Actually the hoop stress in the coil
would be of the order of 300 tons, well within the strength of the winding.

If the charging time of the inductor is 3 min at 2.5 MW—a generous
estimate—the coil would be expected to rise about 5° C in temperature per
shot. Heat from inside the coil would have natural conduction paths
along the leads to the large number of connections between pancakes, and
these could be air cooled. The time between shots will be much more
severely limited by the cooling of the levitated conductors in their Dewar
flask than by the cooling of the inductor. Therefore no expensive water
cooling of the coil would be necessary.

Levitation (with W. Borkenhagen)

There are obvious difficulties in levitating a few tons of Cu
and steel rings in the doughnut during the time of the experiment. The
problem is aggravated by the necessity of precise positioning during a
period of a number of msec. It is assumed that precision is required so
that calculations of the behavior of the plasma in the field will apply
to the actual machine, and so that measurements of plasma diamagnetism
will be successful. In addition to these scientific requirements, there
is the practical necessity that the rings should be close to their
magnetic equilibrium positions at any time when there is a possibility of

of energy being fed into the machine terminals. If, for example, the rings were lying in the bottom of the doughnut, and the field were accidentally energized by a prefire of capacitor bank ignitrons, a large force would be generated driving the rings upward toward their equilibrium position; 10 MJ corresponds to the kinetic energy of a mass of 2 tons moving at a speed of about 100 m/sec. Clearly, if even a small fraction of the stored energy were transformed into kinetic energy of motion of the rings, a catastrophe would result.

The requirement of accurate positioning of the rings is made more difficult by the necessity of operating through an "ultra high vacuum" wall. Since no grease or oil of any kind will be permitted in the system, a bellows seems to provide the best solution. Ordinary metal bellows are probably not able to survive the accelerations required of the withdrawable ring supports, but there appear to be several conceivable means of by-passing this difficulty.
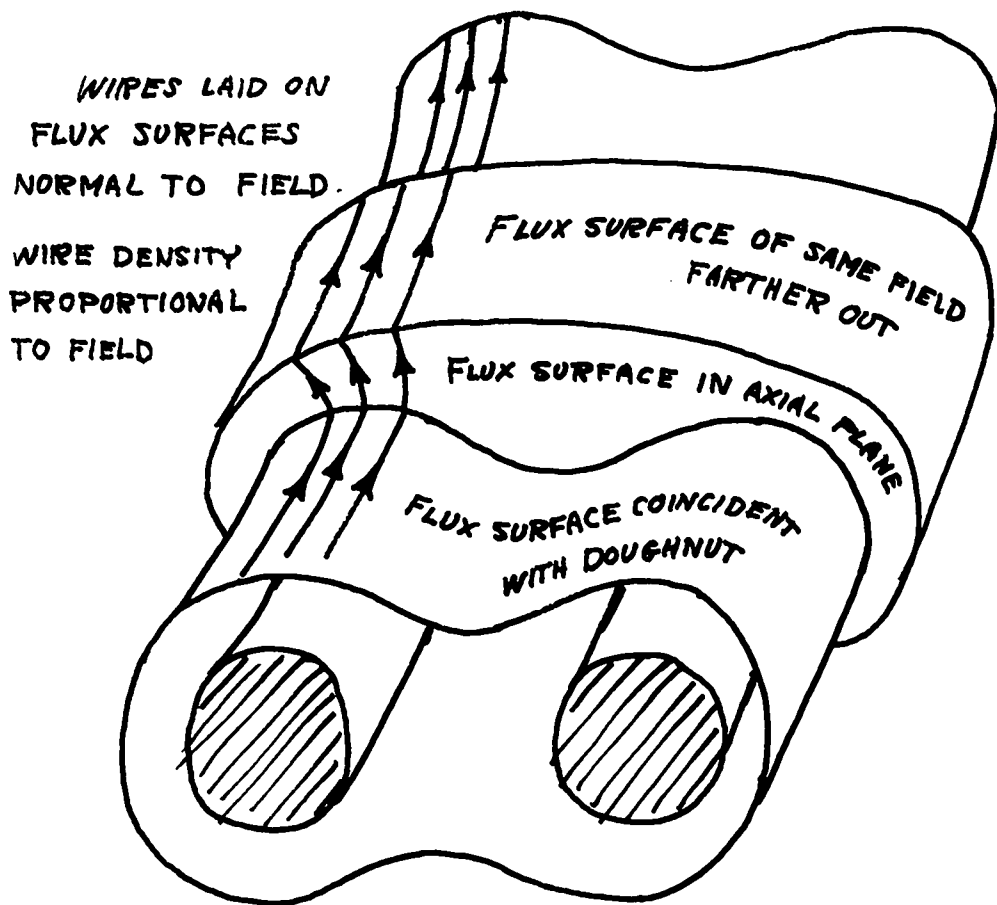
The levitation procedure, as conceived at present, is as follows: Originally the ring conductors are supported by a set of withdrawable pins or crutches. The pins are held in position relative to the doughnut wall by latches, and are arranged to be withdrawn rapidly by stored high-pressure air acting on pneumatic cylinders. The entire doughnut is mounted on a mechanical linkage controlled by a one-turn cam driven by a flywheel. The cam is designed to drive the doughnut into a free fall trajectory in which it remains for 50 msec, for a drop of 1.25 cm. Immediately following the start of free fall of the doughnut, the pins are withdrawn from under the rings. A downward acceleration of 15 g is sufficient to move the pins 10 cm in 10 msec. This leaves the rings falling freely at the same speed as the doughnut and in the original relative position. After the pins are out, the machine is left in free fall for 30 msec, at which time another set of pins is driven into the machine in the same way that the

first set was pulled. Ten msec later they are in contact with the rings and the cam program continues with a deceleration and elevation phase.

Plans are being made to construct a working model of the levitation machinery. Air cylinders and bellows have been ordered, and a working space will soon be available in which the model will be set up.

Injection

As was stated at the outset, it is planned to use the cross field injection technique in the proposed machine. For this purpose it will be necessary to have at least one large hole in the machine wall unencumbered by current conductors, but with as little distortion of containment field inside the hole as possible. Outside the hole there should be a continuation of the containment field for a sufficient distance so that measures can be taken to reject the slow plasma. If the field shape is determined by a conducting metal wall, the outside field can be matched adequately by local coils outside the hole in the wall. If it is determined by wires accurately laid in their calculated positions, the extension of the field in the injection region should strictly be made by bulging the winding all the way around the doughnut as in the sketch on the following page. If the outer flux surface is pulled outward a sufficient distance it should be possible to part some of the wires far enough to allow plasma injection without perturbing the containment field.

WIRES LAID ON FLUX SURFACES NORMAL TO FIELD.

WIRE DENSITY PROPORTIONAL TO FIELD

FLUX SURFACE OF SAME FIELD FARTHER OUT

FLUX SURFACE IN AXIAL PLANE

FLUX SURFACE COINCIDENT WITH DOUGHNUT

CAULKED CUSP DESIGN CALCULATIONS

(D.A. Baker, L.W. Mann)

Approach to Field Design

The requirements of the magnetic field for the Caulked Cusp device were described at the beginning of the preceding section of this report. The following approach has been used to design a suitable field: (1) Calculate a field configuration which has the right topology, i.e., an outer toroidal boundary, representing the primary winding, which encloses a pair of ring conductors corresponding to levitated secondaries, and is everywhere stable in the sense that the vacuum value of $\int d\ell/B$ decreases outward from the proposed plasma region. (2) Scale the resulting field values so that the field strength at the injection point is small enough to allow injection from a coaxial gun. (3) Scale the torus cross section so that an adequate plasma region is separated by several gyro radii from the wall. (4) Scale the inside major diameter of the torus to be compatible with the magnetic core and primary windings required. (5) Examine the resulting configuration from the point of view of field energy and forces.

These steps will be repeated with new configurations until an acceptable result, optimum in some sense, is obtained.

Results

Step (1) has proceeded using a modified version of the MAFCO computer code of Perkins and Brown (IRL) in which current rings are located such as to produce a field of the right topology. Figures 5, 6, 7, and 8 represent flux surfaces of the torus cross-section found in this manner. The outer curve is the outermost "stable line" where the primary is to be located, next inside is the approximate separatrix

31

FIELD LINES AROUND TWO CONCENTRIC RINGS   COIL 1 AT
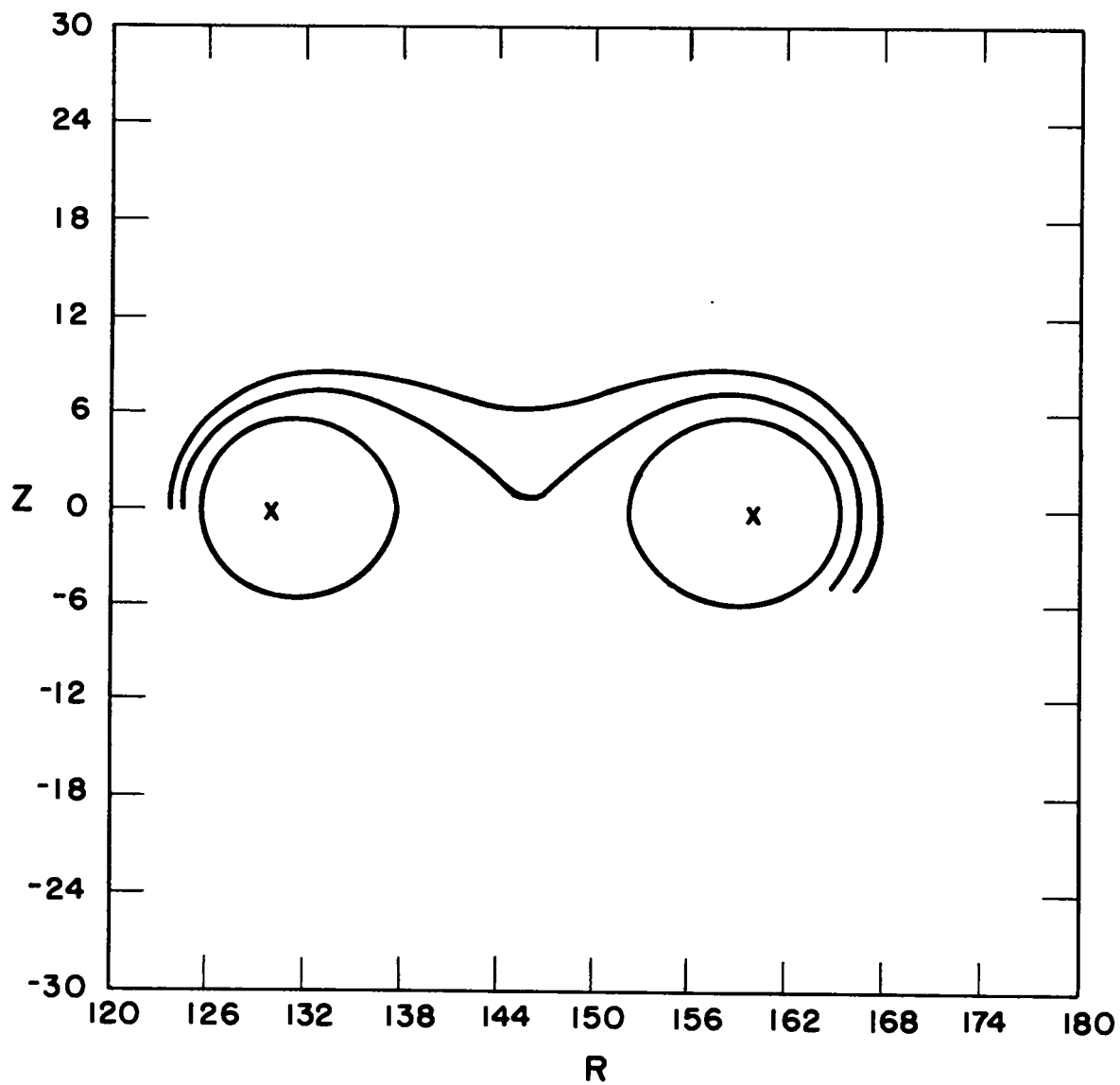130, I = 1800   COIL 2 at 160, I = 1000

Fig. 5.   Flux surfaces of torus cross section

CASE II

FIELD OF FOUR RINGS COIL 1 AT R = 130, I = 1800   COIL 2
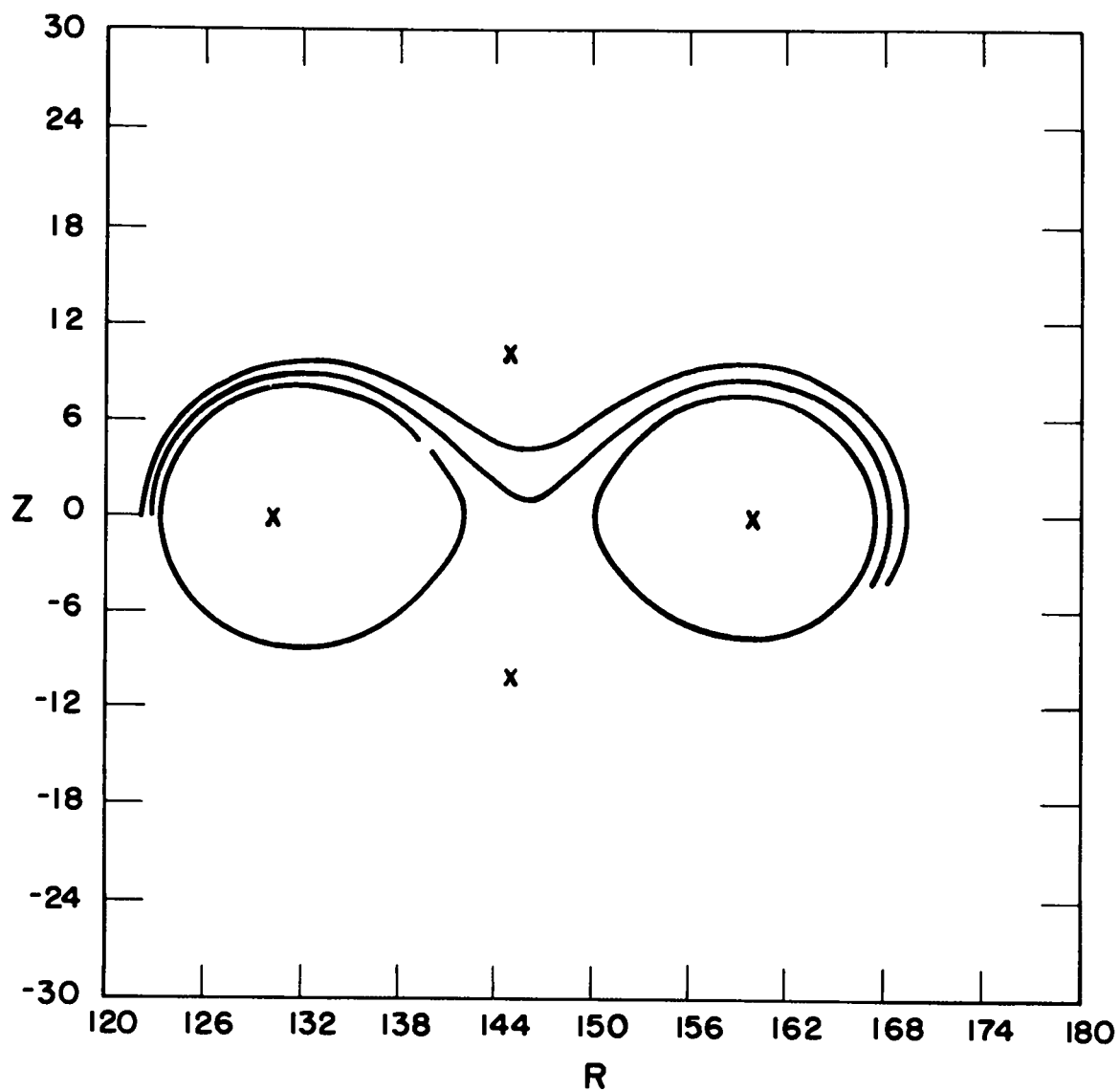AT 160, I = 1000, COILS 3, 4 AT R = 145, Z = +10, -10, I = -200

Fig. 6. Flux surfaces of torus cross section

CASE III

FIELD OF FOUR RINGS COIL 1 AT R = 130, I = 1800   COIL 2
AT 160, I = 1000, COILS 3, 4 AT R = 145, Z = +10, -10, I = 75
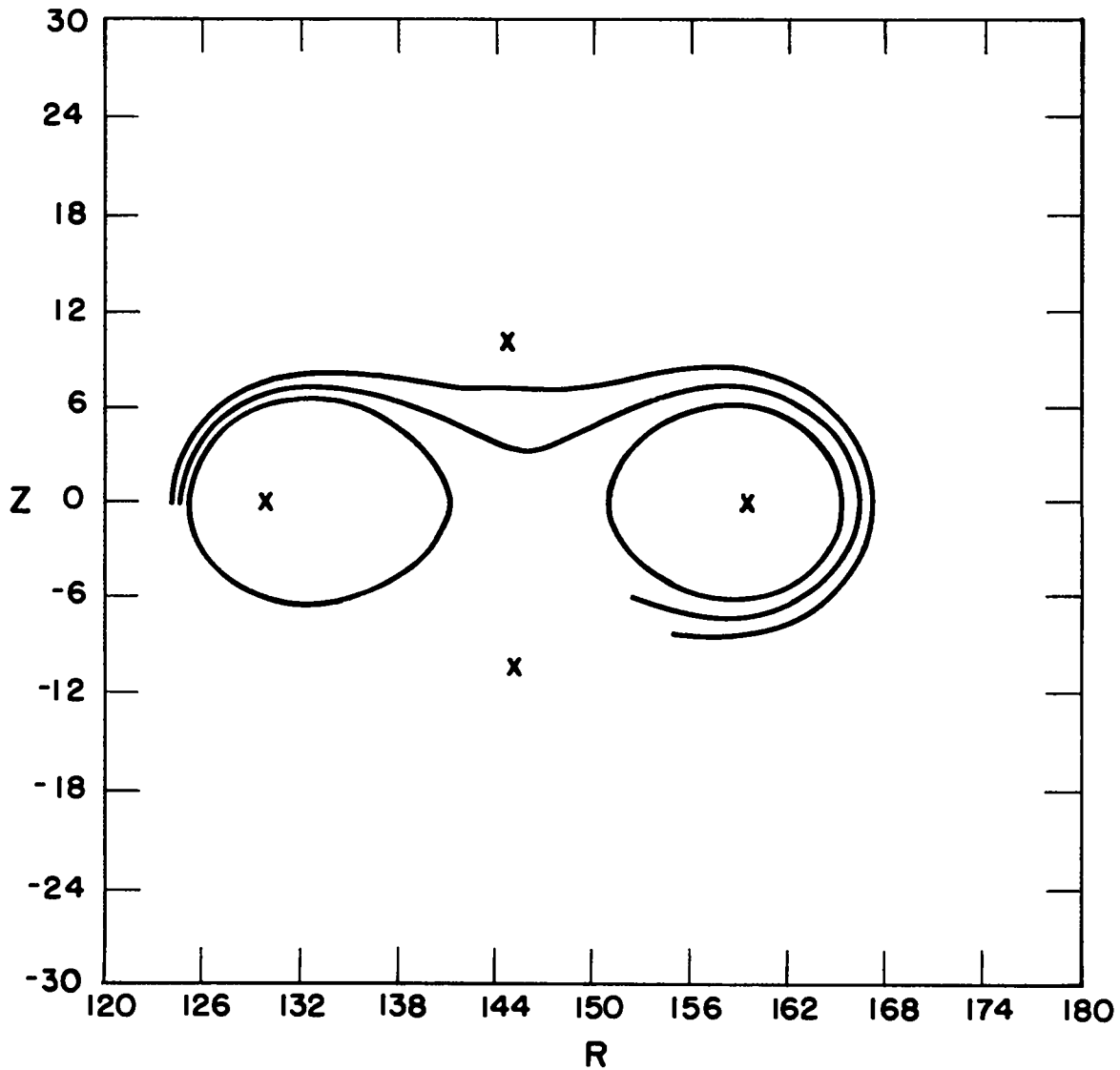

Fig. 7. Flux surfaces of torus cross section

CASE IV

TWO SPLIT COILS, R = 130, Z = +5, -5, I = 900 EACH AND
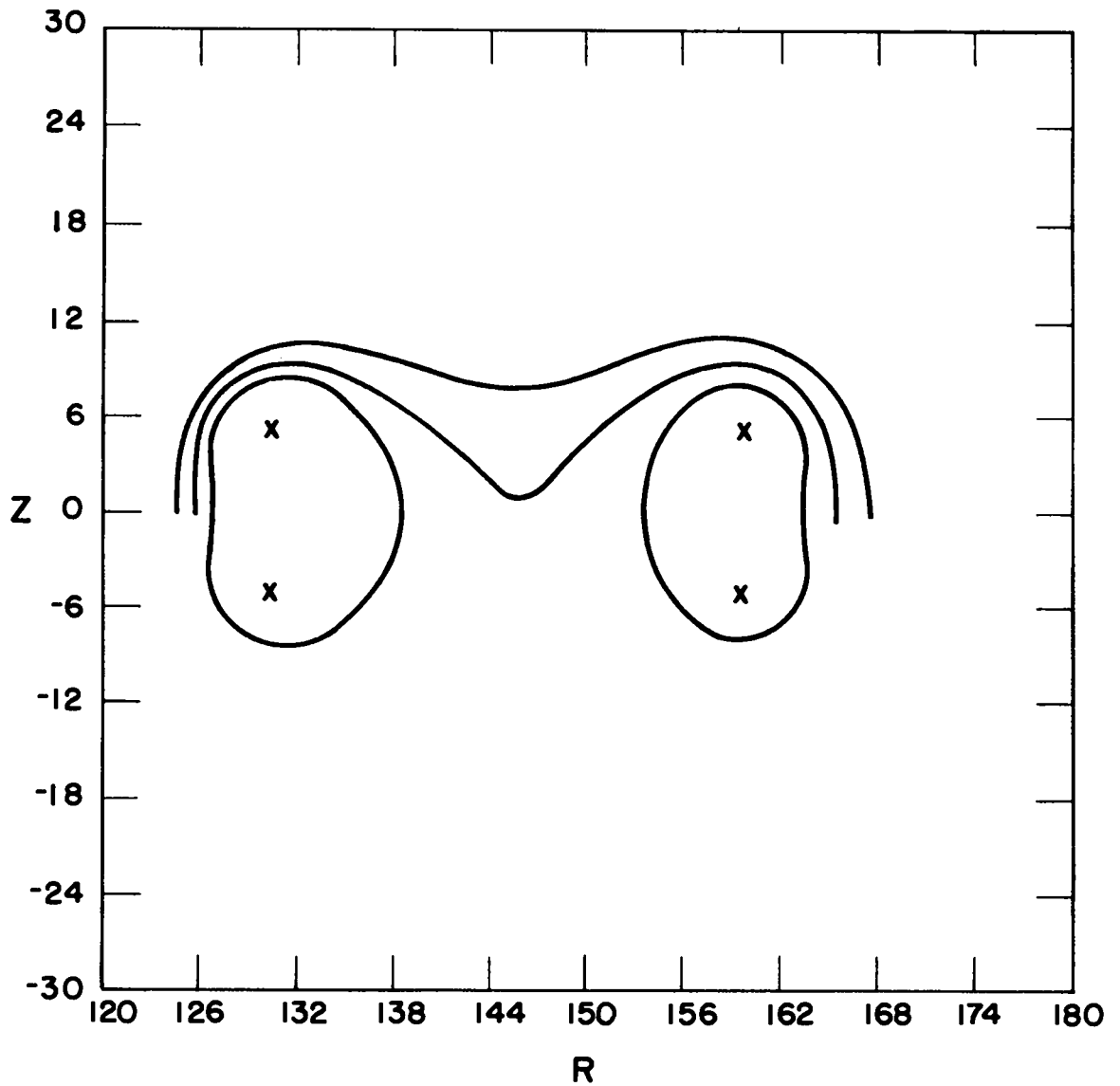R = 160, Z = +5, -5, I = 500 EACH

Fig. 8.   Flux surfaces of torus cross section

where the plasma is to be concentrated, and the two inside curves represent the levitated conductors. More recently the flux surfaces have been determined using a modified version of R. A. Dory's boundary value code. This program allows better control of the flux surfaces to be computed since the current sources need not be determined in advance. An example of a field configuration obtained in this way is shown in Fig. 9.

The results of scaling the problems in Figs. 5-8 are shown in Table I.

TABLE I

Case	Torus Dimensions (cm)		Flux (Webers)	Rod Current (10^6 A)		Total Current (10^6 A)	Confinement Field Energy (MJ)
	ID	OD		Inner	Outer		
I	125.2	420	2.58	4.68	2.60	7.28	9.4
II	163.2	712	4.39	7.75	4.31	12.06	27.0
III	124.0	410	2.52	5.14	2.86	8.00	10.1
IV	117.0	370	2.25	4.35	2.42	6.77	7.62

Notes: Injection field = 10 kG

Wall

$\int Bd\ell = 10^5$ G-cm corresponding to 5 gyro radii for a 10-keV D ion

Separatrix

$\int d\ell/B$ decreases away from separatrix throughout field volume

The injection field in all cases has been scaled to 10 kG. Each torus cross section has been scaled so that for a 10-keV D ion the walls are five gyro radii from the separatrix line at the worst point—the outermost bridge. The torus major inside diameter has been separately scaled so that a backbiased core capable of a 30-kG flux change occupies 70% of the hole area. This leaves approximately 10 cm for primary windings and vacuum flanges. The justification for scaling this diameter independently of the cross section stems from calculations with the boundary value code.

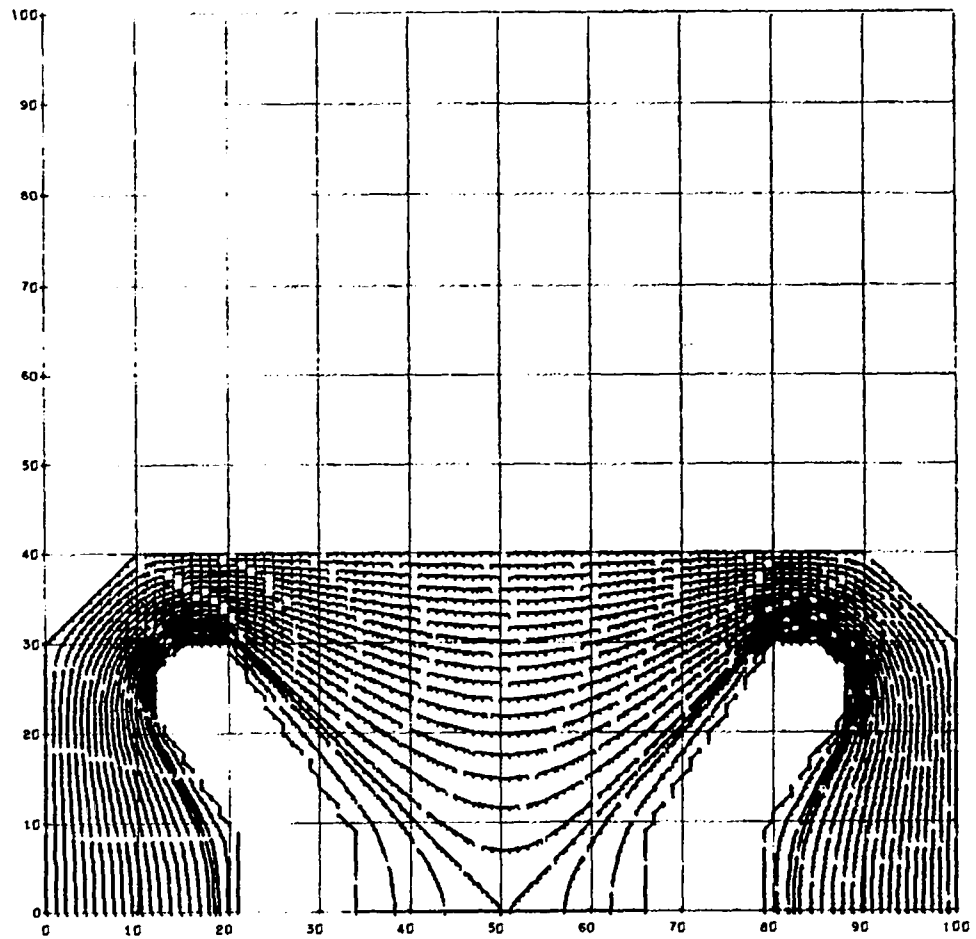DORY CODE FIELD LINES
PROBLEM NUMBER 10G

Fig. 9. Field configuration calculated by Dory's code

It was found that, for a given cross-section geometry, the surfaces are independent of the torus diameter to a very good approximation.

Conclusion

From the comparison of the confinement field energies in Table I, it is clear that Case IV is advantageous. This result has led to the investigation of configurations similar to that shown in Fig. 9.

All of the above calculations are based on the approximation of a small skin depth. For a magnetic field with a long period, further corrections will be required for the final design.

LINEAR MODEL OF CAULKED CUSP

(D.A. Baker, R.S. Dike, and J.E. Hammel; E.L.Kemp)

A full-scale linear section of the Caulked Cusp machine is being built. The section will be 1.5-m long and for ease of construction will have no curvature. The model will be used to study the problems associated with plasma injection into the actual machine. The section will be placed in the vacuum tank now being used for the transverse injection experiments and will be powered by the 1-MJ in Rack 6 of Zeus. The section has eight turns in series giving an $nI = 5$ MA for each interior conductor.

Included in the experiment will be a coil placed outside the injection port. This multipurpose coil will, it is hoped, (a) reduce the perturbation caused by the injection port, (b) remove the slow component of the gun plasmas as described in the section of this report on transverse injection (p. 57), and (c) serve as a focusing guide field for the stream.

Figure 10 is a schematic of the physical arrangement. The field of the external guide coil is a distorted mirror arrangement which is able to reduce the internal field distortion to a few percent. A shorting plate outside the mirror of the guide coil will be included to remove the slow component of the gun stream.
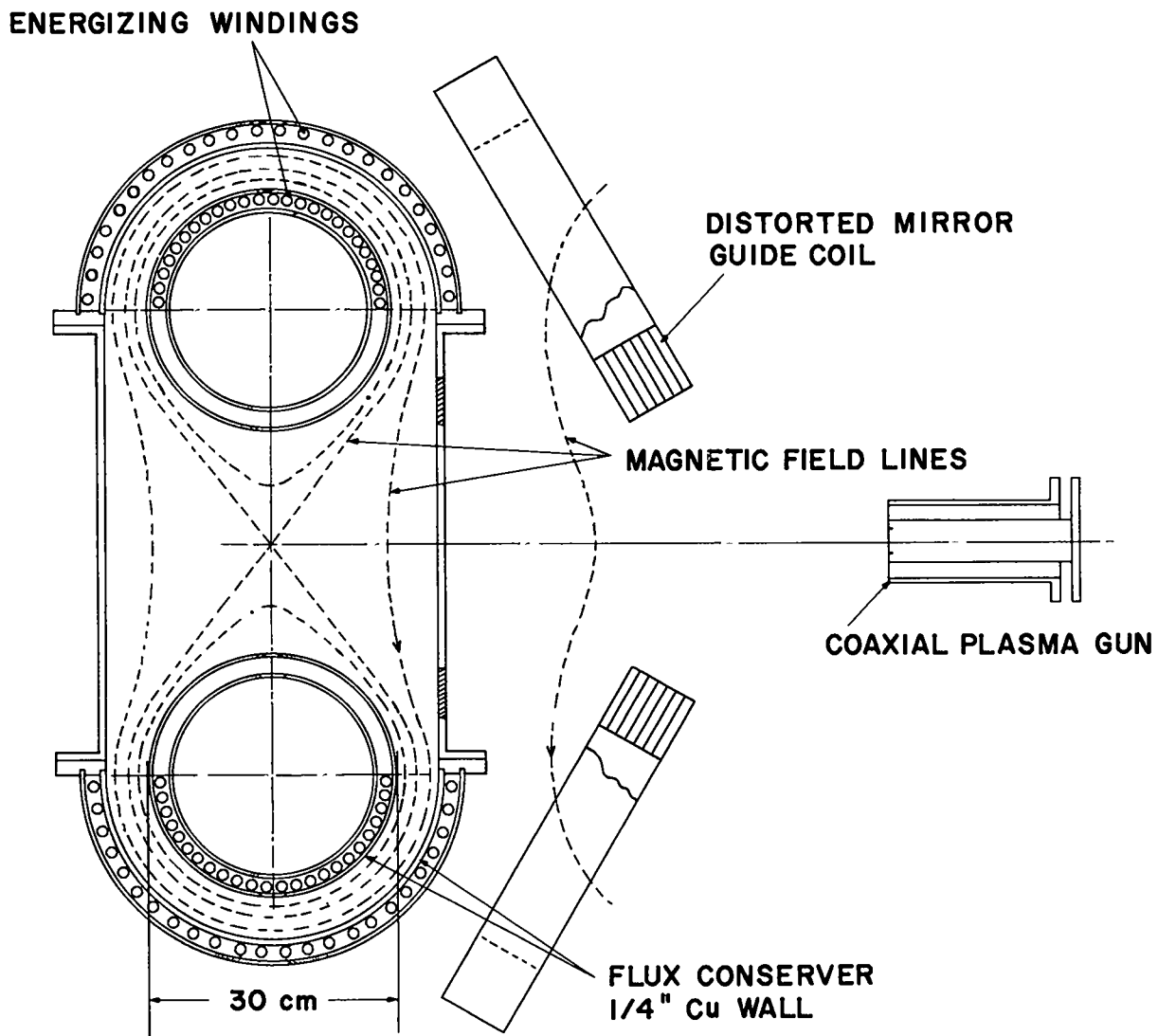
ENERGIZING WINDINGS

DISTORTED MIRROR
GUIDE COIL

MAGNETIC FIELD LINES

COAXIAL PLASMA GUN

FLUX CONSERVER
1/4" Cu WALL

30 cm

Fig. 10. Schematic of linear section of Caulked Cusp machine model

40

FIELD PENETRATION STUDIES

(D.A. Baker, M.D.J. MacRoberts, L.W. Mann)

Introduction

A Fortran program has been written for the IBM-7094 to compute the speed at which pulsed fields penetrate an infinite hollow cylindrical conductor and the electric field at the surface of the conductor. This code can thus be used to determine conductors which minimize magnetic field energy loss and to indicate methods of programming rod currents to minimize the surface electric field on the conductors. The latter feature will reduce the $\vec{E} \times \vec{B}$ drift of plasma to the conductors.

Approach

The electric and magnetic fields in an infinite hollow cylinder will have the following simple form:

$$\vec{E} = \hat{Z} \, E\,(r,t), \qquad a \leq r \leq b$$

$$\vec{B} = \hat{\theta} \, B\,(r,t),$$

where a and b are the inner and outer radius, respectively, of the cylinder. Upon applying Maxwell's field equations and neglecting the displacement term, the differential equation

$$\frac{\partial^2 B}{\partial r^2} + \frac{1}{r}\frac{\partial B}{\partial r} - \frac{B}{r^2} = \mu\sigma\frac{\partial B}{\partial t}$$

can be developed. If the initial condition on the fields is that

$$B(r,0) = E(r,0) = 0; \quad a \leq r \leq b$$

and the boundary conditions are

$$B(a,t) = 0 \quad \text{and} \quad B(b,t) = \frac{\mu\, I\,(t)}{2\pi b} \quad ,$$

$B(r,t)$ can be computed by an implicit numerical differencing scheme.

The electric field is

$$E(r,t) = \frac{1}{r\mu\sigma}\left[B + r\,\frac{\partial B}{\partial r} \right].$$

Results

The manner in which the B field penetrates an infinite hollow conducting cylinder is shown in Fig. 11. The current in the cylinder is of the form

$$I(t) = I_m \sin \omega t,$$

where $I_m = 10^6$ and $\omega = (\pi/2)10^3$.

The set of curves is for a Cu cylinder of inner radius 5 cm, outer radius 10 cm at times of 0.1, 0.5, and 1 msec.

The computed electric field at the surface of a Cu conductor is given in Fig. 12. The case shown is for a sinusoidal rising current which is ideally crowbarred at its peak, i.e., the current and magnetic field remain constant at their peak value for $t \geq \tau/4$.

The parameters used in the calculation were: outer radius = 10 cm, quarter period of the current = 0.25 msec, μ and σ for Cu, tube wall thickness = 1, 2, and 5 mm, and 2 , 4, 6, 8 and 10 cm (solid conductor), total conductor current = 10^6A (1 MA). For a solid conductor, a drift velocity of 0.375 cm/msec is obtained at the conductor surface for the time of peak magnetic field (20 kG). This drift velocity is independent of the value of peak current since, at a given time, E and B each scale linearly with conductor current. It is seen from Fig. 12 that decreasing the wall thickness increases the surface E field at all times. The thinner walls take a shorter time for the fields to soak in and therefore level out sooner to higher values of the dc E field. For wall thicknesses > 2 cm the fields
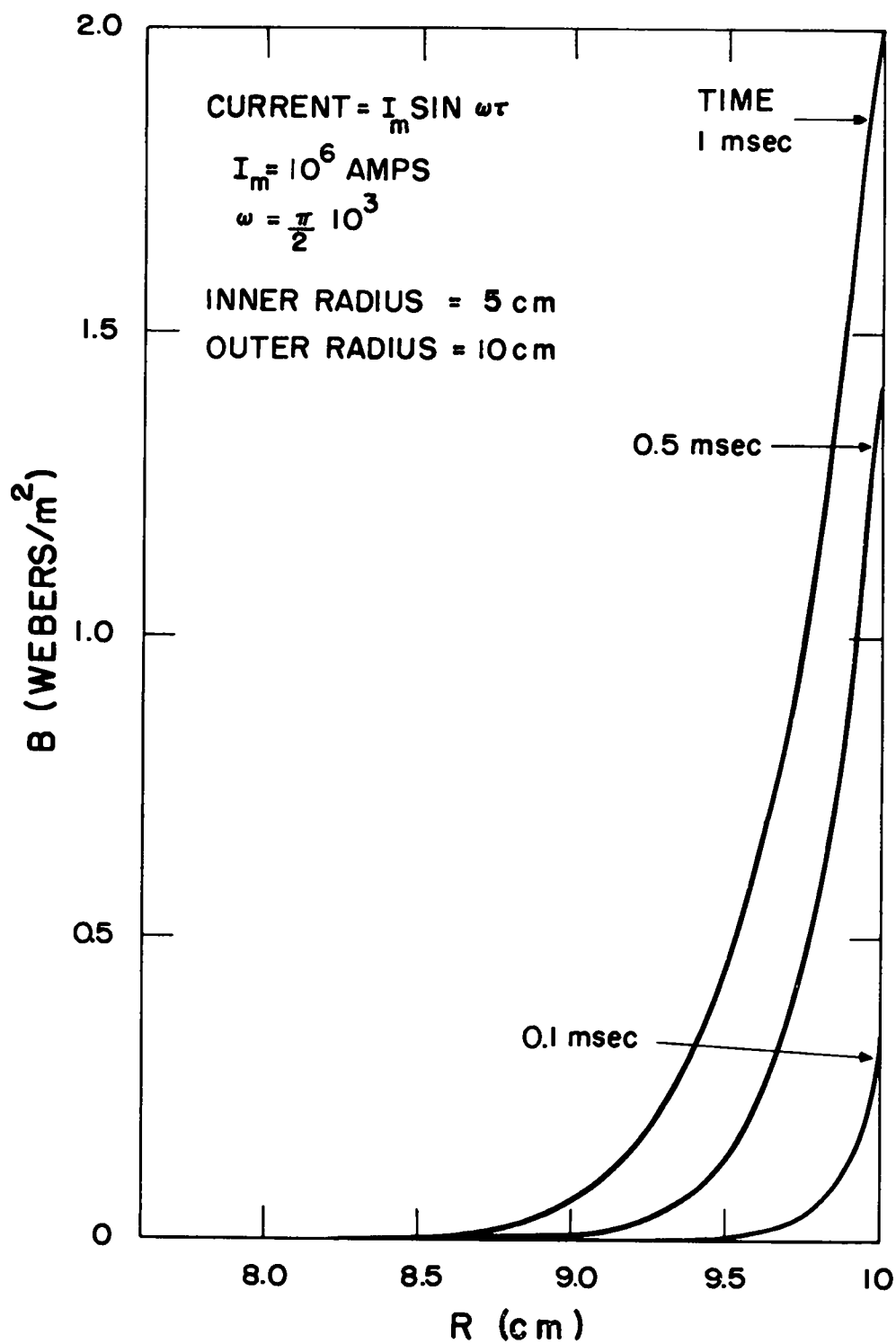
Fig. 11.   Field penetration into a hollow copper cylinder

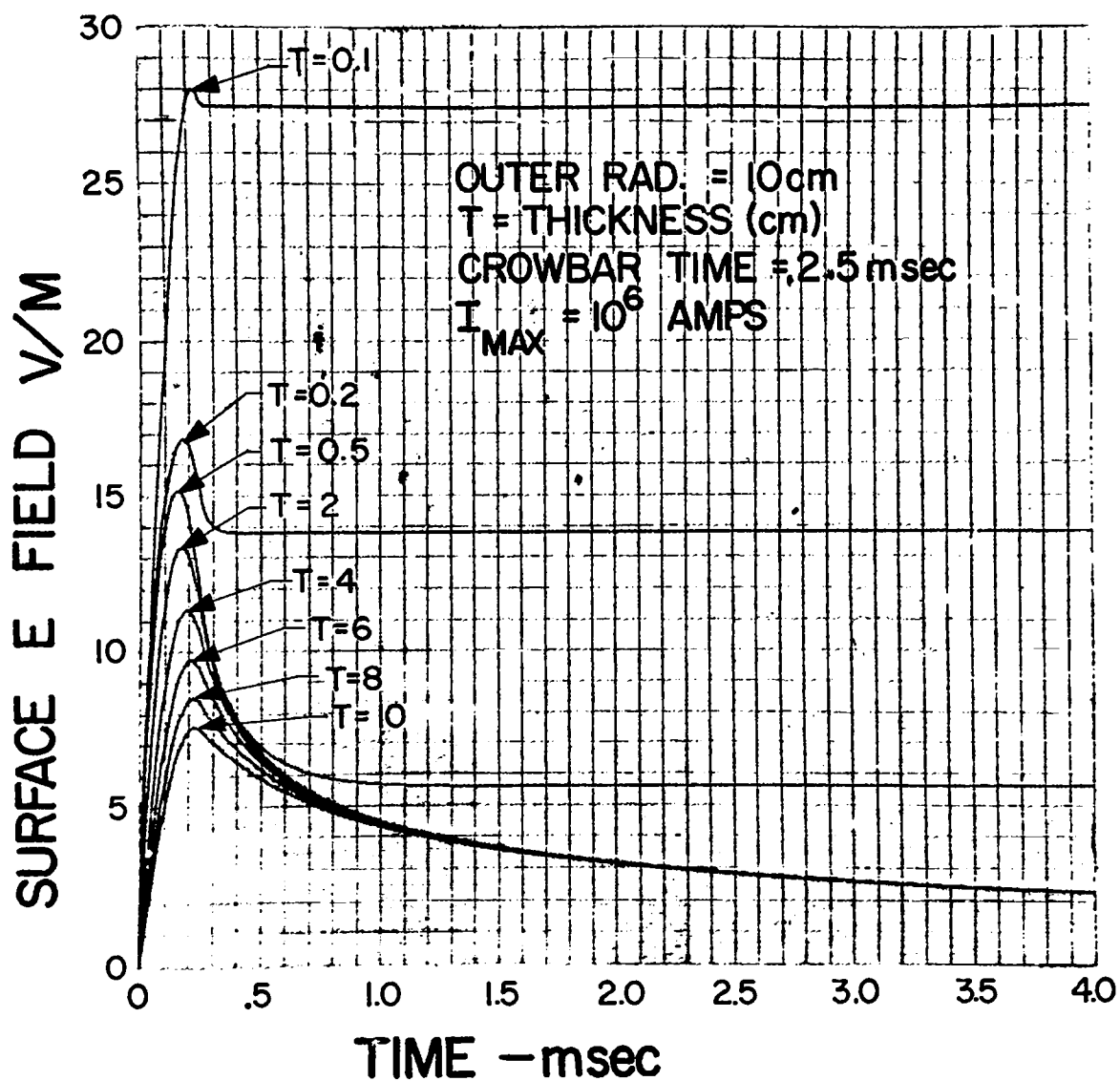## SURFACE ELECTRIC FIELD FOR AN IDEALLY CROWBARRED HOLLOW COPPER CYLINDER

Fig. 12.   Surface electric field for crowbarred hollow copper cylinder

44

have not yet reached their steady state values by 4 msec. Figure 13
shows the effect of increasing the period of the sinusoidal rising
current to 10 msec. The drift velocity in the solid conductor is
reduced to 0.116 cm/msec.

It would be desirable to minimize the surface electric field on
conductors during the time active plasma is present in the magnetic
field in order to minimize the associated $\vec{E} \times \vec{B}$ drift to the conductors.
The computer program was used to determine if programming the rod
current would accomplish this. Figures 14 and 15 show the surface
B and E fields respectively for the case of an exponentially damped
current starting at the maximum of a sinusoidal rise. The data apply
to a cylindrical Cu rod of 20-cm radius with current rising to 1 MA
in 10 msec and then falling exponentially as $I_{max} \, e^{-\alpha t}$. The results
are shown for ten values of α ranging from 0 to 200. In general, as
the damping is increased the surface electric field drops and even
reverses. A case was run to find the programmed magnetic field
required to cause the surface E-field to drop suddenly to zero (and
to remain there) at the time of peak magnetic field. The surface
E-field was reduced to zero at the sacrifice of about 25% of the
maximum B field after the first 500 μsec with an e-folding time of
about 20 msec thereafter.

Conclusions

The computer program will permit the following three types of
studies to be made with regard to the E and B fields associated with
an infinite cylindrical hollow conductor.

1. B field penetration as a function of time, for a parameter
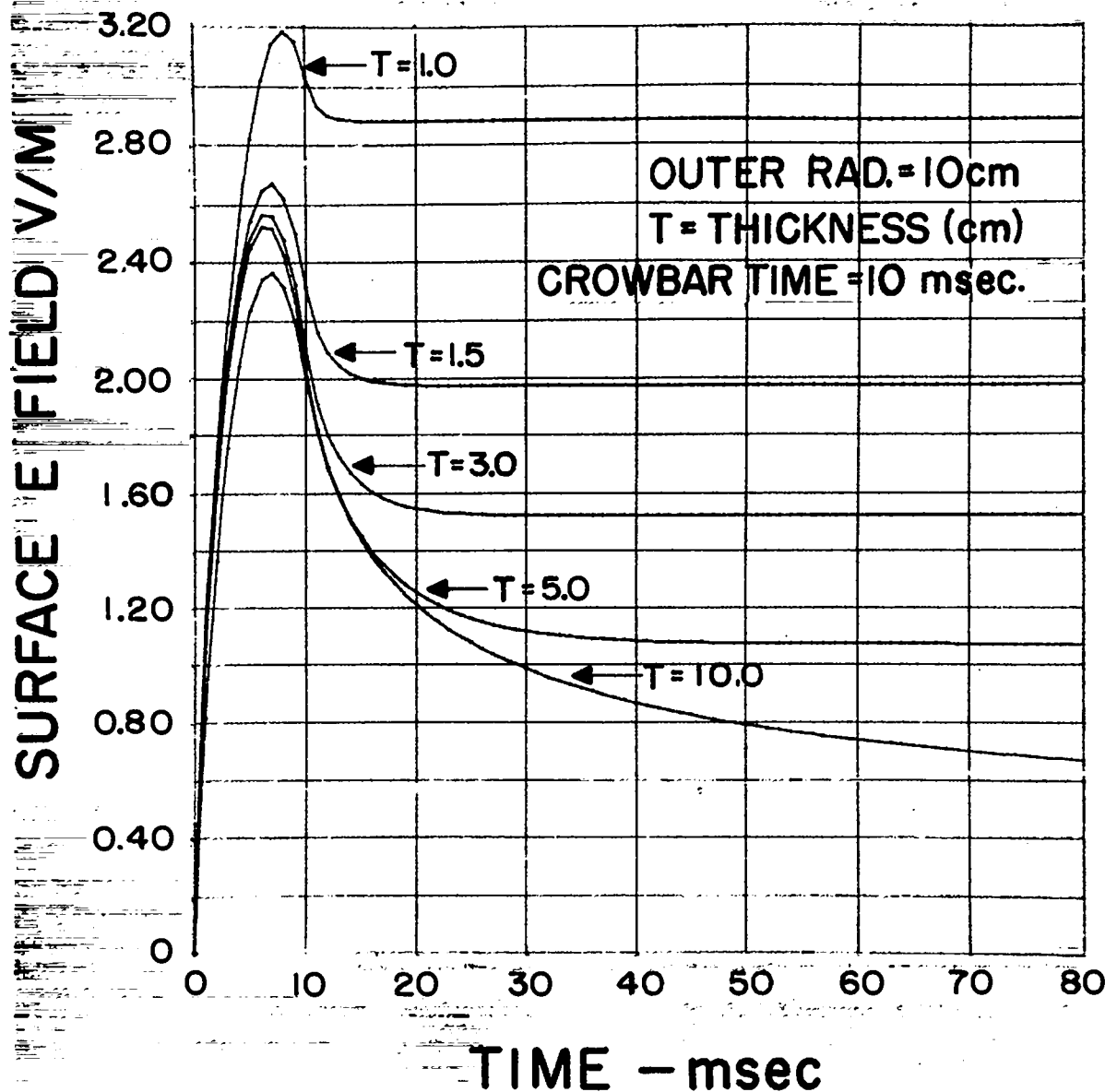set. The code will also allow variation of the conductivity as a
function of the radius.

Fig. 13. Effect of increasing period of sinusoidal current to 10 msec
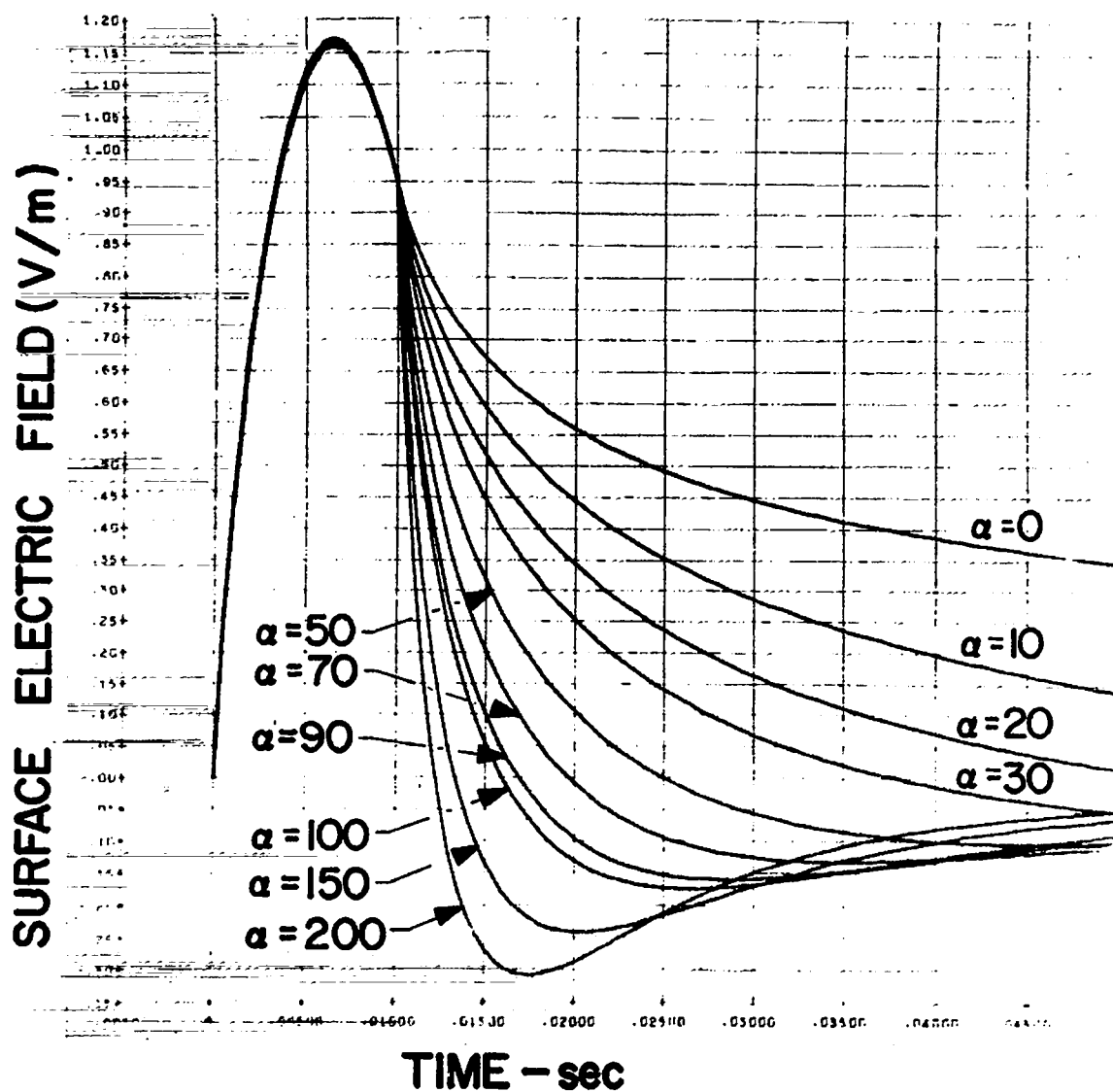
Fig. 14. Surface electric field for different rates of current decrease

47

Fig. 15. Surface magnetic field for different rates of current decrease

48

2. Surface E field as a function of time for a parameter set. A set of dimensionless "universal curves" has been made for use in design work.

3. E field minimization by programming current and magnetic fields. In a caulked cusp design, this method of reducing the E field at the surface of the levitated conductors, and therefore of reducing the plasma drift toward the conductors, results in an increased E field and plasma drift at other positions in the machine.

HYDROMAGNETIC PLASMA GUN PROGRAM

(I. Henins and J. Marshall)

Introduction

Since surprisingly large amounts of highly stripped C and O
ions were observed to accompany the fast plasma from a coaxial plasma
gun (LA(MS)-3085),efforts have been made to reduce these impurities.
The vacuum system has been replaced with a cleaner one, and a new gun, the
design of which was reported, has been put into operation.

New Vacuum System

The new vacuum system uses dry Viton O-rings in place of the
greased neoprene of the previous system. The glass tube is still
glued together with epoxy cement, but the joints are protected from
plasma bombardment by intervening glass sleeves on the inside. Initially,
it was pumped by the same diffusion pump as before, with the same
anticreep Freon-cooled baffle (-50°C). Mass spectroscopic analysis
of the residual gas showed strong hydrocarbon impurities; no comparison
could be made with the previous system since the mass spectrometer was
not used. The pump was a PMC 720 in which back streaming is reduced
by superheating the vapor with immersion heaters extending above the
surface of the oil in the boiler. The oil itself (Convoil 20) should
have been effectively trapped at the baffle temperature, but pyrolytic
decomposition of the vapor, due to the heater design, may produce
untrappable lighter hydrocarbon fragments.

The diffusion pump has now been replaced by a combination ion
pump and Ti sublimator. The pump combination is a Varian 600-1/sec ion
pump with a sublimation well, as sold for ultra high vacuum bell jar
pumping. The well has been modified to have a larger number of
sublimation filaments to avoid the need for frequent opening of the

system to replace filaments. The pumping speed of the system is somewhat reduced by a short section of 4-in. tubing between the well and the end box. The hydrocarbon contamination level is now smaller by about a factor of 20, and the base pressure is approximately 1.5×10^{-7} torr. There has been some trouble with leaks and it has been necessary to polish all gasket surfaces highly to eliminate them.

New Gun

The new gun design reproduced the former gun exactly, except for two changes, which it was hoped would contribute to cleanliness without altering the operating characteristics. One change was the replacement of the hammer-operated fast valve with one operated by thermal expansion and provided with a labyrinth between the valve opening and the inside of the gun barrel. The purpose of the labyrinth is to prevent damage to the Viton valve seal by the gun discharge. The other change was the addition of a Cu baffle fitting into an annular slot in the outer gun electrode at the butt end. This was added in the hope that it might prevent decomposition of the glass insulator, one of the obvious sources of impurities.

One or both of these changes may be responsible for a change in gun behavior which has interfered with the impurity ion analysis method used on the previous gun. Formerly, it had always appeared that, for purposes of external plasma behavior, all of the fast component could be considered to leave the gun muzzle at one instant in time. This property allowed time of flight analysis of fast ions which, coupled with electrostatic particle energy analysis, made it possible to identify the e/m ratios of the various impurities. With the modified gun the slower parts of the fast plasma appear to leave the muzzle later, and the time of flight method is no longer reliable. For this reason a magnetic analyzer has been added to the electrostatic energy analyzer. The system is just coming into operation and no data are yet available.

Results of Gun Operation

At one point in the initial operation of the modified gun, difficulty was had with a sticking Viton O-ring in the fast valve. In diagnosing this difficulty an axial magnetic field was added inside the gun barrel by very early excitation of coils surrounding it so that there was time for field to soak through theCu barrel. The gun B_0 field had a marked effect on the fast plasma as is shown in Figs. 16 and 17 where the gun plasma is injected into an 8.2-kG guide field. The results indicate unintegrated diamagnetic pickup loop signals at various positions along the tube. With the B_0 field (approximately 1000 G in the same direction as the guide field), the plasma front is faster and late structure is lacking in the diamagnetic signal. It is unfortunate, in a sense, that the B_0 produces a favorable effect, because now one more parameter has been added to an already too complicated system.

What appears in Figs. 16 and 17 to be an excessive attenuation of the front of the diamagnetic signal is a spurious effect due to inductive communication of diamagnetic signals from one coil in the guide system to the next. It is removed with compensated diamagnetic pickup loops in place of the simple ones used in this case. However, there is an interesting effect to be seen in Fig. 16 which is believed to be real. Late peaks in the unintegrated loop signals grow as they are propagated along the tube when, in a free particle model, they should decrease with the inverse square of the distance. The effect is not understood although it may be evidence of an instability.

A positive electrostatic signal is observed to propagate along the system at a much higher speed than first diamagnetism. This signal appears to be associated with the pinch-like discharge which
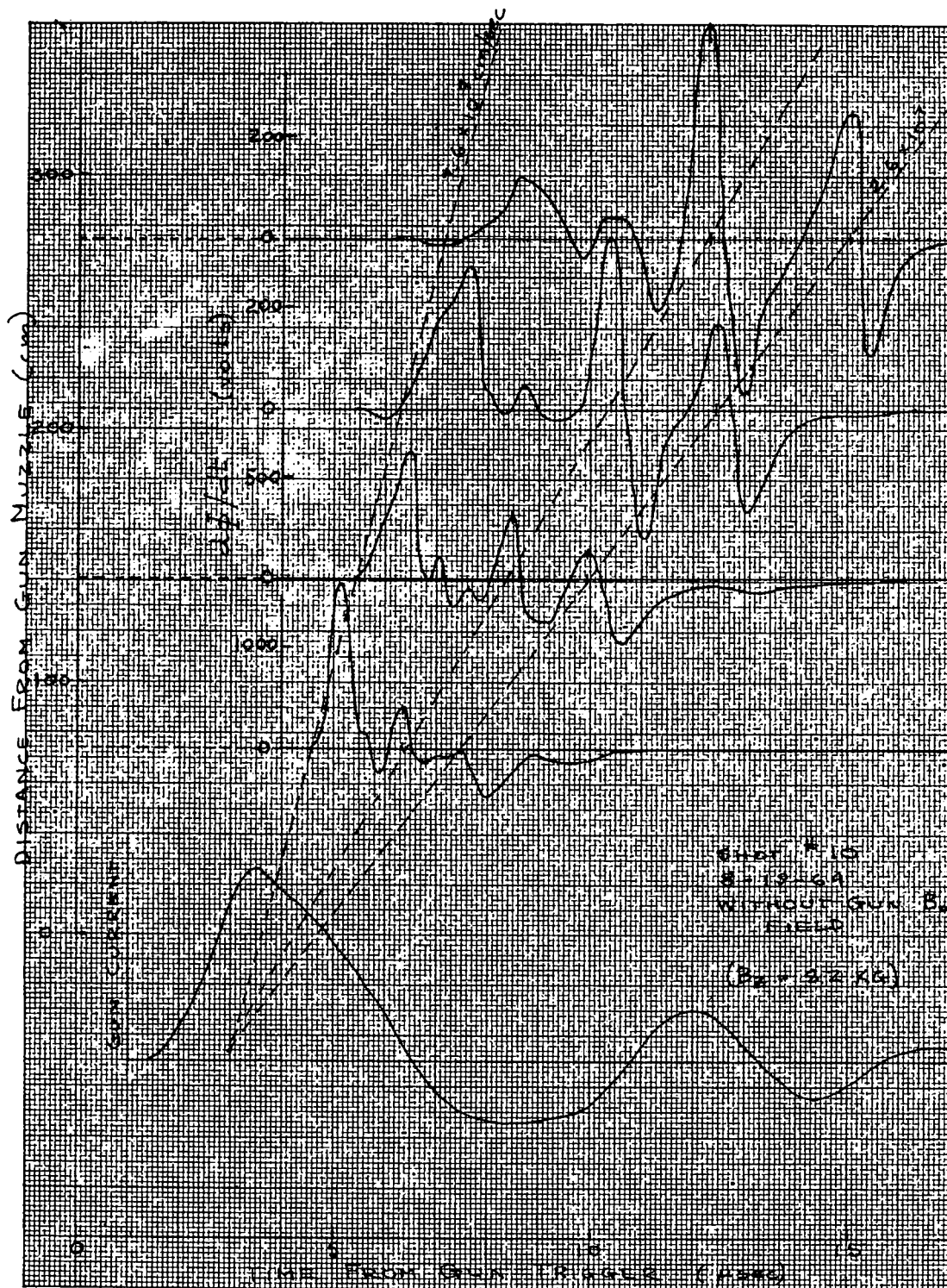
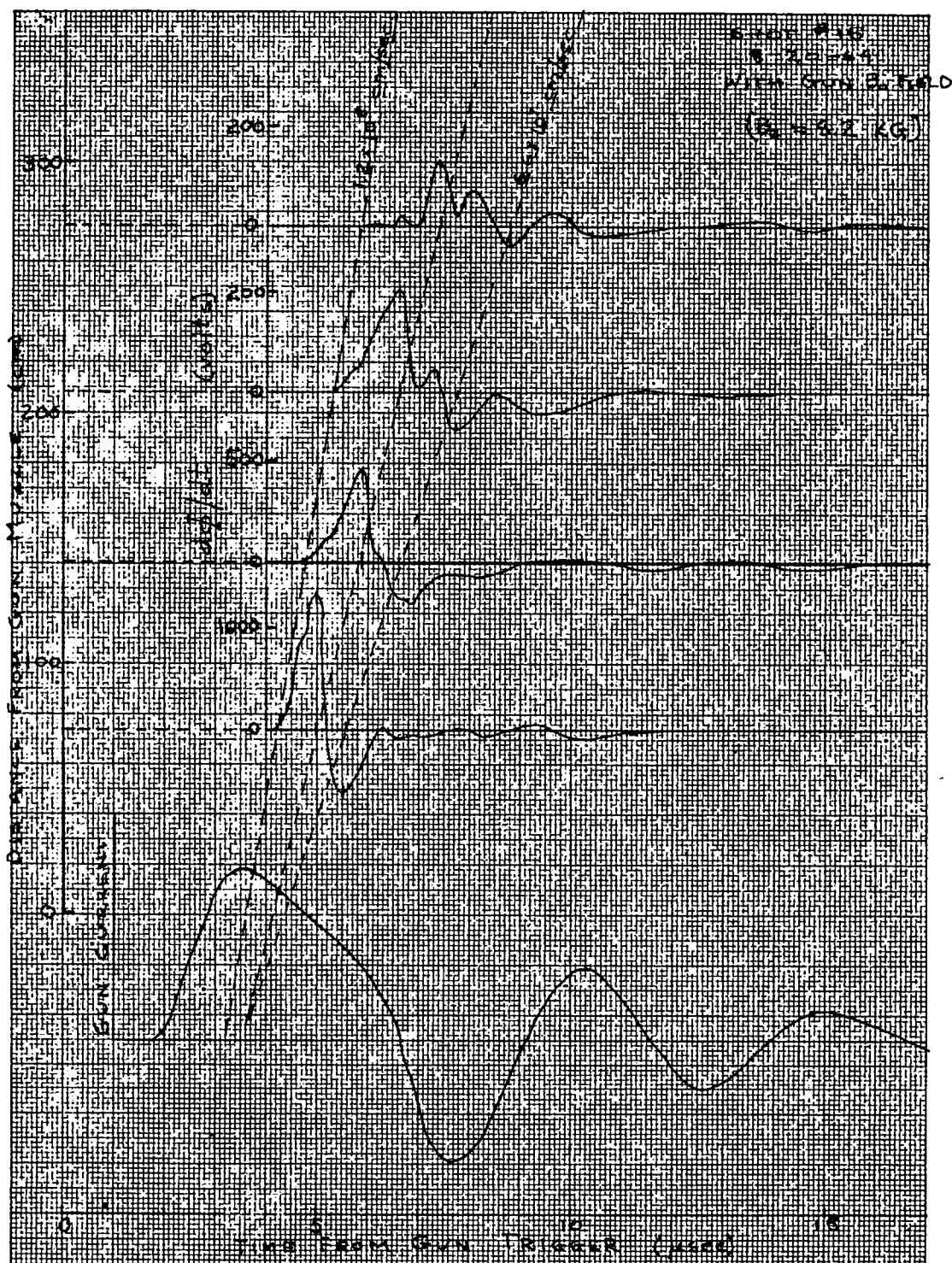Fig. 16. Characteristics of fast plasma without gun B_O field

Fig. 17. Characteristics of fast plasma with gun B_O field

blows out of the gun muzzle into vacuum when the current front reaches the muzzle. The results of the measurements are shown in Fig. 18. The potentials observed are those at the surface of the glass envelope, and are not necessarily contradictory to the negative potentials previously reported from internal probes. The difference may be due to the large gyro radius of the ions in the plasma as compared to the electrons, thus making possible a positive sheath on the surface of the plasma.

The presence of highly stripped C and O impurities in the fast plasma (C^{5+} and O^{6+} have been observed) appears to be further evidence that most of the fast plasma component is derived from the wall. The proportions of C and O in the plasma are very much larger than what they must be in the D_2 feed. The evidence as to impurities in the new gun is still incomplete so that it is not known whether C is present or not. Preliminary indications are that there are still fast impurities present.
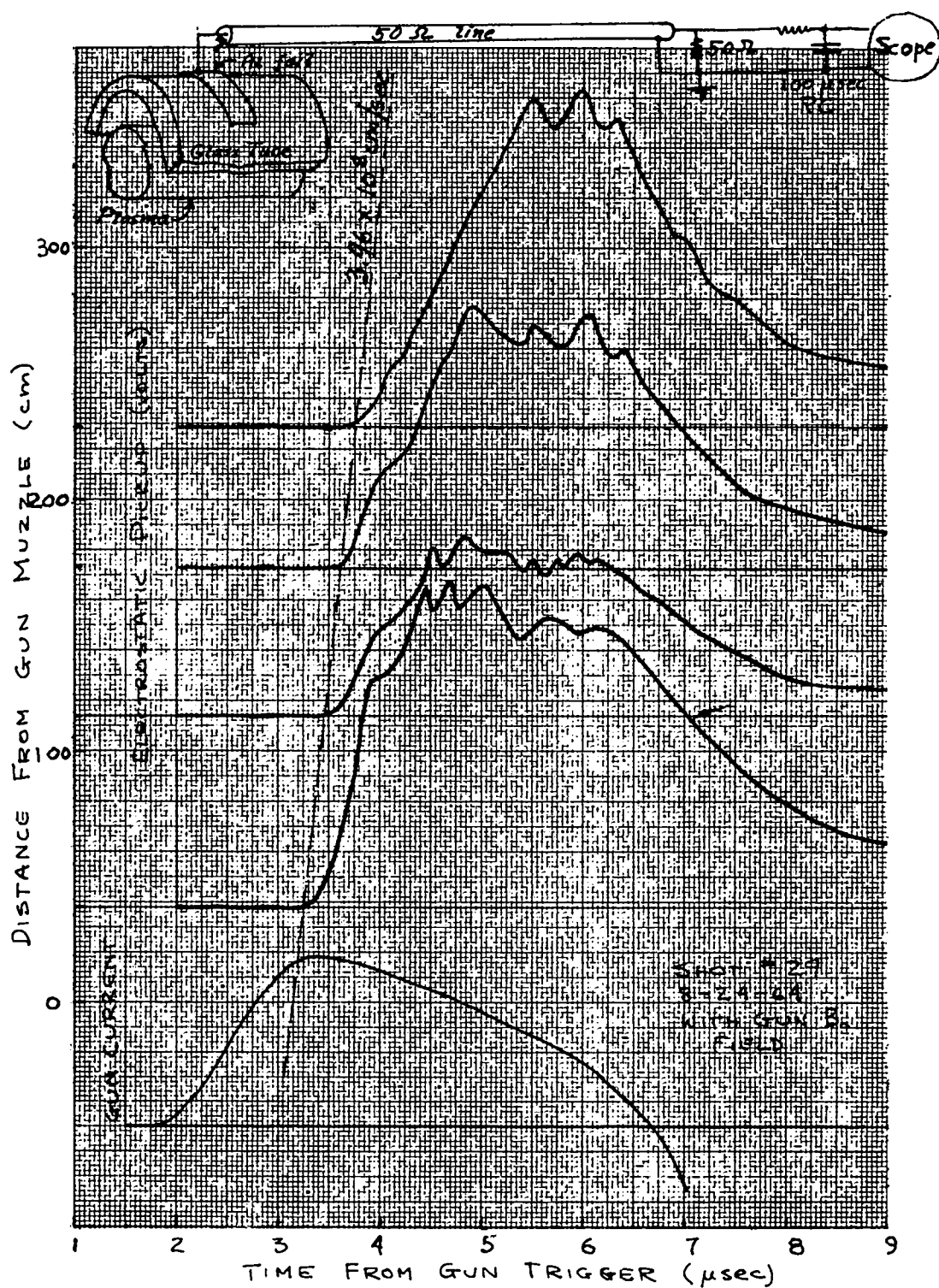
Fig. 18. Electrostatic pickup with gun B₀ field

ELECTRON DENSITY MEASUREMENT IN TRANSVERSE INJECTION EXPERIMENT

(D. A. Baker, J. E. Hammel, and F. C. Jahoda)

Introduction

A substantial advance in knowledge of the plasma in the transverse injection experiment was made through the use of the interferometry technique with the He-Ne laser. First, the electron densities measured with the laser have essentially confirmed the values derived with low precision from shorting current probes. Moreover, the measurement promises to be valuable with the additional information it provides on the penetration of the transverse B-field by the plasma stream.

Extension of the Interferometry Technique

In the external laser interferometry technique,[1] the beam from a He-Ne laser was reflected back by a fixed mirror after making two traversals of the plasma. The two wavelengths (3.3μ and 6328Å) emitted by the He-Ne from the same upper level were utilized in the measurement. At a fixed pumping rate, the steady state laser output in the two lines is complementary, so that slow variations in one can be monitored by variations in the other. The visible line was used for optical alignment and detection, whereas the infrared line provided the greater sensitivity for the electron-induced phase shift. By detecting in the visible, counting of fringes was limited in the original technique to rates less than 1 Mc/sec. This restricted frequency response is caused by the high Q of the laser circuit necessary to sustain laser action at 6328Å. Another limitation is associated with the non-linearity of the feed-back process which restricts quantitative measurement of the phase shift to units of one complete cycle.

Two changes initiated at LASL have improved both of these limitations by more than an order of magnitude. By detecting the I.R. directly with indium arsenide (KH-33, Block Eng. Inc.), the lower Q of $3.39-\mu$ laser circuit allows the laser to follow phase changes up to 7 Mc/sec. The indium arsenide detector used seems to be good at frequencies up to 20 Mc/sec.

In order to measure quantitatively electron induced phase shifts in units less than one complete phase change, a controlled modulation was super-imposed on the output level of the laser by an effective linear motion of the external mirror. This motion is obtained by a mirror 40-cm off axis on a rotating arm. The modulation is produced during the small portion of the cycle when the arm is nearly normal to the laser radiation. On the order of 200 equally spaced fringes can be observed when the mirror is 12 ft from the laser. To obtain longer periods of observation, a pendulum of 250-cm length has now been installed to produce the mirror motion. In practice it is found that a displacement of 0.1 fringe is readily observed. This corresponds to an integrated electron density change of 3.3 x $10^{15}/cm^2$ for a double pass through the plasma by the 3.39 μ radiation.

Figure 19 shows schematically how both the rotating mirror and infrared detector were applied to the density measurement. Figure 20 is the modulated output of the indium arsenide detector before and during the plasma stream passage.

Results of Density Measurement

Figures 21 and 22 give the electron density of the plasma at a point 8-cm upstream from the magnetic mirror axis. A striking feature of the results is the marked effect of the transverse magnetic field on the time history of the electron density. For example, with regard to the arrival time of the front of the stream, the higher the field the earlier the leading edge arrives. This change in arrival time could be caused by an increase in the velocity of a portion of the stream, which might be associated with electric fields in the direction of the stream velocity.

Another important feature of the results is the large decrease in the density of the late material (Fig. 22) at 5.5 kG when a shorting region is placed in the stream path. Measurements made past the mirror axis show the density of the late material is reduced to a value below the resolution of the laser measurement whereas the fast component suffers a very small decrease in density.

Reference

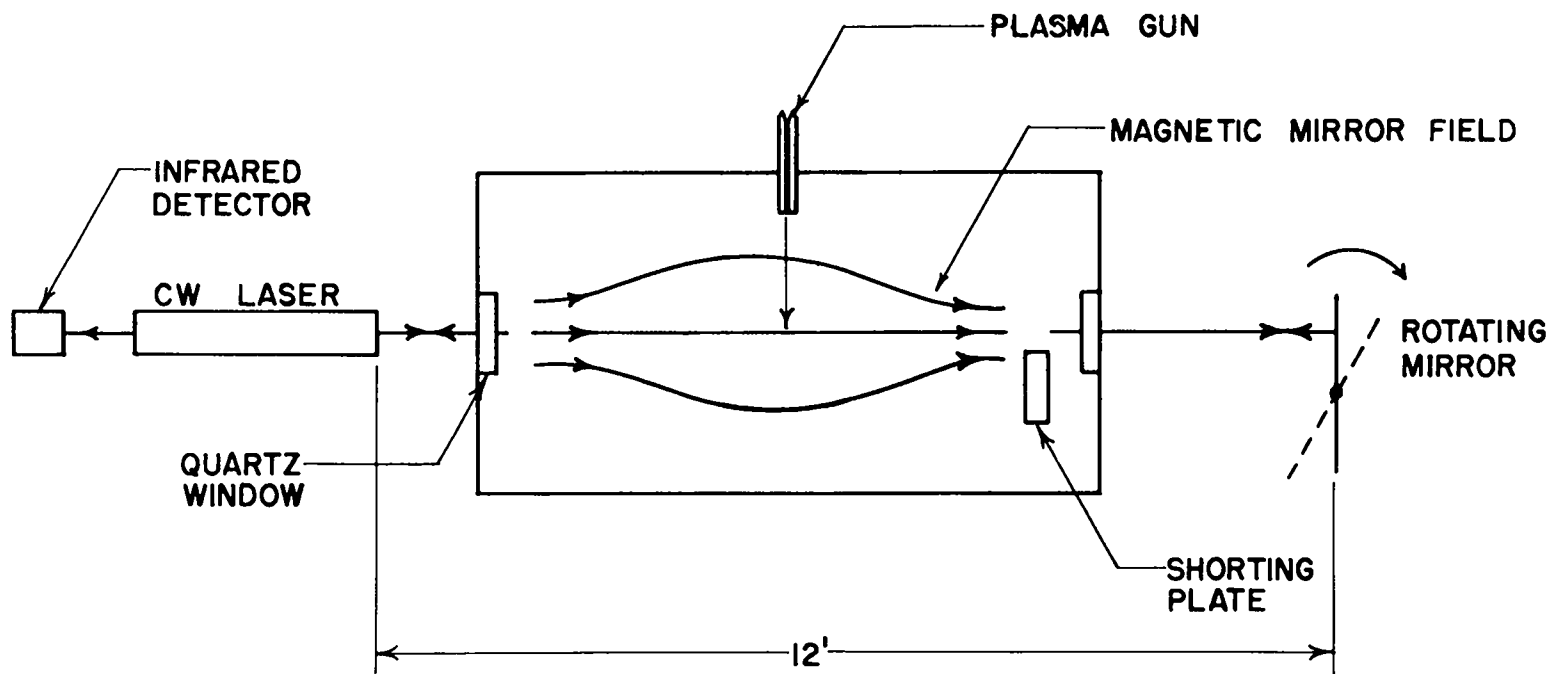[1]Ashby and Jephcott, Appl. Phys. Letters, 3, 13 (1963)

Fig. 19. Application of rotating mirror and infrared detector to electron density measurement

SHORTING
CURRENT
6 KA/DIV.

LASER
INFRARED
OUTPUT

2 μS/DIV.

3.39 μ LINE PHASE SHIFT BY FAST GUN PLASMA

TRANSVERSE B-FIELD = 5.5 KILOGAUSS

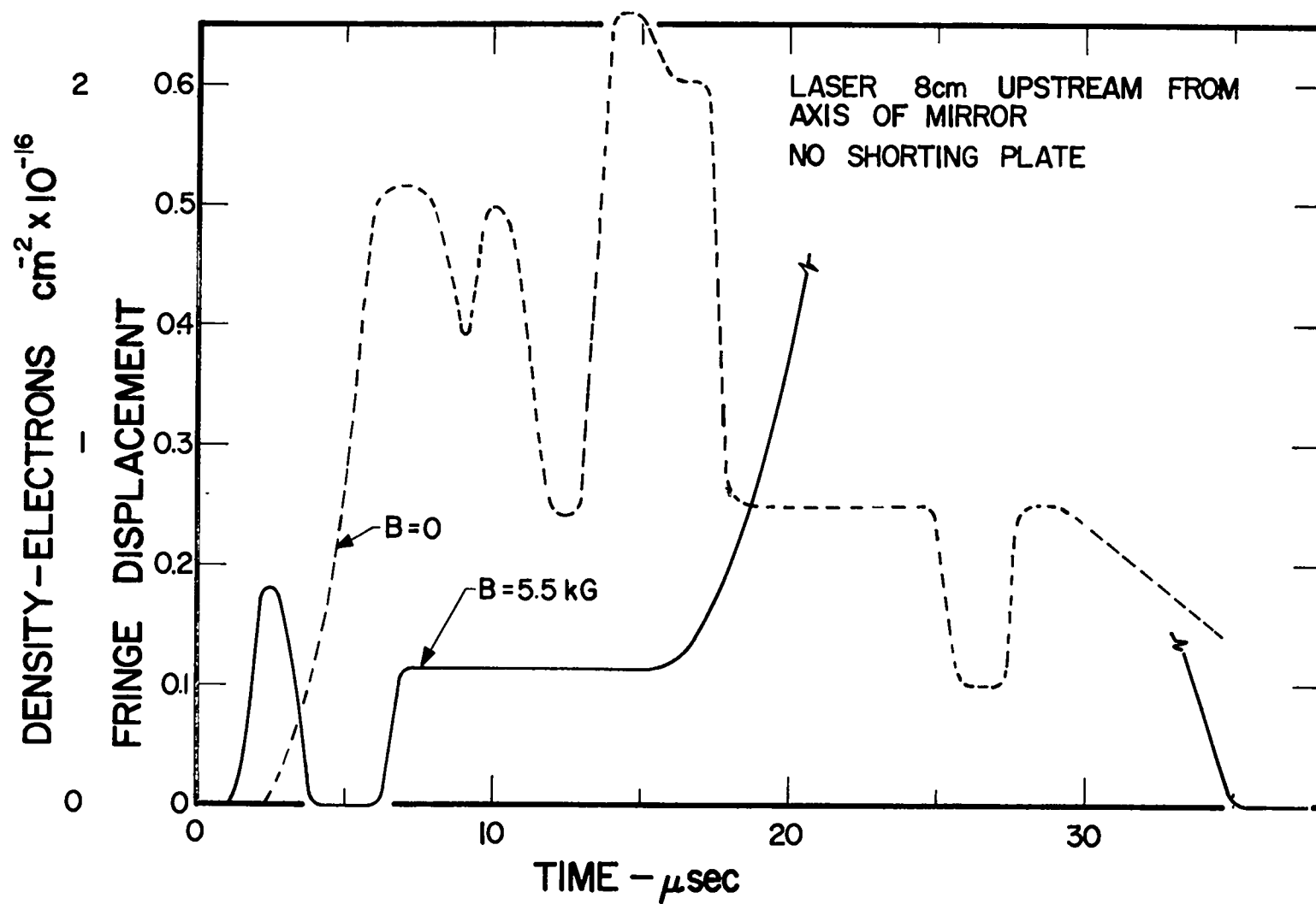Fig. 20. Modulated output of detector before and during plasma passage

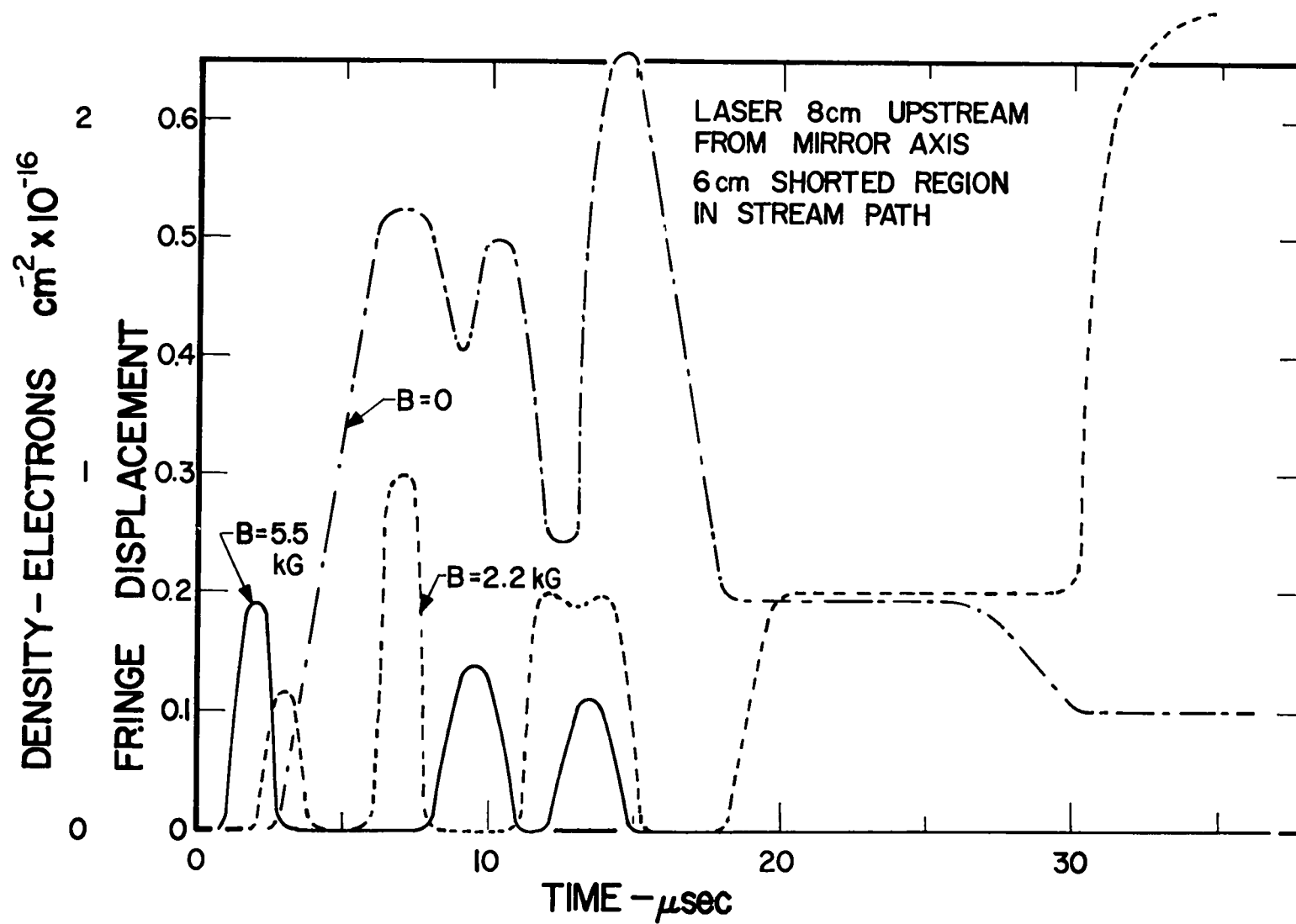Fig. 21. Electron density of plasma with no shorting plate

Fig. 22.   Electron density of plasma in shorted region

HIGH-DENSITY PLASMA FOCUS

(J. W. Mather)

Introduction

A schematic of the hydromagnetic coaxial gun used in the high-density plasma focus studies is shown in Fig. 23. The current sheaths shown shaded are based on the results of magnetic probe measurements. Condenser energy is supplied from a 90-μF, 20-kV bank with currents of $\sim$ 800 kA rising in $\sim$ 2.3 μsec. The operation of the coaxial gun at high pressures (1-6 torr) leading to the formation of a dense plasma can be thought of as (1) the direct acceleration of a current sheath in the gun proper and (2) the rapid radial collapse of the current sheath as it leaves the end of the center electrode (muzzle end).

For a fixed geometry, a simple expression (in MKS units) is derived, based on the "snowplow" M theory, which expresses the average rate of motion, $\bar{v}$, of the current sheath in the gun proper in terms of the applied voltage, V, mass density, ρ_o, and outer and inner radii, R and r, of the electrode as

$$\bar{v} = \frac{1}{2\pi} \sqrt[4]{\frac{u_o}{2}} \sqrt[4]{\frac{V_o^2}{\rho_o r^2} \cdot \frac{1}{\left[\frac{u_o}{2\pi} \ln \frac{R}{r} + b\right]^2}} \quad ,$$

where b is the parasitic inductance per unit length. This relation describes reasonably well the dynamics of the current sheath leading to the current singularity. Changes in the geometrical factor R/r do change $\bar{v}$ qualitatively, but the range of R/r is limited to small values.

The rapid collapse of the current sheath signified by the occurrence of a current singularity is accompanied by a large voltage spike which is associated with a change of inductance ($\Delta L/\Delta t$). This effect is probably

CURRENT
SHEATH

TIME RESOLVED
X-RAY CAMERA

PYREX GLASS
INSULATOR

$\sim 1m$

B_θ

$\sim 22cm$

5cm

PLASMA
FOCUS

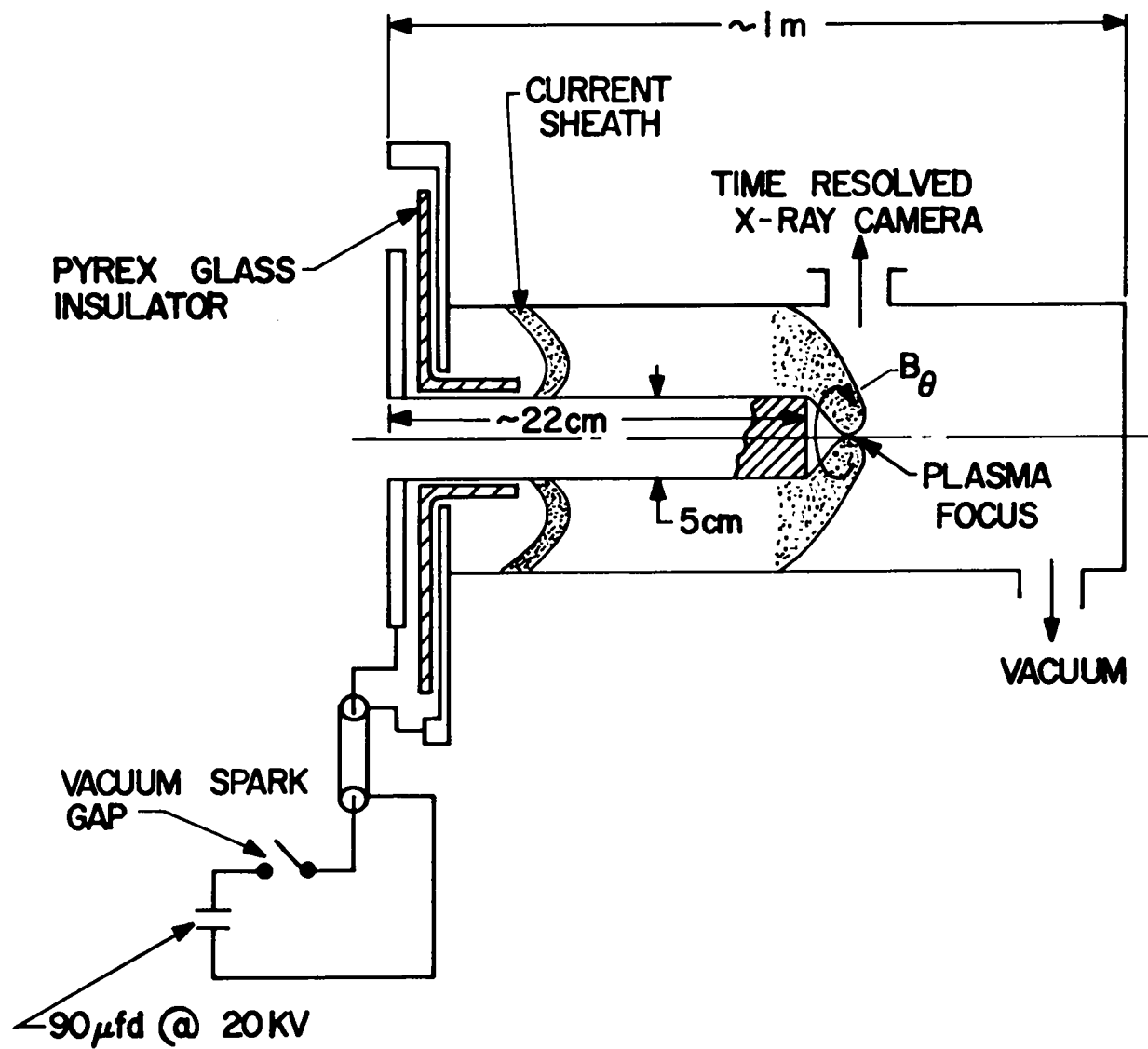VACUUM

VACUUM SPARK
GAP

90 μfd @ 20KV

Fig. 23. Schematic diagram of hydromagnetic coaxial gun

produced as a result of a fast dynamic pinch effect. The position of the plasma focus relative to the face of the center electrode (CE) depends to first order on the axial momentum of the current layer prior to collapse. For a given CE length, the applied voltage or gas pressure is adjusted to cause the current layer to reach the end of the CE at peak current time, i.e., when the magnetic energy is maximum behind the sheath.

Voltage Measurements

Measurements at the breech end of the gun generally show a voltage spike at gas breakdown and then a smooth time dependence indicating an inductive change as the current sheath proceeds along the center electrode. However, at peak current time (upper trace in Fig. 24) the voltage signal (lower trace) exhibits a large increase which is time-correlated with the singularity in the total current trace. Several voltage spikes are evident which perhaps correspond to multiple pinches. Sweep time of Fig. 24 is 0.5 μsec/cm.

Spatial and Time-resolved Soft X-Rays

Figure 25 shows some typical soft x-ray images of the dense plasma taken through a 1/4-mm pinhole with absorber thicknesses of 1.46 and 3.26 mg/cm^2 Al. The CE face is to the left and is indicated by dark circular spots. A viewing port is cut through the perforated outer electrode to give an unobstructed view of the central region.

It is generally observed that multiple plasma foci form for neutron yields > 10^{10}/burst at a position of ~ 1 to 1.5 cm beyond the face of the CE. The operating D$_2$ gas pressure for these particular discharges is ~ 3 torr. The volume of the foci ranges from 0.08 to ~ 0.4 mm^3. It appears for a given set of operating conditions that the total volume of the intense x-ray region increases with neutron yield.

In Fig. 26 is shown a typical set of time-resolved soft x-ray signals obtained at a sweep speed of 0.5 μsec/m. The absorber thicknesses

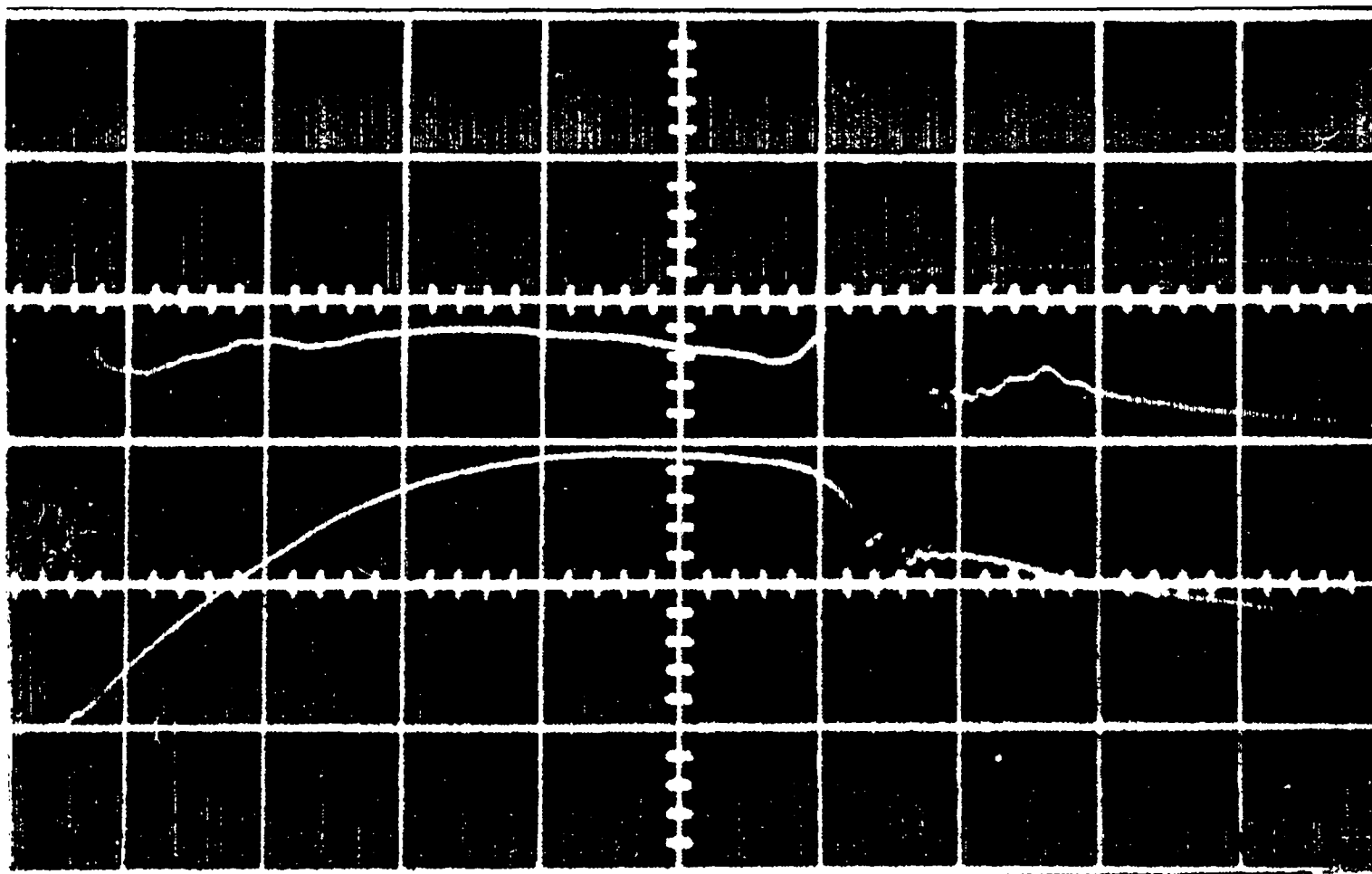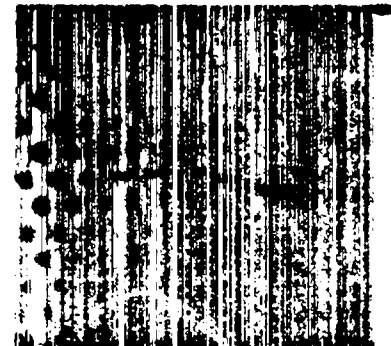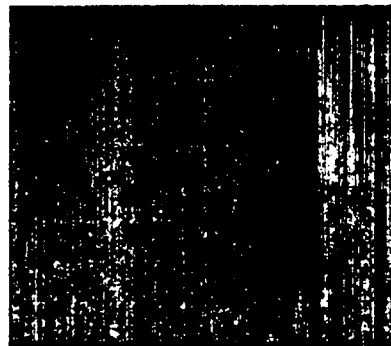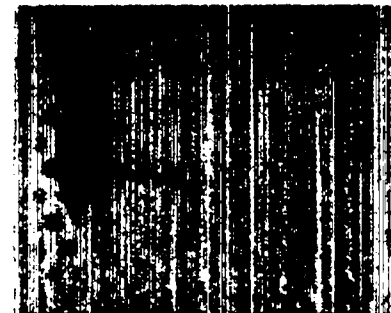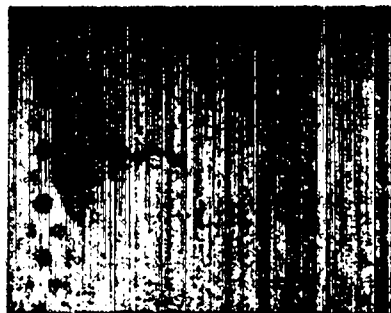Fig. 24. Current (upper trace) and voltage (lower trace) at breech end of gun

Soft x ray (Al. abs.) - Pos. Volt.

1.46 mg/cm^2

3.26 mg/cm^2

Pinhole - $\frac{1}{4}$ mm D.
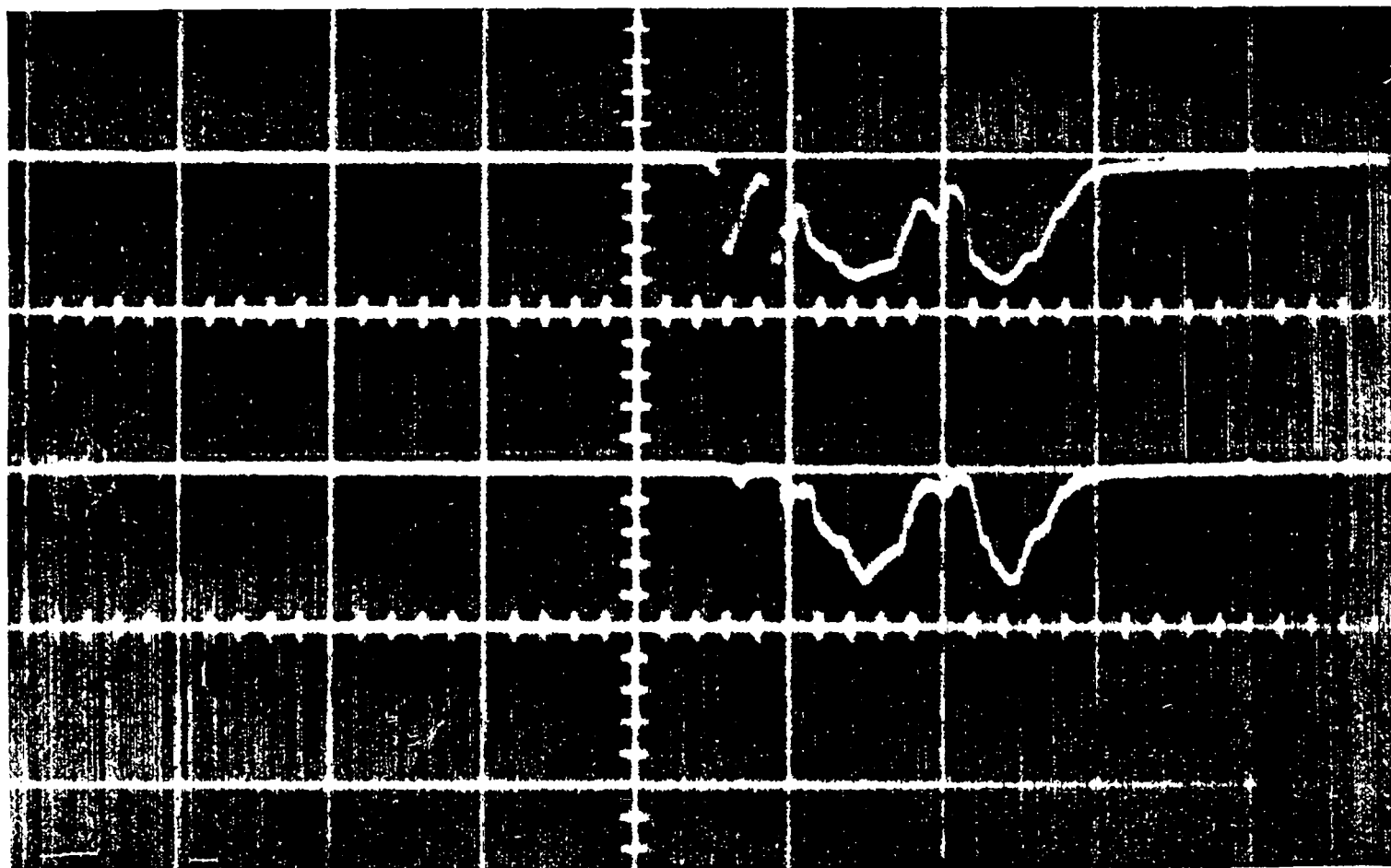
Fig. 25. Soft x-ray images of dense plasma

69

Fig. 26. Time-resolved soft x-ray signals

for the upper and lower traces are 3.14 and 6.25 mg/cm², respectively.
If it is assumed that the dense plasma is emitting a pure D bremsstrahlung,
then the ratio of these signals determines the electron temperature, T_e,
as a function of time. For these particular signals, T_e varies from
~ 600 eV to 3 keV. In other experiments, T_e reaches ~ 5 keV.

An interesting fact is that the neutron pulse leads the time
dependent x-ray pulse by ~ 0.1-0.2 μsec, as is particularly evident for
large neutron yields. This may be partially explained in the following
manner. If the pinch effect is the primary mechanism for producing the
dense plasma, then the ions are preferentially heated and the electrons
are cold. In time, depending upon the particle density and temperature,
the electrons relax toward the ion temperature. For example, at particle
densities of ~ $10^{19}/cm^3$ and T_e ~ 1 keV, the ion-electron relaxation time
τ_{ie} is ~ 0.1 μsec. For higher temperatures and lower densities, τ_{ie} is
larger. Figure 27 shows a typical x-ray signal and a fast neutron pulse
(lower trace).

Center of Mass Motion of the Dense Plasma

By the very nature of the dense plasma formation, it is to be
expected that motion of the dense plasma would occur away from the CE
simply on the basis of a large axial momentum of the current sheath prior
to collapse. Furthermore, if the collapsed current undergoes the m = 0
instability, it is expected that large electric fields might be generated
due to this type of instability; hence the neutron yield distribution
should be sensitive to the polarity of the applied voltage. Measurements
of the neutron yield in the forward and backward direction show no
appreciable asymmetry for a positive or negative CE voltage. In fact the
yield ratio $R(0°/180°)$ is ~ 1 with counting accuracy of ~ ± 5%. If an
asymmetry of ~ 10% in the ratio is assumed in the worst case, the center
of mass motion of the dense plasma would correspond to v_{cm} ~ 5 x 10^7 cm/sec.
This kind of plasma motion would, it seems, be very evident in the smearing
of the soft x-ray images in a time of ~ 0.5 μsec. Such smearing has, however,
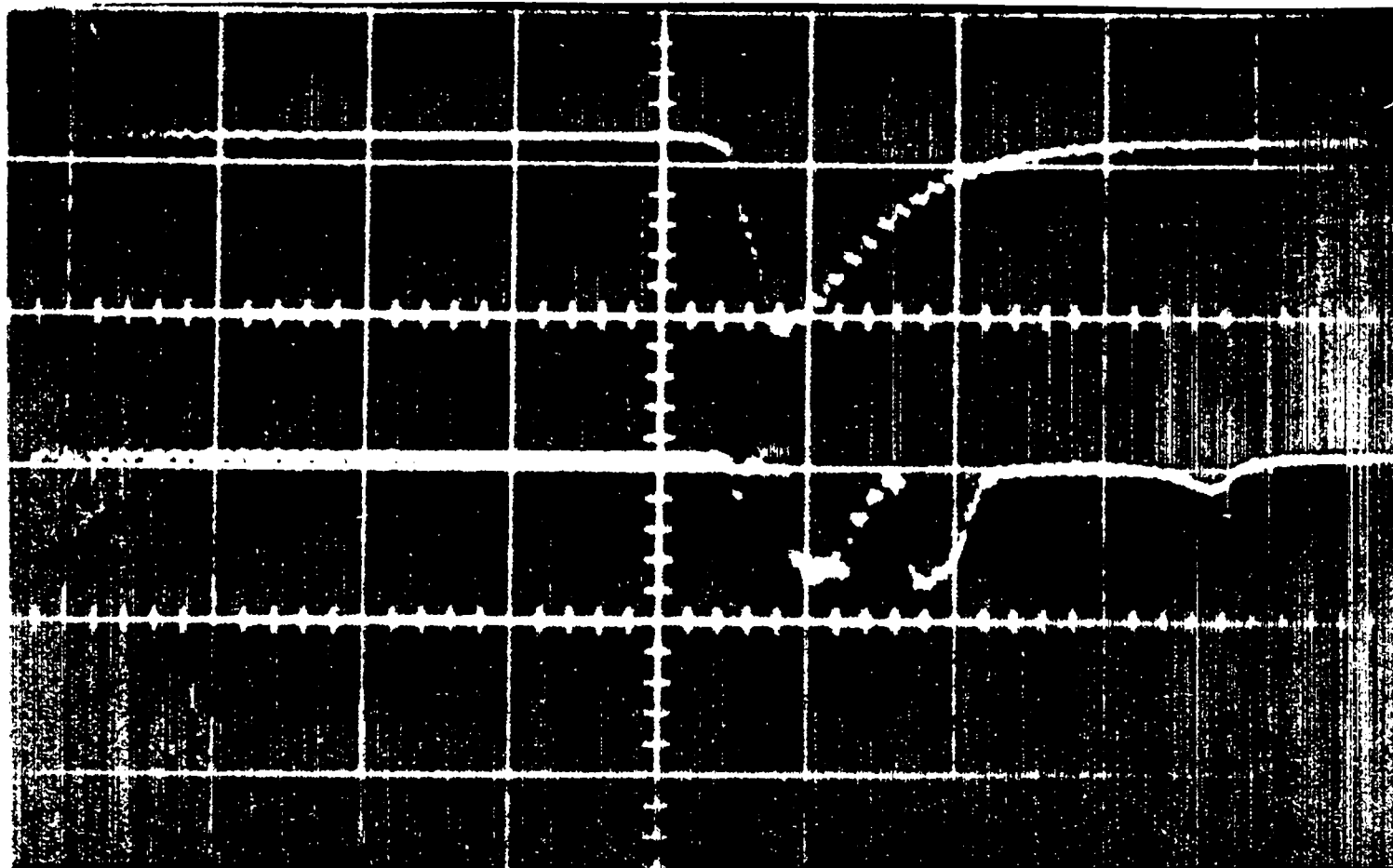not been observed.

Fig. 27. X-ray signal (upper trace) and fast neutron pulse (lower trace)

Erosion of Frontal Face of Center Electrode

The dense plasma focus is readily produced for either positive or negative applied voltage. However, when a positive voltage is applied to the Cu CE, a cavity gradually forms in its front face. This erosion, after many discharges, takes the form seen in Fig. 28. On the other hand, negative voltages cause only a slight depression. Metallographic examination of the walls of the cavity, starting at the face of the Cu electrode, shows gradually increased hardness as the bottom of the cavity is approached; at the bottom the hardness is approximately twice the ordinary annealed value, and reaches to a depth of ~ 0.5 mm. These observations suggest that the hardness is due either to recoil of the dense plasma or to magnetic pressure effects; and the erosion of the metal surface is a result of intense electron current heating. A W insert in the face of the electrode shows less cavitation, whereas brass behaves similarly to Cu.

Summary

In summary, it appears that (1) multiple plasma foci are formed nonsimultaneously in time and space beyond the center electrode, (2) the multiplicity is a result of the $m = 0$ "sausage type" instability of the collapsed current filament, (3) the electron temperature lags the ion temperature, assuming neutron production is a result of a thermal plasma, and (4) no appreciable center of mass motion of the dense plasma is observed for either positive or negative voltage. From the time and spatial dependence of soft x-rays, neutron yields of $\sim 10^{10}$/burst (assuming $T_e = T_i$), and a time duration of ~ 0.3-0.5 µsec (half maximum width), an estimate of the particle density n, would be 2-3×10^{19}/cm^3. These numbers lead to an nτ value of $\sim 6 \times 10^{12}$.
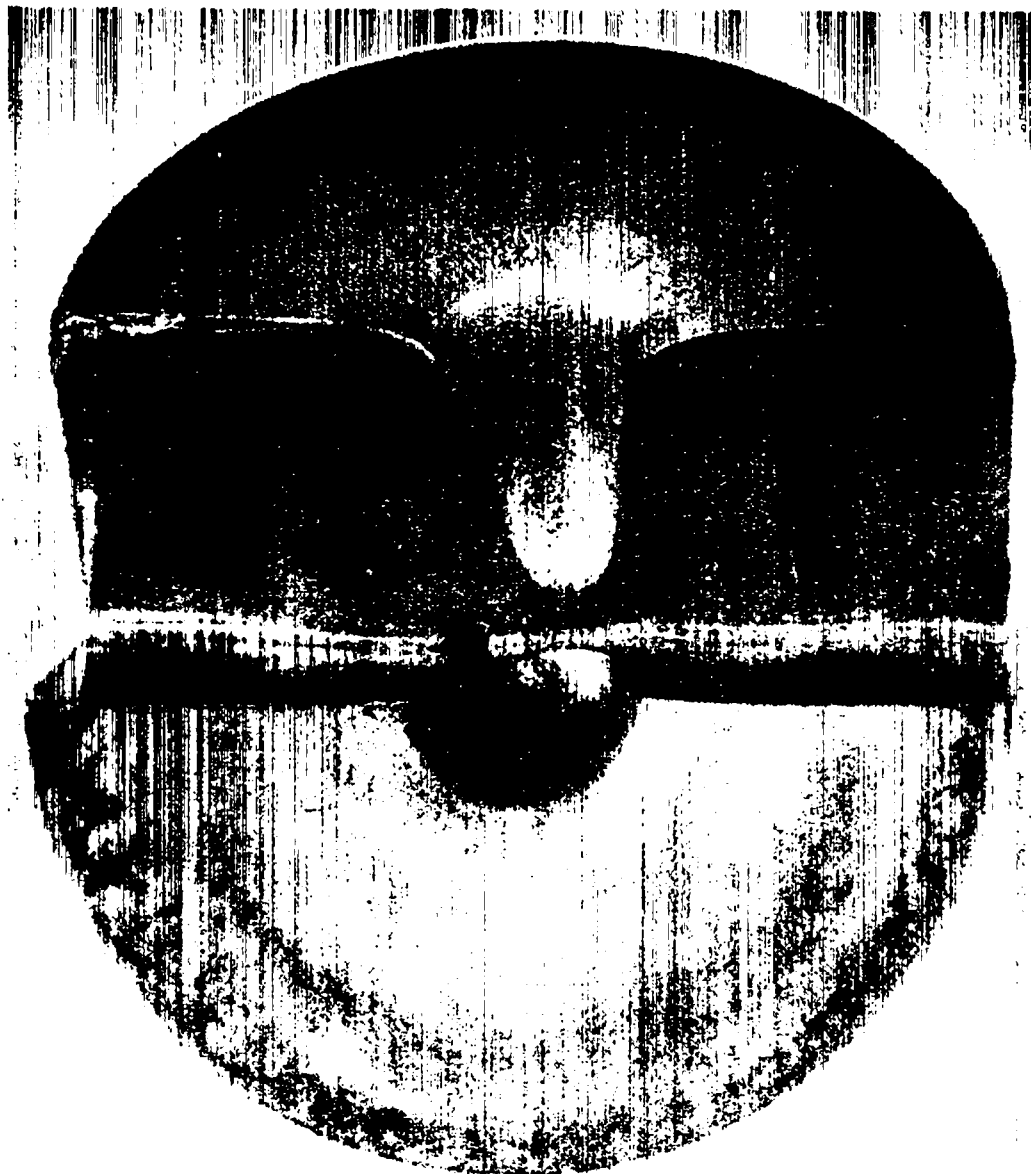
73

Fig. 28. Erosion of the front face of copper center electrode

SCYLLA IV: "LOW-PRESSURE" REGIME

(E.M. Little, W.E. Quinn, and G.A. Sawyer)[*]

Introduction

The production, heating,and confinement of plasma by a rapidly rising magnetic field in a theta-pinch geometry have been studied in many laboratories and it has been established that dense, high-energy plasmas are produced in these devices.[1] In the first theta-pinch experiments it was anticipated that plasma formation and heating would occur by a combination of hydromagnetic shock heating followed by adiabatic compression.[2] However, the production of a hot plasma was found to require the presence of a reversed magnetic bias field in the initial stage of the discharge.[3,4] In the earliest theta-pinch experiments, the reversed bias magnetic field was created by the rapidly oscillating compression field as field trapped during a given half-cycle and held by the plasma until the next half-cycle. In later experiments, it was applied independently as a "bias" field. The present experiments with the Scylla IV theta-pinch at low filling pressure have produced a stable, hot plasma without the presence of a magnetic bias field, similar to that reported by Goldman, et al.[5] This formation of hot plasma is apparently in accordance with the initial conception of the theta pinch at LASL by J. L. Tuck.[2]

The density and configuration of the Scylla IV plasma in this "low-pressure" regime have been studied by the use of a Mach-Zehnder interferometer with ruby laser illumination. The measurements allow the plasma end loss to be determined and compared with theory. In addition, measurements of the soft x-ray and neutron emissions have been made with the interferometer as a function of the initial D_2 pressure.

Experimental Arrangement

The Scylla IV device has been described elsewhere.[6] The experiments to be reported here utilized 0.6 MJ of the total 3.8-MJ available energy storage. The compression coil is energized by two separate capacitor banks: (1) A 40-kV, 10-kJ preionization bank with low inductance and short rise time is used to ionize the deuterium gas. (2) A 50-kV, 570-kJ primary bank with very low inductance (2.2 μH) provides the fast rising magnetic field, which has been characteristic of the previous Scylla devices, for shock heating and compression.

The plasma was produced in a 1-m length, 10-cm diameter coil which was operated both with and without magnetic mirrors. In the experiments with magnetic mirrors, the geometrical mirror ratio of the coil was 1.44. The preionization bank produces a 330 kc/sec oscillating magnetic field with peak magnitudes up to 10 kG and maximum azimuthal electric field, E_θ, of 0.4 kV/cm just inside the discharge tube wall. The primary bank produces a peak magnetic field in the coil of 93-kG with a rise time of 3.7 μsec. The maximum value of E_θ just inside the discharge tube wall is 1.1 kV/cm.

A single crowbar switch is used to short the compression coil at or after the current maximum of the primary bank. The shorting operation reduces the oscillating magnetic field in the coil and the voltage reversal on the capacitor bank during later current half-cycles. The discharge tubes were made of 99% Al_2O_3 to fit the contours of the comperssion coil. The inside diameter of the tubes in the central coil region was 8.6 cm.

The D_2 gas at a filling pressure in the range of 10 to 50 μHg is ionized, "shock" heated, and compressed in the single-turn coil. The operational sequence is as follows: (1) The discharge tube at a base pressure of 10^{-3} to 10^{-4} μHg is loaded with D_2 to an appropriate pressure with an equilibrium flow between inlet and pump out. (2) The preionization bank is applied to the compression coil to preionize the D_2 by the induced azimuthal electric field.[6] This oscillating field damps out in approximately 15 μsec. (3) The 50-kV primary bank is applied to the highly ionized

afterglow 30 μsec after the start of the preionization bank to produce a rapidly rising magnetic field in the compression coil. (4) The crowbar spark gap is triggered at the first maximum of the magnetic field of the primary bank.

Plasma Radiations

Neutron Emission

One of the significant features of the low-pressure regime is the production of a neutron-emitting plasma in the absence of an initial magnetic bias field. Neutrons from the d-d reaction were measured with two Ag counters placed on the compression coil, one at the center and the other near one end, as well as with a plastic scintillation detector. Neutron emissions in the range of 4 to 9 x 10^8 per discharge have been observed at initial D_2 filling pressures of 10 to 50 μHg. The average neutron yield (see Table IV) is not significantly dependent on the initial D_2 pressure in this pressure range.

Typical time distributions of the neutron emission with the magnetic field are shown in Fig. 29. In both the mirror and the mirrorless coil, the neutron emission rate attains a maximum before the peak of the magnetic compression field. This observation is consistent with the particle losses indicated by interferograms.

An attempt has been made to determine the length of the plasma with a massive neutron collimator having five collimating channels which span half of the coil length. The results, although somewhat erratic due to background problems and statistics, indicate that the hot plasma has a length of approximately 80-cm in the 1-m mirrorless coil.

Soft X-Ray Emissions and Plasma Electron Temperatures

Plasma electron temperature, T_e, measurements have been made with an axial dual soft x-ray detector[7] using two Be foils with thicknesses

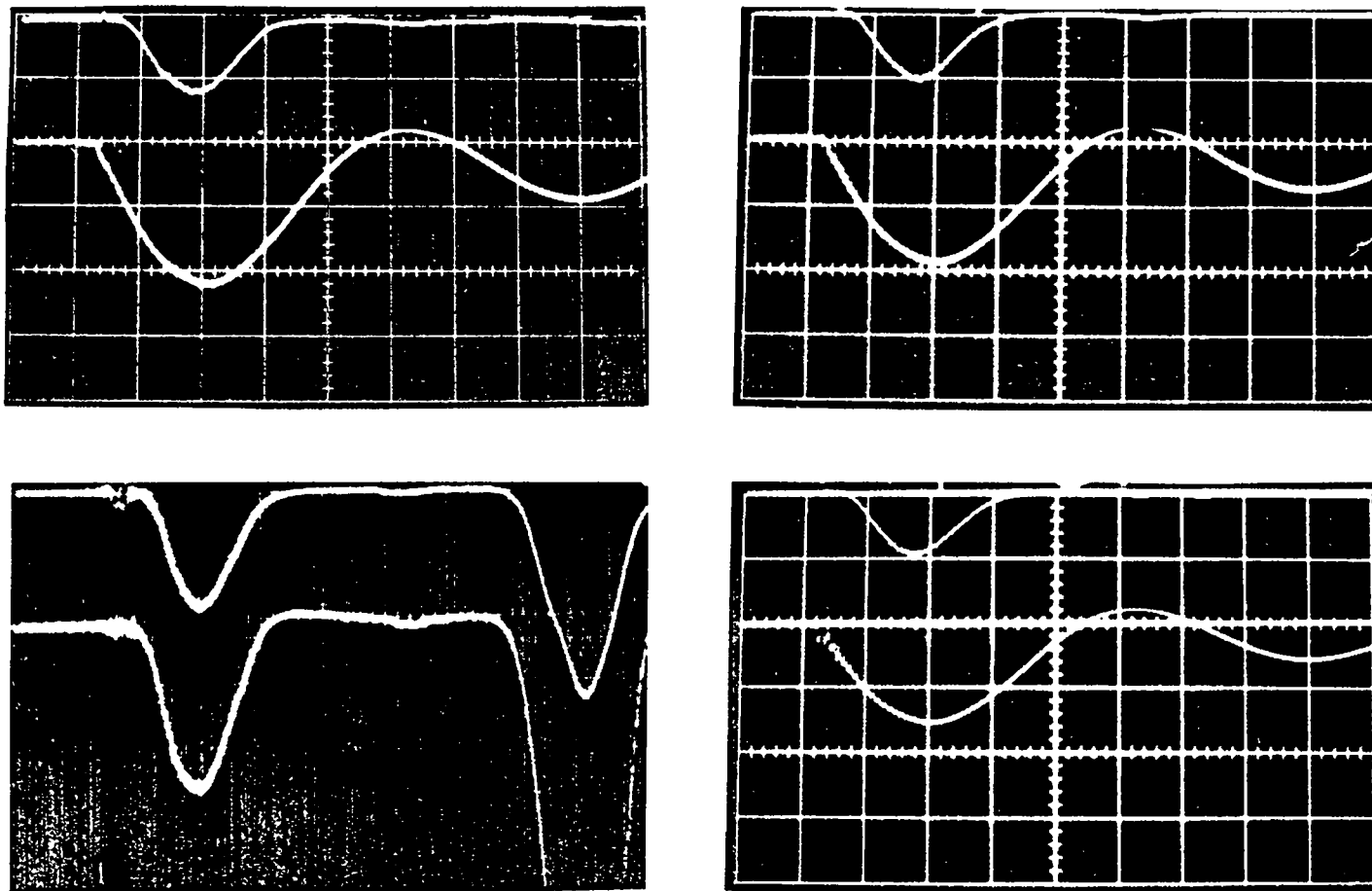Fig. 29. Applied magnetic compression field and neutron and soft x-ray emissions. Upper left shows the neutron signal at an initial pressure of 25 µHg. Lower left: soft x-ray signals through Be foil thicknesses of 24.7 mg/cm^2 (top trace) and 10.7 mg/cm^2 (bottom trace) at an initial pressure of 15 µHg in the mirrorless coil (upper right) and the mirror coil (lower right). Time scale: 2 µsec/div.

77

of 10.7 and 24.7 mg/cm^2. In addition, a single axial soft x-ray detector with a 22.4 mg/cm^2 Be absorber foil was used simultaneously to measure the absolute intensity of the soft x-ray emission. The absolute detector was calibrated with a Cs^{137} γ source. The absorber foil attenuation was folded into the detector sensitivity factor. The solid angle subtended by the plasma at the detector aperture was calculated by integrating over the plasma volume as determined from interferometer and neutron collimation experiments.

A summary of the soft x-ray emission measurements is presented in Table II, in which I_x is the absolute soft x-ray intensity emitted by the plasma, n_e is the electron density as determined with the interferometer for identical operating conditions, and R is the ratio of measured x-ray intensity to the theoretical bremsstrahlung intensity emitted by a pure D$_2$ plasma with the indicated electron temperature and density. The radiation power in the bremsstrahlung from a pure D$_2$ plasma is calculated from[8]

$$P = 1.5 \times 10^{-32} \, n_e n_i \, g(kT_e)^{\frac{1}{2}} \text{ watts/cm}^3 \, , \qquad (1)$$

where kT_e is in eV and g is the Gaunt factor. The last column of Table II gives the percent of O impurity which is required to bring the measured continuum intensity results into agreement with the theoretical values assuming all the O exists in the discharge as O VIII.[9] The continuum radiation data indicate that the impurity level of the discharge is much less than that of previous Scylla discharges at higher pressures. In fact, if the impurity is assumed to be O and that it exists in the discharge mainly in the O VIII state during the time of soft x-ray emission,[9] then the impurity is about 0.1%. If the majority of the impurity were in the O IX rather than O VIII, the proportion in the plasma would be reduced by a factor of approximately 4.8; on the other hand, it would be increased by a factor of 88 if the impurity were O VII.

The T_e's in the low-pressure plasma without reversed magnetic bias field are approximately 300 eV (Table II) and are essentially independent

TABLE II

Averaged Soft X-Ray Emission Data

P_{D_2} (μHg)	No. of Discharges	T_e (eV)	(I_x)Meas. (W/cm^3)	n_e (x 10^{16} cm^{-3})	(I_x)Theo. (W/cm^3)	$R\left(\dfrac{I\ Meas.}{I\ Theo.}\right)$	% O VIII Impurity
10	4	328 ± 56	244	2.1	119	2.05	0.029
25	12	282 ± 31	915	4.1	422	2.17	0.032
50	30	300 ± 30	1607	5.4	776	2.07	0.030
70	11	296 ± 15	2113	~ 6	928	2.28	0.035
125	8	295 ± 15	28,260	~ 10	2535	11.14	0.28

of the D_2 pressure over the range of 10 to 125 µHg. This value is to be compared with T_e's of the order of 1000 eV observed in plasmas with "optimum" reversed B_0 in the same geometries.[6] This difference in the T_e values probably arises from differences in the heating mechanism during the early phase of the discharge and indicates that the annihilation of the reversed B_0 is effective in heating the electrons. In the present experiments, the addition of a small amount of reversed B_0 at the D_2 pressure of 50 µHg increased the electron temperature.

Figure 30 shows T_e, as measured by the Be absorbers, plotted as a function of time for two initial D_2 pressures. The T_e remains near its maximum value as the intensity of the soft x-ray emission decreases soon after the magnetic field maximum. It is probable that this decrease results from particle losses as indicated by the interferograms.

Interferometric Measurements

A Mach-Zehnder interferometer has been used to obtain plasma electron densities, to observe plasma shapes and stability, and to determine the particle losses from the Scylla IV plasma.[6] To a good approximation, the optical path length difference introduced by a plasma of length L is

$$P = \int_0^L [(n-1)/\lambda]\, d\ell = r_e\, \frac{\lambda}{2\pi} \int_0^L n_e d\ell, \qquad (2)$$

where r_e is the classical electron radius. For $\lambda = 6943$ Å a shift of one fringe corresponds to $\int n_e d\ell = 3.2 \times 10^{17}$ cm².

Experimental Arrangement

The interferometer has a 2-m test optical path which spans the Scylla IV compression coil and discharge tube as shown in Fig. 31. A pulsed ruby laser, operated either in the giant pulse mode with a power level of about 500 kW and a pulse width of less than 0.1 µsec or continuously

Fig. 30. Applied magnetic field and plasma electron temperatures
as functions of time in the mirrorless coil

COMPRESSION COIL

DISCHARGE TUBE

VALVE

QUARTZ WINDOW

VALVE

QUARTZ WINDOW

INTERFERENCE FILTER

LENS

TO STREAK CAMERA

FILM PLANE

DIAPHRAGM

VACUUM PUMP

FRINGE LOCATION

COMPENSATION CHAMBER

LASER BEAM

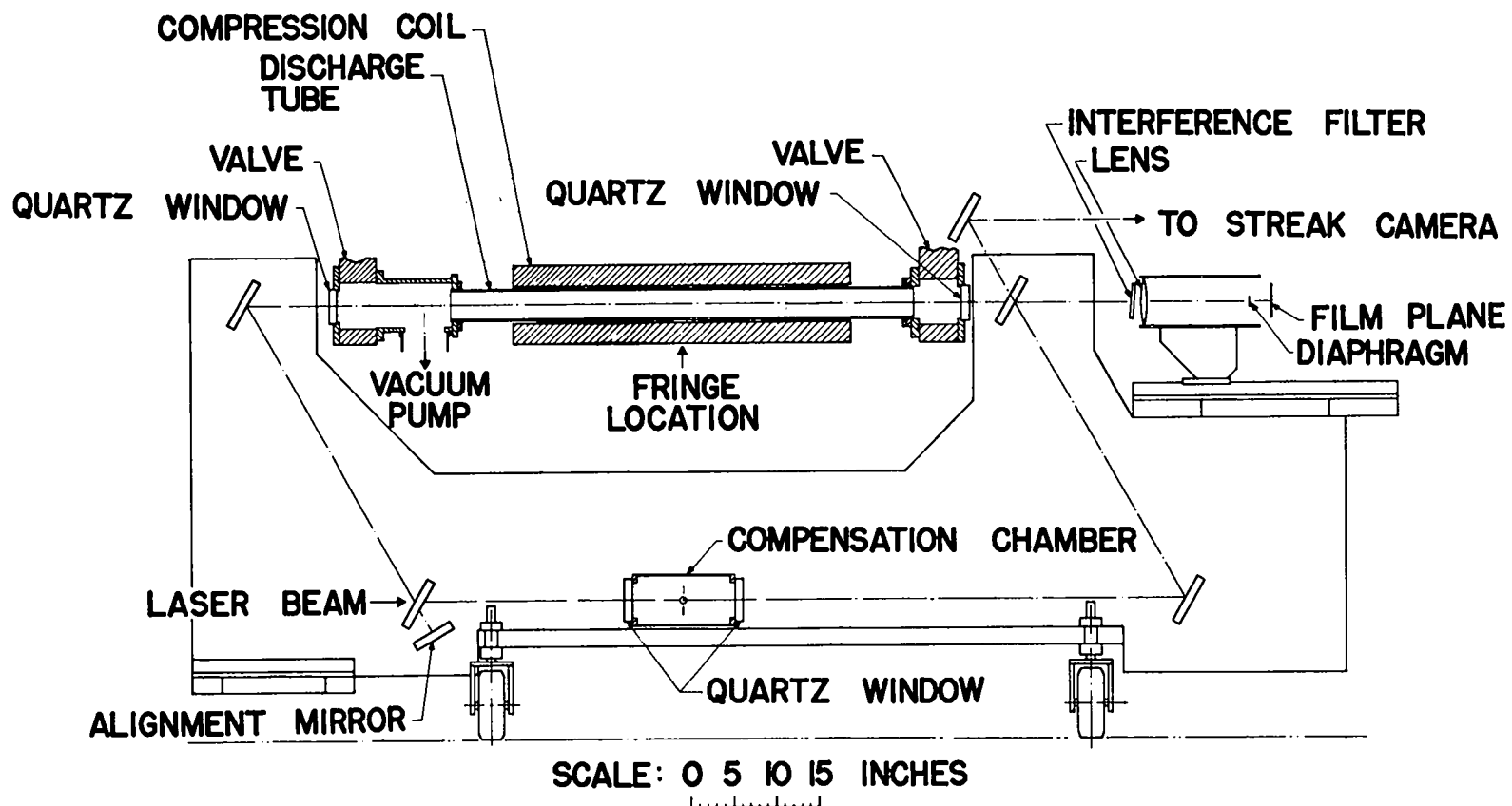QUARTZ WINDOW

ALIGNMENT MIRROR

SCALE: 0 5 10 15 INCHES

Fig. 31. The Mach-Zehnder interferometer

for about 200 μsec at a power level of 5 kW, was used to illuminate the interferometer. An inverted telescope served to expand the 1-cm diameter laser beam to a 10-cm cross section. A narrow band interference filter and a 3-mm diameter pinhole were used to discriminate against the plasma light.

Measurements

The interferometer was adjusted without plasma to have 3 to 10 fringes over its field. The data (Figs. 32 through 35) show that the plasma gave large fringe shifts. All the plasma is swept into the compressed core, so that the region outside shows undistorted vacuum fringes. The absolute fringe shifts can be obtained in either of two ways: (1) The fringe pattern can be analyzed across a diameter of the discharge tube perpendicular to the vacuum fringes by measuring the positions of displaced fringes relative to the vacuum fringe pattern. Subtraction of the "background" fringes from those corresponding to regions of plasma density gives the absolute fringe shifts. (2) The fringe pattern can be analyzed along a diameter parallel to the vacuum fringes by measuring the position of the displaced fringes. This gives the absolute fringe shift due to the plasma density directly.

It has been shown that fringe shifts resulting from the deviation of light rays by refractive effects in the plasma are negligible for Scylla IV.[6]
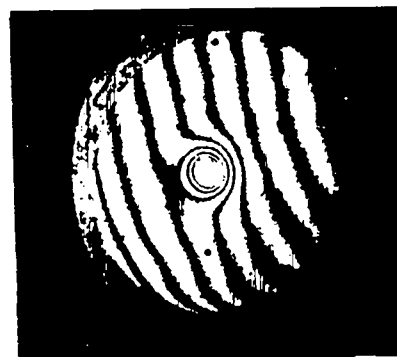
Results with Giant Pulsed Laser

Time sequences of interferograms during the discharge half cycle were obtained in the 1-m mirror coil at pressures of 15, 25, and 50 μHg (Fig. 32) and in the 1-m mirrorless coil at pressures of 10, 15, and 25 μHg as shown in Figs. 33 through 35. Each interferogram was taken on a single discharge with the ruby laser operating in the giant pulse mode. The time resolution, determined by the laser pulse width, is less than 0.1 μsec. The interferograms show time sequences of stable neutron-producing plasmas

15μ, 1.6μs   15μ, 3.3μs   25μ, 3.3μs

50μ, 1.8μs   50μ, 3.3μs   25μ, 3.3μs
                            $B_o = -0.9\,kG$

Fig. 32. Interferograms during the magnetic half-cycle at various times after application of the magnetic field. The lower right interferogram is with an initial reversed bias magnetic field, the others are without this field.

Δt=0.2μsec 2.4 3.6

4.9 6.1

$P_o = 25 \mu Hg$

Fig. 33. Time sequence of interferograms during the magnetic half-cycle at various times with an initial pressure of 25 μHg

$\Delta t = 1.0 \mu sec$ 1.9   3.6

5.3   6.5

$P_o = 15 \mu Hg$

Fig. 34. Time sequence of interferograms during the magnetic half-cycle at the various times with an initial pressure of 15 µHg

$\Delta t = 0.6 \mu sec \qquad 2.1 \qquad 2.7$

$4.1 \qquad 5.4$

$P_o = 10 \mu Hg$

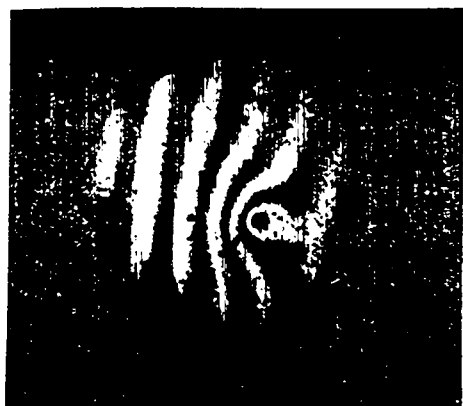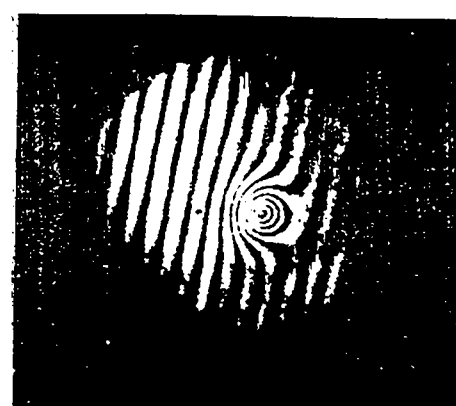Fig. 35. Time sequence of interferograms during the magnetic half-cycle at various times with an initial pressure of 10 µHg

created in the absence of magnetic bias fields in both the mirror and mirrorless coils over a pressure range of 10 to 50 µHg. With an initial D_2 filling pressure from 10 to 25 µHg, the vacuum fringe patterns exist outside the central plasma core throughout the discharge half-cycle. This indicates the absence of ionized plasma in the vicinity of the discharge tube wall. An upper limit on n_e outside the plasma core of 10^{15} electrons/cm^3 is obtained from the interferograms. At a pressure of 50 µHg, there is some distortion of the vacuum fringes (Fig. 32) outside the central plasma region by the time of maximum magnetic field. The absence of ionized matter outside the central plasma core at the lower pressures is to be contrasted with a typical interferogram (Fig. 36) at a pressure of 70 µHg with reversed bias magnetic field.

The time-sequence interferograms taken in the low-pressure regime without bias-field show the following: (1) The plasma is stable throughout the magnetic half-cycle. (2) The vacuum fringe pattern is present outside the plasma core and in the vicinity of the discharge tube walls showing the absence of ionized plasma. The characteristic influx of impurities from the wall as seen at higher pressures is not observed. (3) After the maximum of the magnetic field ($\Delta t = 3.7$ µsec), the diameter of the plasma fringe pattern does not increase as the magnetic field decreases, but the number of fringes decreases. This shows that the plasma is being lost from the central plasma core. Figures 37 and 38 give the reduced data, showing graphs of the fringe shifts from Eq. (2) vs distance across the discharge tube diameter. These graphs correspond to the interferograms in Figs. 32 through 35. The fringe shifts give the integral of n_e over the plasma length. If this length is taken to be 80 cm, as indicated by neutron collimation data, the resulting n_e's at maximum magnetic field time are in the range of 2 to 4×10^{16} cm^{-3} as given in Table IV.

The total number of electrons, N_e, in the discharge can be obtained from the reduced interferogram data without a knowledge of the plasma length. This procedure requires only the assumption of a uniform plasma density throughout the plasma volume as is certainly the case for a

A

B

0.4 μsec   1.6   2.3   3.2

p = 70μ Hg

B_0 = 5.0kG

C

Fig. 36. Time sequence of interferograms (B) during the magnetic half-cycle with an initial reversed bias magnetic field. (A) Oscillogram of the applied magnetic field with a time scale of 2 μsec/div. (C) Streak photograph aligned on the same time scale as (A).

Fig. 37. Graphs of the reduced data of Fig. 33 showing the fringe shifts, $\alpha \int n_e d\ell$, at the indicated pressures and magnetic half-cycle times

Fig. 38. Graphs of the reduced data of Figs. 33, 34, and 35 showing the fringe shifts produced by the plasma at the indicated magnetic half-cycle times

β = 1 plasma. At an interferometer illumination of λ = 6943 $\mathring{A}$, it can be shown that N_e is then given by

$$N_e = 2.5 \times 10^{17} \, (\Delta f) \, \overline{d^2} \, , \tag{3}$$

where Δf is the number of fringe shifts produced by the plasma and $\overline{d^2}$ is the mean square diameter of the fringe shift 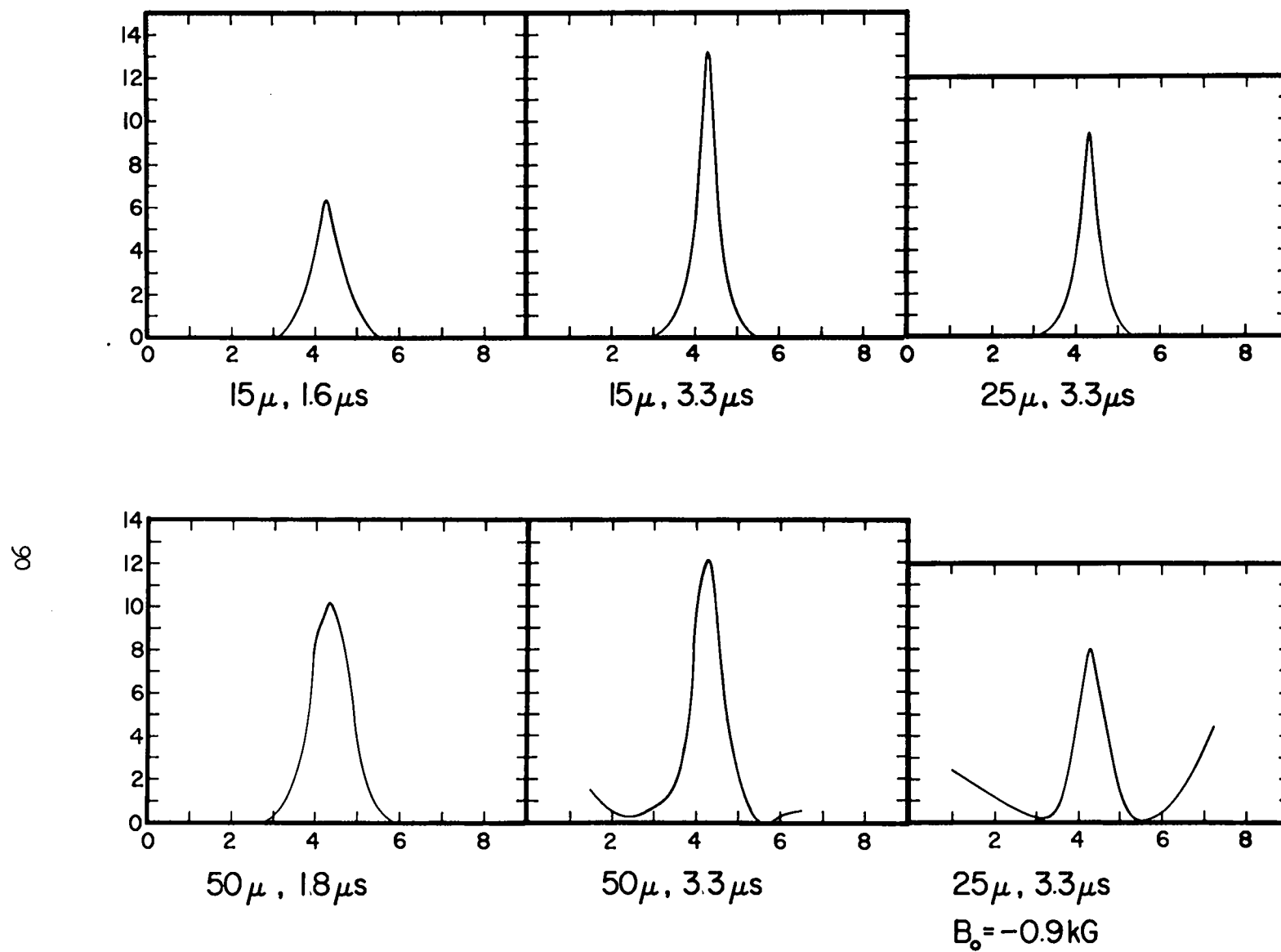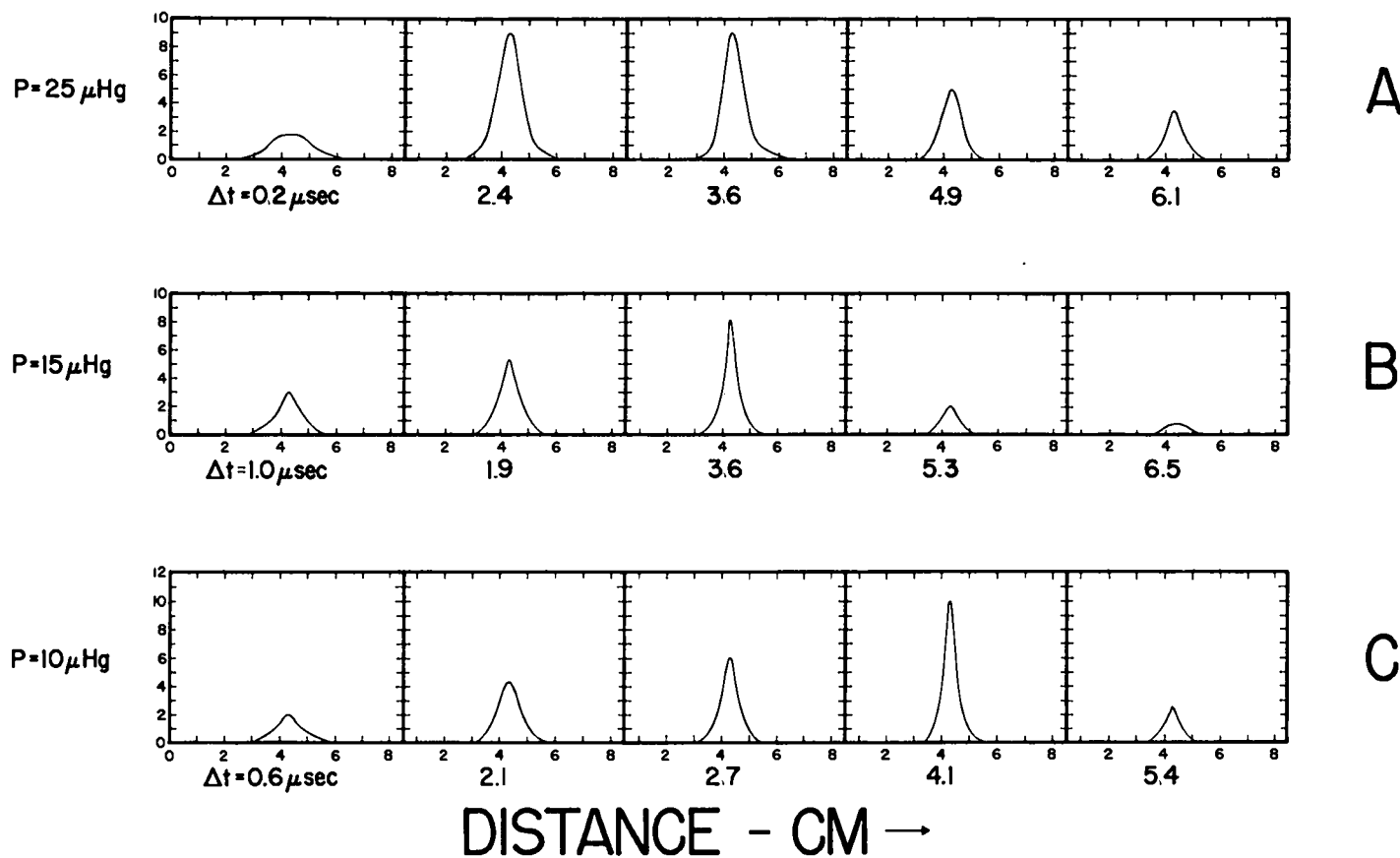distribution. Figure 39 presents graphs of N_e vs the applied magnetic field obtained from interferograms recorded at the observed pressures. It should be recalled that each point on the plots is derived from an interferogram taken on a single discharge. The graphs indicate that the total particle number begins to decrease prior to the magnetic field maximum. Containment times before peak field are 6.3 and 5.7 μsec, whereas after peak field they decrease to 4.1 and 3.3 μsec. The relatively lower initial time points are believed to result from poor statistics and inadequacies in the analysis of the fringe patterns during the initial stage of the discharge. The total particle number should remain constant until losses cause it to decrease. It should not increase with time unless new particles are coming in from the walls or ends. The interferograms indicate, however, that an influx of particles from the walls is not occurring.

Results with Continuous Laser Illumination

The foregoing measurements yielded only one interferogram per discharge. In order to obtain continuous records, the ruby was chilled with liquid N_2 and was allowed to oscillate freely. It then emitted light in a continuous manner for a short time and high-speed photography was employed to obtain the necessary time resolution. Figure 40 shows the continuous emission produced by the free oscillations of the cooled ruby. The Scylla discharge was made to occur at the time of peak laser illumination.

Several high-speed methods were tried in photographing the fringe patterns. The results obtained on 35-mm, 1N-film with a f/2.9 NLC streak camera sweeping the 1-mm slit image on the film at 3 mm/μsec were deficient
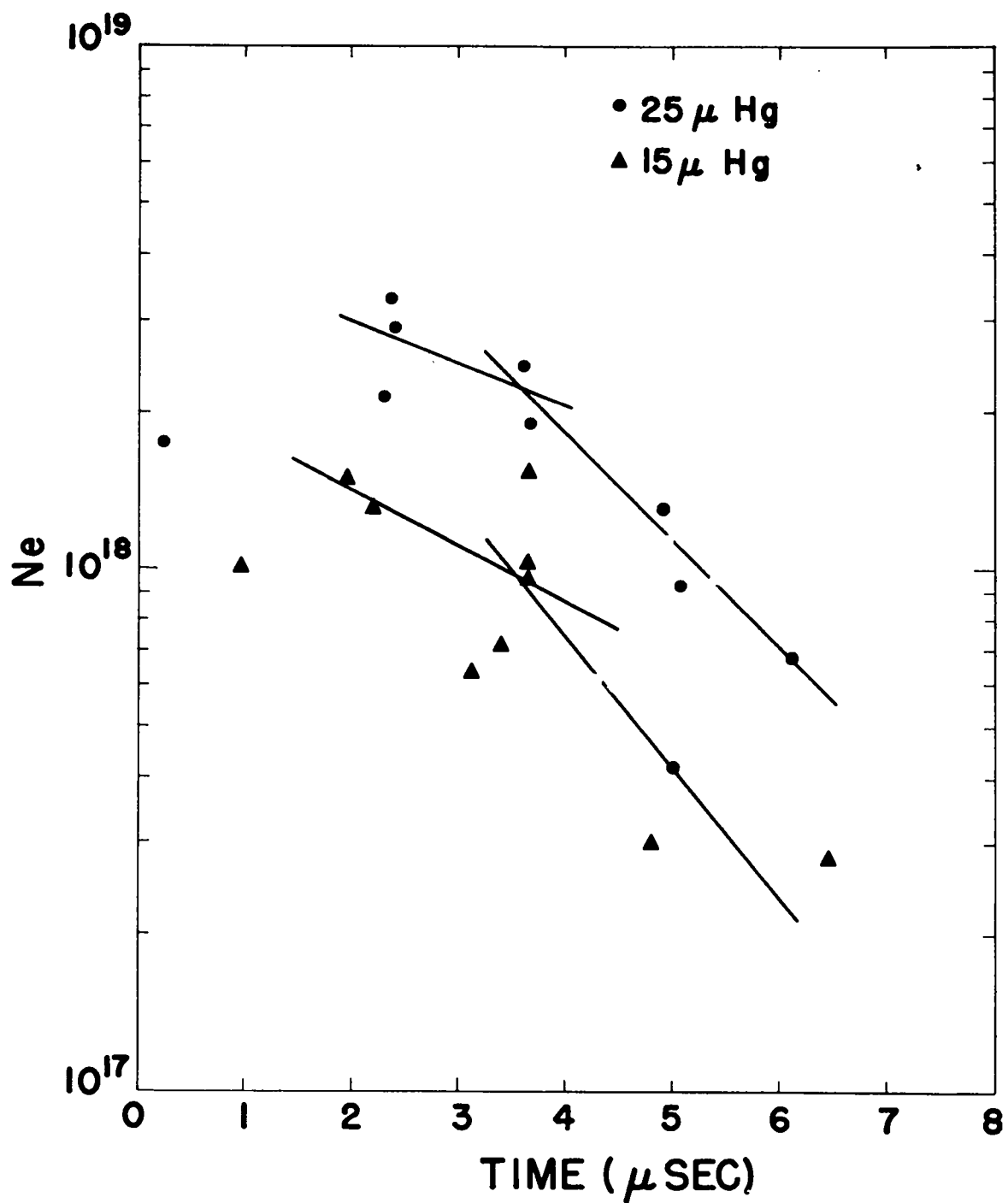
Fig. 39. Total number of plasma electrons, N_e, in the discharge as a function of time during the magnetic half-cycle for data corresponding to Figs. 33 and 34
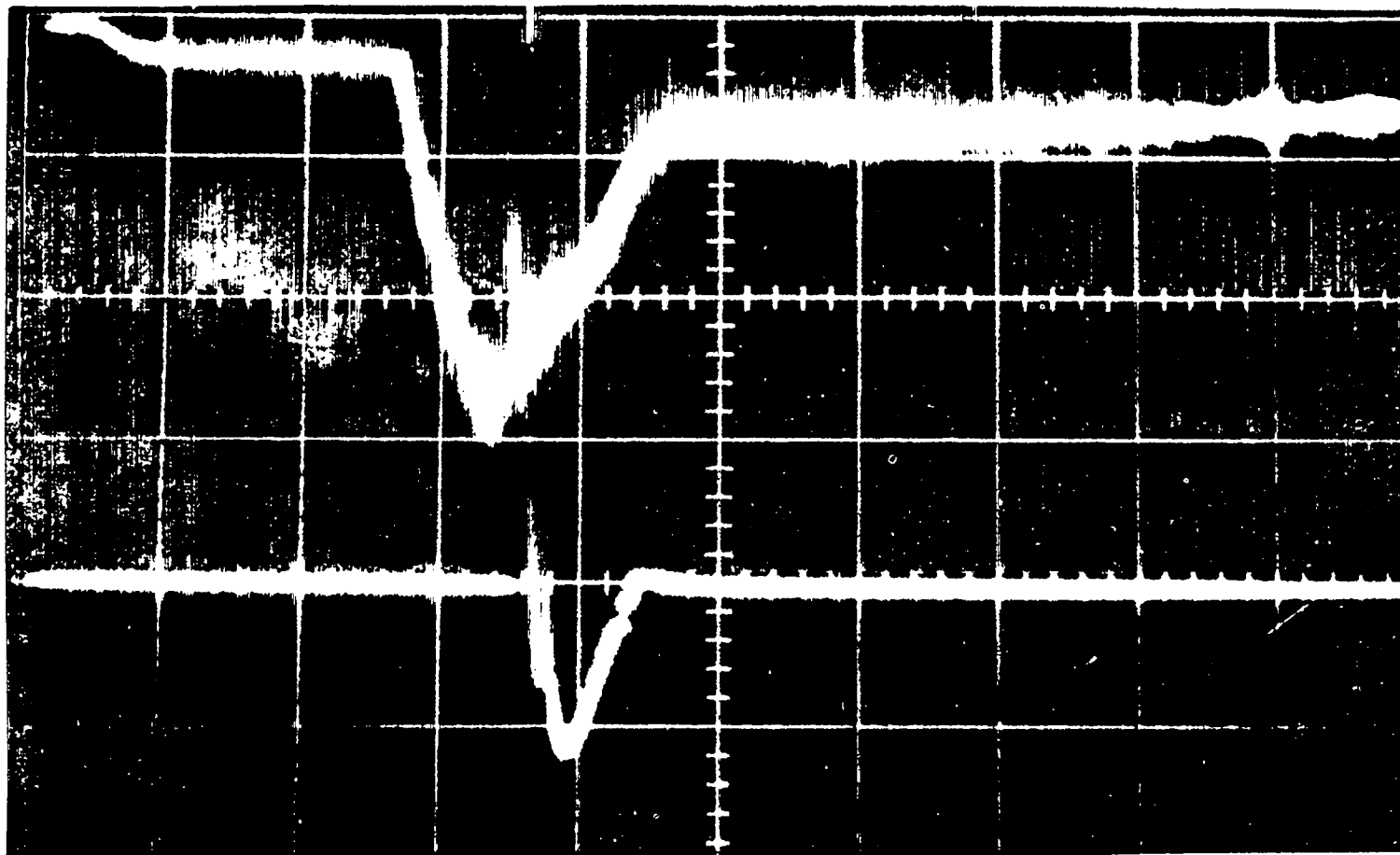
Fig. 40. Emission of a cooled ruby laser on a time scale of 100 μsec/div.
The initial signal is caused by the flash lamp emission which provides the laser
excitation.

in both intensity and resolution of the fringe pattern. Similar results were obtained with the STL camera operating in the streak mode. With the STL instrument operating as a framing camera, the fringe patterns of Fig. 41 were obtained in sets of three per discharge. The results confirm the previous conclusion of plasma stability throughout the magnetic half-cycle and the absence of ionized impurities outside the central plasma core, and indicate that the plasma is being lost. In addition, no appreciable drift of the plasma toward or away from the coil feed point is indicated. The interferograms of Fig. 41C, taken at a pressure of 50 μHg, show a fairly dense, stable plasma with the absence of ionized impurities in the vicinity of the walls.

The graphs of Fig. 42 present the reduced data of fringe shifts vs distance across the discharge tube diameter. With the assumption of an 80-cm plasma length, the n_e's at maximum magnetic field are 1.0, 2.1, and 5.4×10^{16} cm^{-3} at the respective initial pressures of 10, 25, and 50 μHg.

Figure 43 shows the total number of electrons in the discharge as a function of time, as derived from the reduced data plots of Fig. 42 with the aid of Eq. (3). The points connected by lines were obtained from interferograms taken on a single discharge. The results indicate that two different loss rates occur during the discharge. Correspondingly, there are two associated containment times (e-folding times): $(\tau_c)_1$ which characterizes the containment time between two-thirds B_{max} and B_{max} on the rise of the field and $(\tau_c)_2$ which relates to the containment between B_{max} and one-third B_{max} on the decay of the field. The values of these characteristic times, obtained from the slopes of Fig. 42 are given in Table III as a function of the initial filling pressure.

P=10 μHg   A

Δt = 1.2   2.8   4.4   4.9   6.5   7.9μsec

P=25 μHg   B

Δt = 0.4   2.2   3.7   4.1   6.0   7.4μsec

P=50 μHg   C

Δt = 0.3   1.3   1.9   2.8   4.0   5.2   6.4   7.8μsec

Fig. 41.   Interferograms with "continuous" laser illuminations recorded with an STL framing camera. In (A) and (B) each set of three consecutive fringe patterns was recorded on a single discharge. In (C), the first and third, the second and fourth, and the last three interferograms were taken on single discharges at the indicated magnetic half-cycle times.
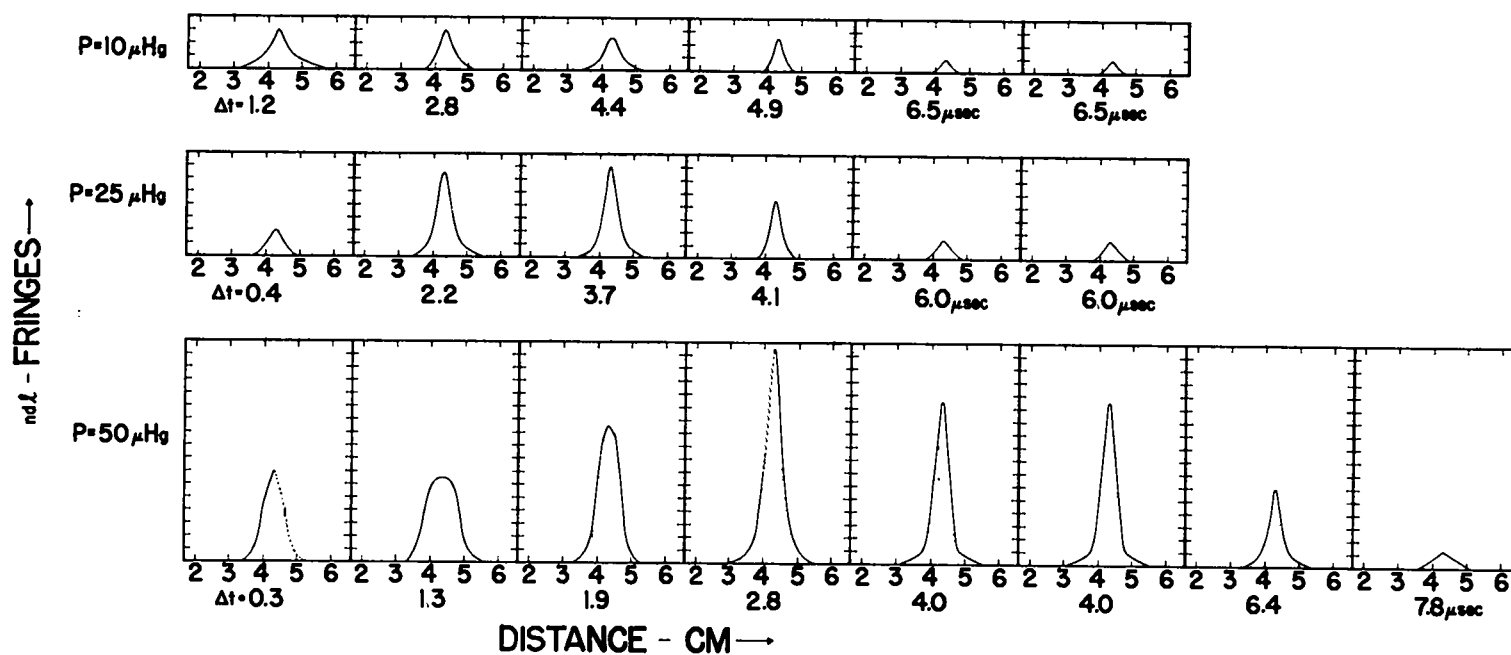
Fig. 42. Reduced data of Fig. 41 showing fringe shifts due to the plasma as a function of the discharge tube diameter
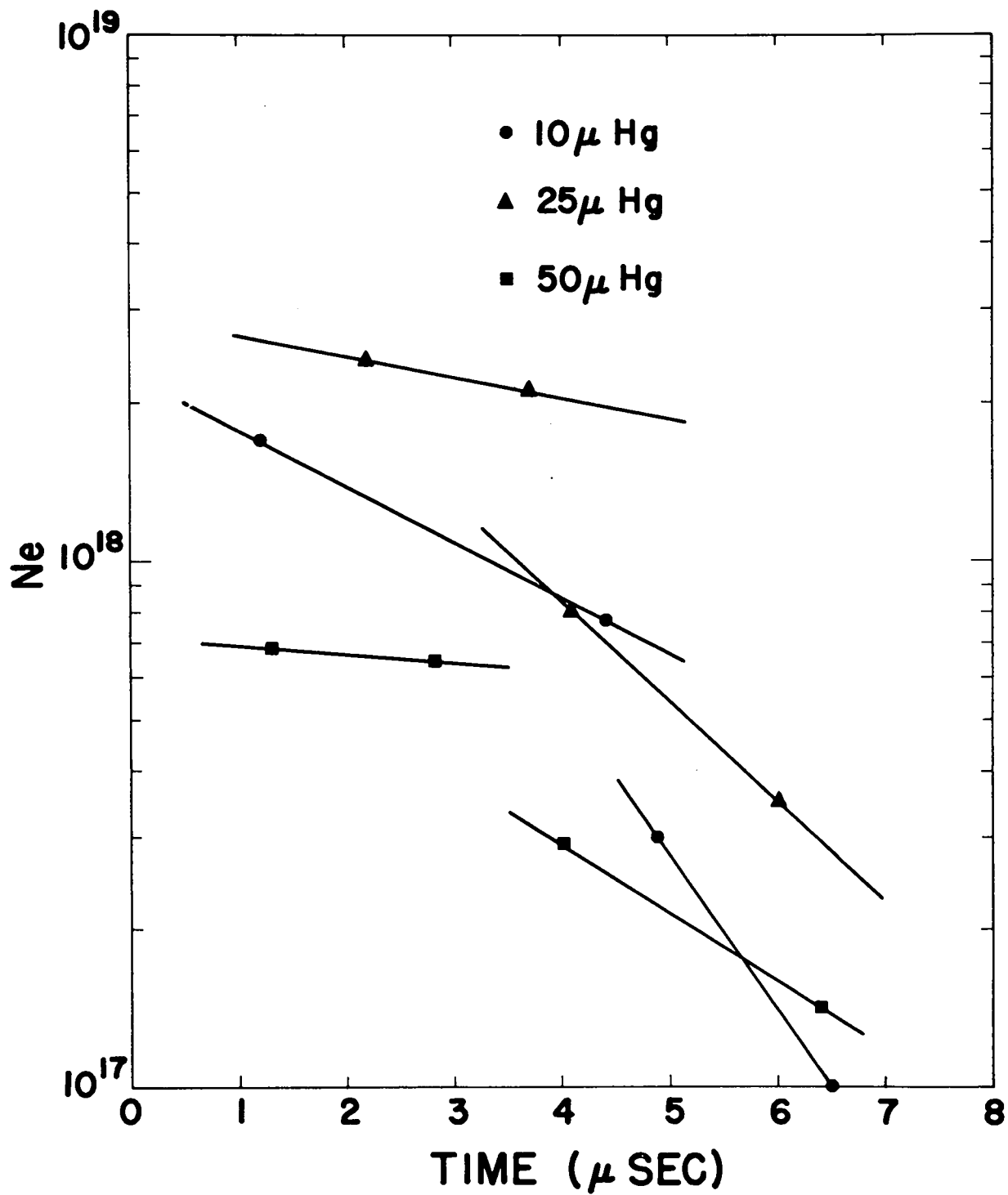
Fig. 43. Total number of plasma electrons, N_e, in the discharge during the indicated magnetic half-cycle times for the data of Figs. 41 and 42

TABLE III

Plasma Containment Times

P_{D_2}	$(\tau_c)_1$	$(\tau_c)_2$
10 μHg	5.9 μsec	2.4 μsec
25	12.1	3.4
50	29.2	4.7

Ion Energies

The measurements described above make possible an independent determination of the average plasma ion energy from pressure balance with the magnetic field. On the assumption that the plasma contains no magnetic field, which has been established for the Scylla plasmas produced with an initial reversed magnetic field,[6] the external magnetic pressure can be equated to the sum of the pressures of the plasma components,

$$B^2/8\pi = n_e\, kT_e + n_D\, kT_D + n_c\, kTc, \tag{4}$$

where the subscripts e, D, and c refer to electrons, deuterons, and contaminant ions, respectively. The magnetic field, B, is determined from circuit constants, T_e from the x-ray measurements, and n_e from the interferometric and neutron collimation length measurements. Since the impurity level has been shown to be low, contaminants are neglected. Then charge neutrality requires $n_D = n_e$ and T_D is determined. Table IV lists the average D ion energy T_D (PB) obtained from pressure balance assuming a $\beta = 1$ plasma for various indicated initial D_2 filling pressures.

The D-ion energy can also be derived from the observed neutron emission rate on the assumption that the neutrons are completely thermo-nuclear resulting from a fully developed Maxwell distribution of D ions. Table IV gives various plasma parameters determined from the interferometer data and the neutron emission for the mirrorless coil: V is the plasma volume obtained from $\overline{d^2}$ and a plasma length of 80 cm; $\overline{Y_n}$ is the average neutron emission for 10 or more discharges; T_D(PB) is defined above;

TABLE IV

Plasma Parameters

P_{D_2} (μHg)	$\overline{d^2}$ (cm^2)	V (cm^3)	$n_e(\Delta t \sim 3.7\ \mu sec)$ (cm^{-3})	$\overline{Y}_n$	$T_D(PB)$ (keV)	$T_D(\sigma v)$ (keV)
50	1.32	83	5.4×10^{16}	3.0×10^8	3.7	1.4
25	0.89	56	4.1×10^{16}	5.8×10^8	3.8	2.2
15	0.59	37	2.6×10^{16}	5.6×10^8	6.6	3.0
10	0.64	40	2.1×10^{16}	5.5×10^8	8.6	3.2

T_D (σv) is the D ion energy obtained from the neutron emission, the plasma volume, and the density based on a Maxwellian distribution.

There is a large discrepancy between the two sets of T_D values, but it is not unreasonable. The total confinement time for the plasma (3 μsec) is barely an ion-ion collision time, and so if the ions were created as monoenergetic, there would be insufficient time to develop a Maxwellian tail. Such a plasma requires a higher mean pressure to produce the same thermonuclear yield.[10] When the neutron yield is calculated for a monoenergetic ion energy distribution, the ion energies required for pressure balance and by the neutron yield are in reasonable agreement.

Particle Losses

For any value of the mean free path, with the magnetic field small and the particle orbits nonadiabatic in the plasma region, the plasma particles are lost essentially by free flow through an orifice of radius r_E.[11] The smallest value that r_E can have is the particle Larmor radius. In the Scylla devices, the experiments strongly indicate that a high-β plasma is produced with the absence of magnetic field in the plasma region.[6] On a simple model, the rate at which particles are lost out of the ends of the compression coil is given by

$$\frac{dN}{dt} = -2 A_E \frac{n\bar{v}}{4} , \qquad (5)$$

where $\bar{v}$ is the average velocity of the ions, $2 A_E$ is the effective area of the two open ends, and n is the particle density. Since the total particle number $N = n A_p \ell$, where A_p is the cross-sectional area of the plasma and ℓ the plasma length,

$$\frac{dN}{dt} = -\frac{N}{2} \frac{A_E}{A_p} \frac{\bar{v}}{\ell} = -\frac{N}{\tau_c} , \qquad (6)$$

so that the containment time is

$$\tau_c = 2 \frac{A_p}{A_E} \frac{\ell}{\bar{v}} \; .$$

(7)

A difficulty arises in determining the loss end area A_E. It will depend on the thickness of the boundary between the plasma and the external field and to the extent that the field has penetrated the plasma near the ends. In addition, A_E should be inversely proportional to the mirror ratio of the compression coil. However, A_E can be determined from Eq. (7) since the other quantities are known or can be reasonably estimated; A_p and τ_c are obtained from the interferograms, ℓ from neutron collimation, and $\bar{v}$ from pressure balance assuming a $\beta = 1$ plasma.

Table V presents r_E values for various ion energies at the indicated pressures for the τ_c's of Table III. In addition, the D-ion Larmor radii, r_d, computed for the indicated magnetic fields, are presented for comparison with r_E. As previously discussed, the D-ion energy distributions are evidently not completely Maxwellian but probably lie between monoenergetic and Maxwellian. Consequently, the agreement between r_E and r_d in Table V is probably better than should be anticipated since r_E depends on the component of the particle velocity parallel to the magnetic field and r_d on the component perpendicular to the field.

Summary

A neutron-producing plasma with ion energy $\sim$ 3-4 keV has been produced at filling densities 10-50 μHg without negative bias magnetic fields in a 570-kJ theta-pinch. Axial interferograms, taken with a Mach-Zehnder interferometer, show that a stable compressed plasma core exists throughout the magnetic half-cycle with no ionized impurities outside the core, and no drift toward the wall. The interferograms give peak plasma densities of 2 to 5 x 10^{16} cm^{-3}, and also indicate a loss of particles as a function of time. Plasma containment times before peak compression are 6 to 30 μsec.

TABLE V

Comparison of the Particle Loss Aperture Radius r_E with Deuteron Ion
Larmor Radius r_d

W_d	$r_E(\tau_{c1})$ (cm)	r_d(B=75 kG) (cm)	$r_E(\tau_{c2})$ (cm)	r_d(B=45 kG) (cm)
P_{D_2} = 10 µHg				
2 keV	0.49	0.12	0.77	0.20
5	0.39	0.19	0.61	0.32
10	0.33	0.27	0.52	0.45
P_{D_2} = 25 µHg				
2 keV	0.28	0.12	0.51	0.20
5	0.22	0.19	0.41	0.32
10	0.19	0.27	0.34	0.45
P_{D_2} = 50 µHg				
2 keV	0.23	0.12	0.57	0.20
5	0.19	0.19	0.47	0.32
10	0.16	0.27	0.40	0.45

The observed loss rates are approximately in agreement with predictions of
free flow through an orifice whose radius is equal to an ion Larmor radius.
Soft x-ray measurements yield ~ 300 eV electron temperature for all filling
pressures. Absolute intensities of the soft x-ray emissions show the impurity
level to be < 0.1%. The ion energy for the low-pressure regime deduced from
pressure balance between plasma and magnetic field (assuming β = 1) is about
a factor two higher than the ion energy deduced from the measured neutron yield.
The discrepancy indicates that the ion distributions are more nearly monoenergetic
than Maxwellian.

References

1. W. E. Quinn, Progress in Nuclear Energy (Pergamon Press, London, 1963) Series XI, Vol. 2, p. 166.

2. K. Boyer, W. C. Elmore, E.M. Little, W. E. Quinn, and J. L. Tuck, Phys. Rev. 119, 831 (1960).

3. A. C. Kolb, C. B. Dobbie, and H. R. Griem, Phys. Rev. Letters 3, 5 (1959).

4. E. M. Little, W.E. Quinn, and F. L. Ribe, Phys. Fluids 4, 711 (1961).

5. L.M. Goldman, H.C. Pollock, J.A. Reynolds, and W.F. Westendorp, Phys. Rev. Letters 9, 361 (1962).

6. F.C. Jahoda, E.M. Little, W.E. Quinn, F.L. Ribe, and G.A. Sawyer, J. Appl. Phys. 35, 2351 (1964).

7. E.M. Little, W.E. Quinn, F.L. Ribe, and G.A. Sawyer, Nuclear Fusion, 1962 Suppl. Part 2, 497.

8. G. Elwert, Z. Naturforsch, 9A, 637 (1954).

9. F.C. Jahoda, E.M. Little, W.E. Quinn, F.A. Sawyer, and T.F. Stratton, Phys. Rev. 119, 843 (1960).

10. W.B. Riesenfeld, Private communication.

11. H. Grad, New York University Report, NYO-7969 (1957).

NUMERICAL STUDIES OF THE THETA PINCH IN THE "LOW DENSITY" REGIME

(T.A. Oliphant, Jr. and F.L. Ribe)

In previous reports, comparison of the experimental behavior of the Scylla I theta pinch was made with the results of the two-fluid hydromagnetic code of Hain and Roberts (cf. IAMS-2916, p. 36, and IAMS-2911). This comparison showed the H-R code to be incapable of predicting the ion temperatures observed with reversed bias fields B_0 at filling pressures in the vicinity of 100 µHg. In addition, temperatures at peak compression were found to vary sensitively with the Richtmyer-Von Neumann shock constant, indicating that the shock term was not being handled properly in the H-R code, which used Eulerian coordinates for integrating the differential equations.

The θ-pinch problem has been recoded in Lagrangian coordinates, and the results for Scylla I parameters showed the temperatures and other parameters at peak compression to be independent of the R-VN shock constant over a reasonable range of its values (LAMS-2944).

Recent work on the General Electric and Scylla IV θ-pinches (see preceding section) has indicated that large ion temperatures (and neutron yields) can be obtained at low pressures ($p_0 \sim 10$ µHg) without negative bias fields. The action of negative B_0 is anamolous in the sense that the ion heating involves effects other than stable magnetohydrodynamic and the collisional effects accounted for by normal transport coefficients. In the new ("low-pressure") regime, where this anamolous action is presumably not present, it is important to compare the results with the hydromagnetic code to see if the observed ion temperatures can be accounted for.

The numerical results with the new code show a well-defined shock ahead of the contact (plasma-magnetic field) surface during the early, dynamical stages of the θ-pinch. For Scylla IV parameters, at $B_0 = 0$, $T_0 = 2$ eV, and initial densities $n_0 = 0.72$, 1.8, 3.6, and 7.2×10^{15} cm^{-3}, the computed

ion temperatures at peak compression (B_{max} = 120 kG) are 6.5, 3.0, 1.5, and 0.83 keV, as shown in Fig. 44. This reproduces the behavior of the LASL and G.E. high voltage θ-pinches in which, at B_0 = 0, the ion energy at peak compression increases through these values as the D_2 filling pressure is decreased from 10 to < 1 μHg. The computed electron temperatures are lower than those of the ions.

These results indicate that the θ-pinch in its low-pressure mode is indeed operating in a classically predictable way. This is illustrated by the scaling shown in Figs. 44 and 45. In Fig. 45, ion and electron temperatures at the end of the first implosion (first maximum of T_e, T_i, and n) are plotted vs n_0. It is seen that T_e is independent of n_0, showing its independence of the shock; T_i varies as $n_0^{-1/2}$, as would be expected from any simple model of a dynamic sheath (cf. LAMS-2471). The time of the first implosion also varies predictably as $n_0^{1/4}$, so that the compression ratio B_{max}/B_{impl} should vary approximately as $n_0^{-1/4}$. In fact the compression ratio varies as $n_0^{-0.3}$, as shown by the T_e results of Fig. 44.

The variation of T_i with n_0 at peak compression is expected to have an exponent of approximately 0.8 on the basis of simple shock heating, followed by compression. The actual exponent in Fig. 44, is 0.9, and the difference probably reflects the fact that shock heating actually occurs over two or three of the initial dynamic oscillations.

These results were obtained with R-VN "smearing" of the shock thickness to approximately one mesh spacing whereas in practice the ion-ion mean free path rapidly becomes larger than a computation mesh spacing. This means that the true collisional viscous term becomes larger than the R-VN viscous term and that true viscosity controls the shock structure. Further numerical runs are in progress in which the code computes with true viscosity when its effect becomes larger than that of the R-VN term.
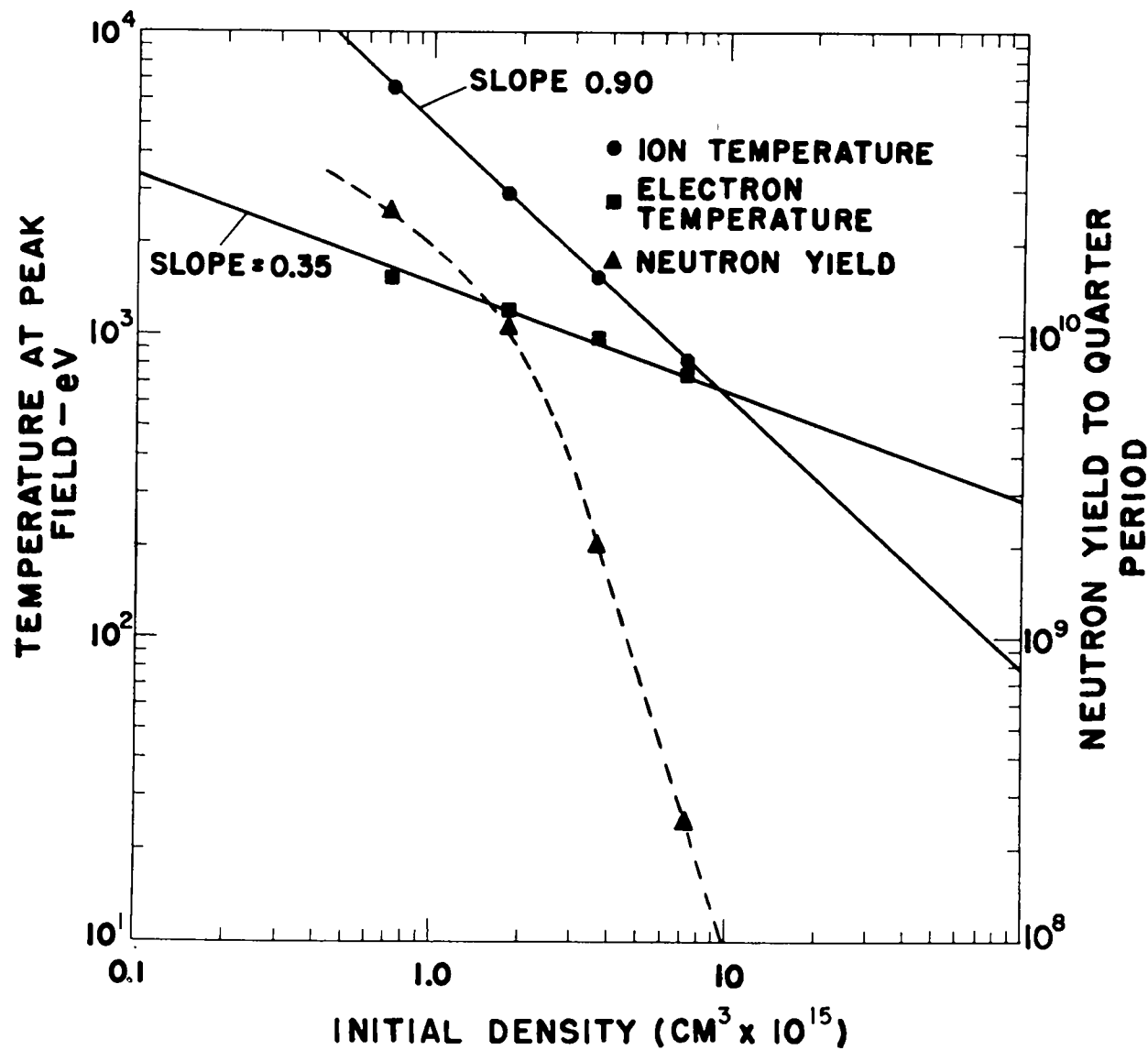
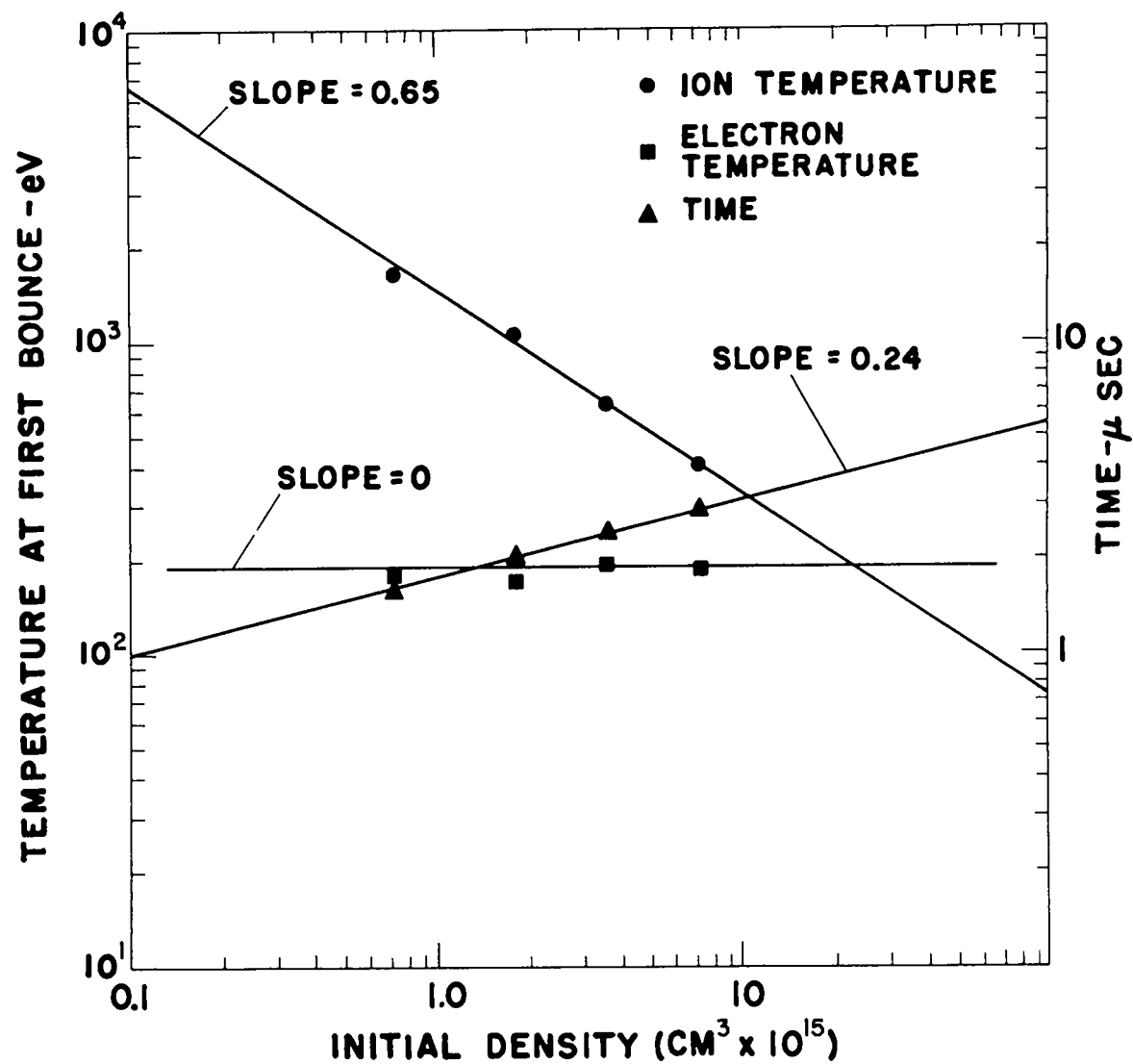Fig. 44. Computed ion temperatures at peak compression

107

Fig. 45. Electron and ion temperatures as functions of initial density at end of first implosion

ULTRAVIOLET SPECTROSCOPY

(N.J. Peacock, G.A. Sawyer, K.Thomas)[*]

Studies of the vacuum ultraviolet spectrum of Scylla are being pursued because of their astrophysical interest. Scylla, with an electron temperature of 200-500 eV, is capable of exciting the many unidentified lines in the vacuum ultra-violet solar spectrum. The experiments have been carried out in conjunction with the High Altitude Observatory, Boulder (LAMS-3004, p. 82). Recent work has been concentrated on the Fe spectrum. With a trace of Fe added to the Scylla discharge in the form of $Fe(CO_5)$,[**] it has been possible to show that a very prominent group of solar spectral lines in the region 170-220 $\mathring{A}$ are due to Fe. These lines, only recently observed in the sun with rocket-borne spectrographs, had previously been unidentified.

The top line of Fig. 46 is a trace of the basic Scylla spectrum and the second line shows the spectrum with Fe added to Scylla. The locations of definitely established Fe lines are marked with carets. The bottom line indicates the solar spectrum observed by H.E. Hinteregger of the Air Force Cambridge Research Center in a rocket flight from White Sands, New Mexico. Several prominent Fe lines may be observed in the solar spectrum, e.g., at 180.41 and 195.13 $\mathring{A}$.

Figure 47 reproduces spectrograms taken on a new 2-m grazing-incidence spectrograph at LASL with and without Fe added to the Scylla discharge. In addition to the many prominent O lines, there are a large number of lines clearly due to Fe. The spectrogram was analyzed using the digital read-out microphotometer developed at LASL by D. Steinhaus. Wavelengths for

---

[*] In collaboration with L. L. House and W. A. Deutschman of the High Altitude Observatory, Boulder.

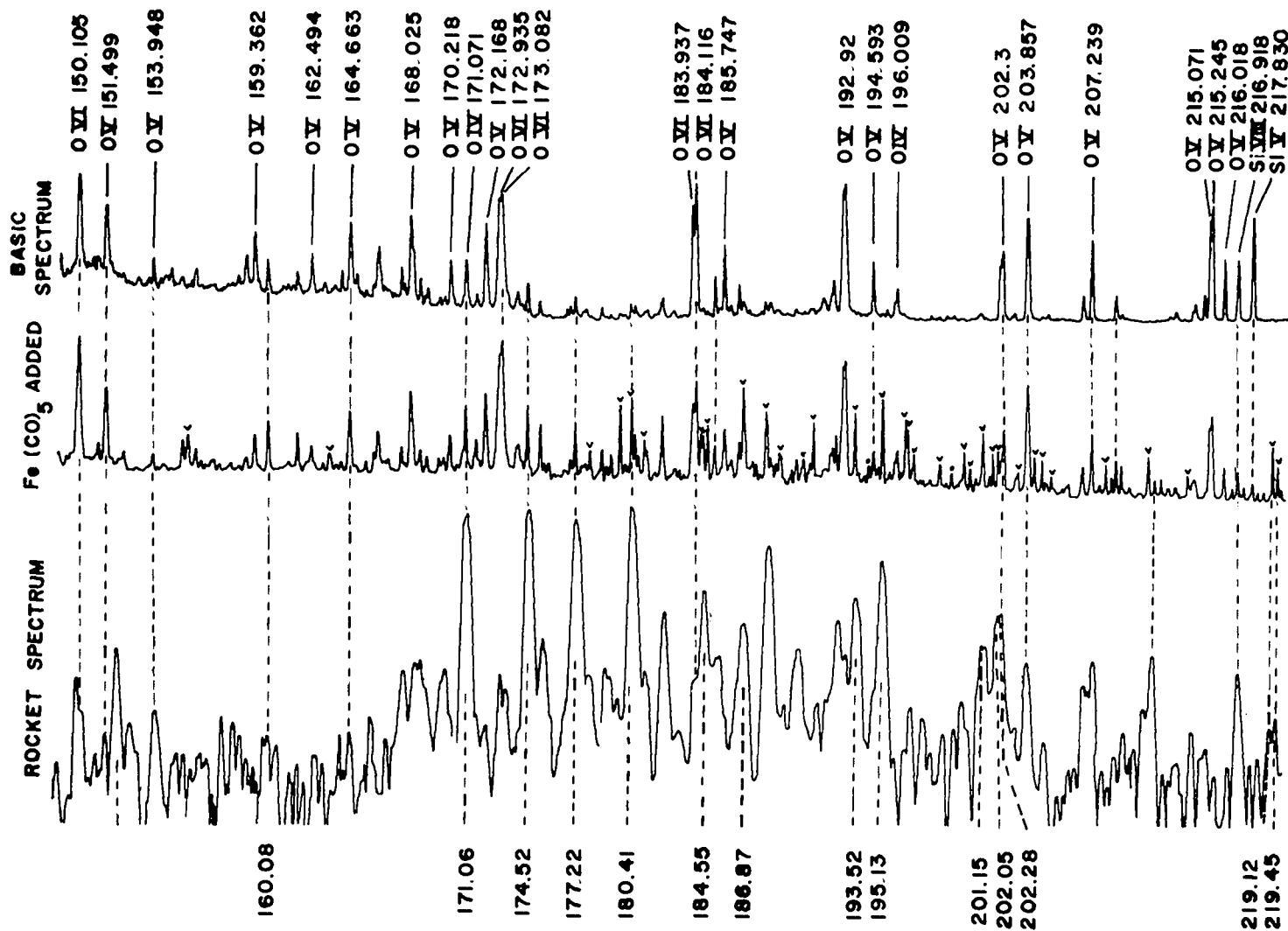[**] The use of $Fe(CO)_5$ as a gaseous Fe compound was suggested by J. L. Tuck.

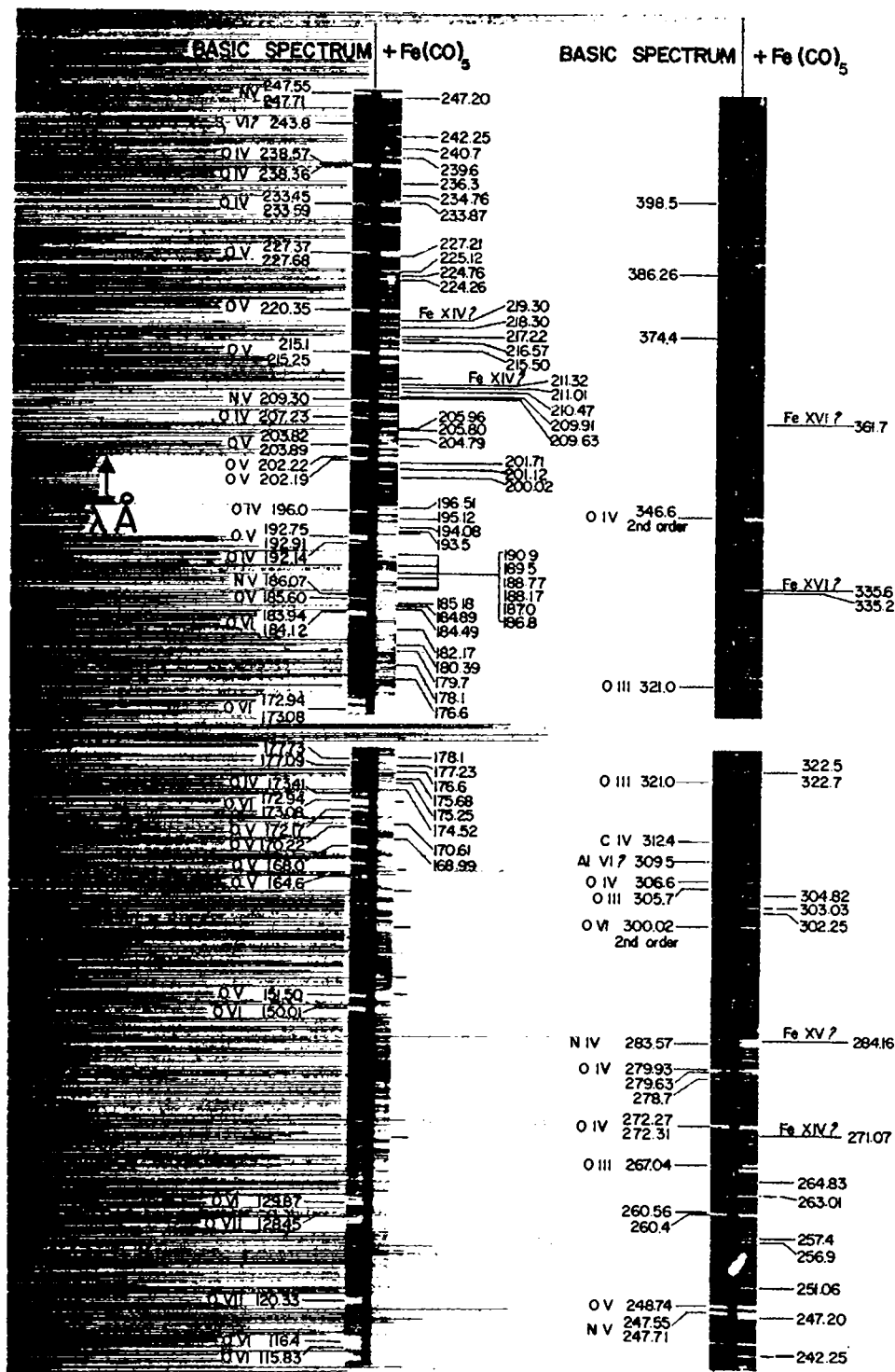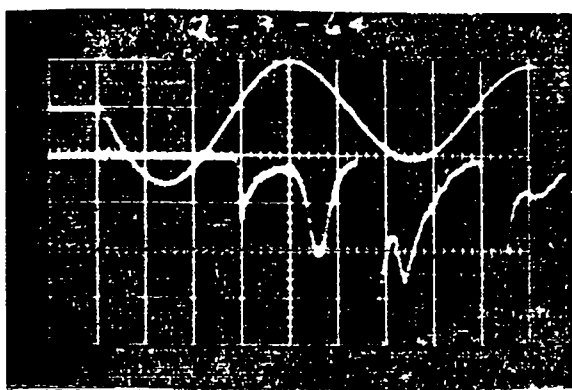Fig. 46. Spectra of Scylla, Scylla with Fe added, and of the sun obtained from a rocket
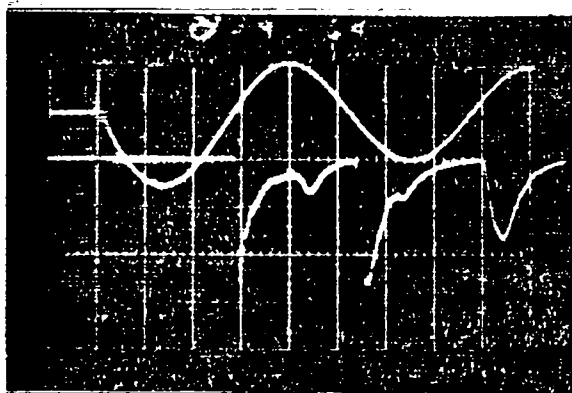
Fig. 47. Spectrogram of Scylla with and without Fe

the Fe lines indicated on the figure are mostly accurate to 0.02 $\overset{o}{A}$. Tentative identifications of a few Fe transitions are also shown.

Unfortunately, the stage of ionization in Fe responsible for most of the observed lines is still unknown. One helpful tool in identifying the ionization state is the time history of the spectral line as observed in Scylla. Such time histories of several O lines are shown in Fig. 48. The significant differences in time histories for lines of different O species are illustrative of the effects it is hoped to see in Fe lines if these lines are to be sorted out according to species. Lines of highly stripped atoms appear in the second half-cycle of Scylla III as it is now being operated, without preionization. The more easily excited species burn through quickly and then reappear after peak field. O VII emission is approximately centered around peak magnetic field showing that it reaches maximum population at maximum Scylla temperature. If similar results can be obtained with Fe, it will be possible at least to separate Fe IX from Fe XVII, although it may be impossible to distinguish adjacent species.

The data shown were taken on Scylla III. The experiment has recently been transferred to Scylla I, and is being continued there.

O V
$\lambda = 192.8 \,\overset{\circ}{A}$
$2p \,^3P_2 - 3d \,^3D_3$
$V_{ex} = 74.2\,ev$

O VI
$\lambda = 183.9 \,\overset{\circ}{A}$
$2p \,^2P_{3/2} - 3s \,^2S_{1/2}$
$V_{ex} = 79.0\,ev$

O VII
$\lambda = 128.4 \,\overset{\circ}{A}$
$2p \,^3P_2 - 3d \,^3D_3$
$V_{ex} = 665.1\,ev$

Fig. 48. Time histories of O lines in Scylla

SCYLLA IV POWER CROWBAR INSTALLATION AND MACHINE OVERHAUL

(E.M. Little and W.E. Quinn)

Introduction

Three megajoules of the original Zeus capacitor bank have been
connected to the Scylla IV system to power crowbar the fast 0.5-MJ
primary capacitor bank. This installation began in June when a high-voltage
breakdown occurred between the Scylla IV collector plates. In addition to
the repair of the collector plates, the primary capacitor bank has been
recabled with an improved cable of the RG 17/14 type (LA(MS)-3085, p. 50).

Collector Plate Breakdown

The high-voltage breakdown in the collector plate system occurred
after more than 1000 full energy discharges. It probably resulted from
electrical fatigue of the polyethylene insulation (6 - 0.25 mm layers)
between the parallel collector plate system. The deposition of the primary
bank energy (520 kJ at 48 kV) in the breakdown area produced cavities in
both Al alloy plates not unlike those caused by high explosives. These
cavities were approximately 5 cm in diameter with a depth of 3 cm. An
overall depression resulted in the inner plate surfaces over an area
having a diameter of 25 cm. Figure 49 is a photograph of the damaged
plate area. The repair of the collector plate system required a
complete disassembly of the system. The damaged area of the 2.3 m x 4.6 m x
7.5-cm plates was repaired by a 20-cm diameter "cold weld" plug, i.e.,
a tight expansion fit achieved through the use of liquid N_2.

The collector plates were reassembled with 23 layers of 0.075-mm
Mylar-sheet electrical insulation between them. Since the Mylar sheet
was 122-cm wide, staggered butt joints were employed in the laying of
the sheets to make the effective insulation thickness 1.65 mm. Each
layer of Mylar was coated with a thin film of Dow Corning silicone
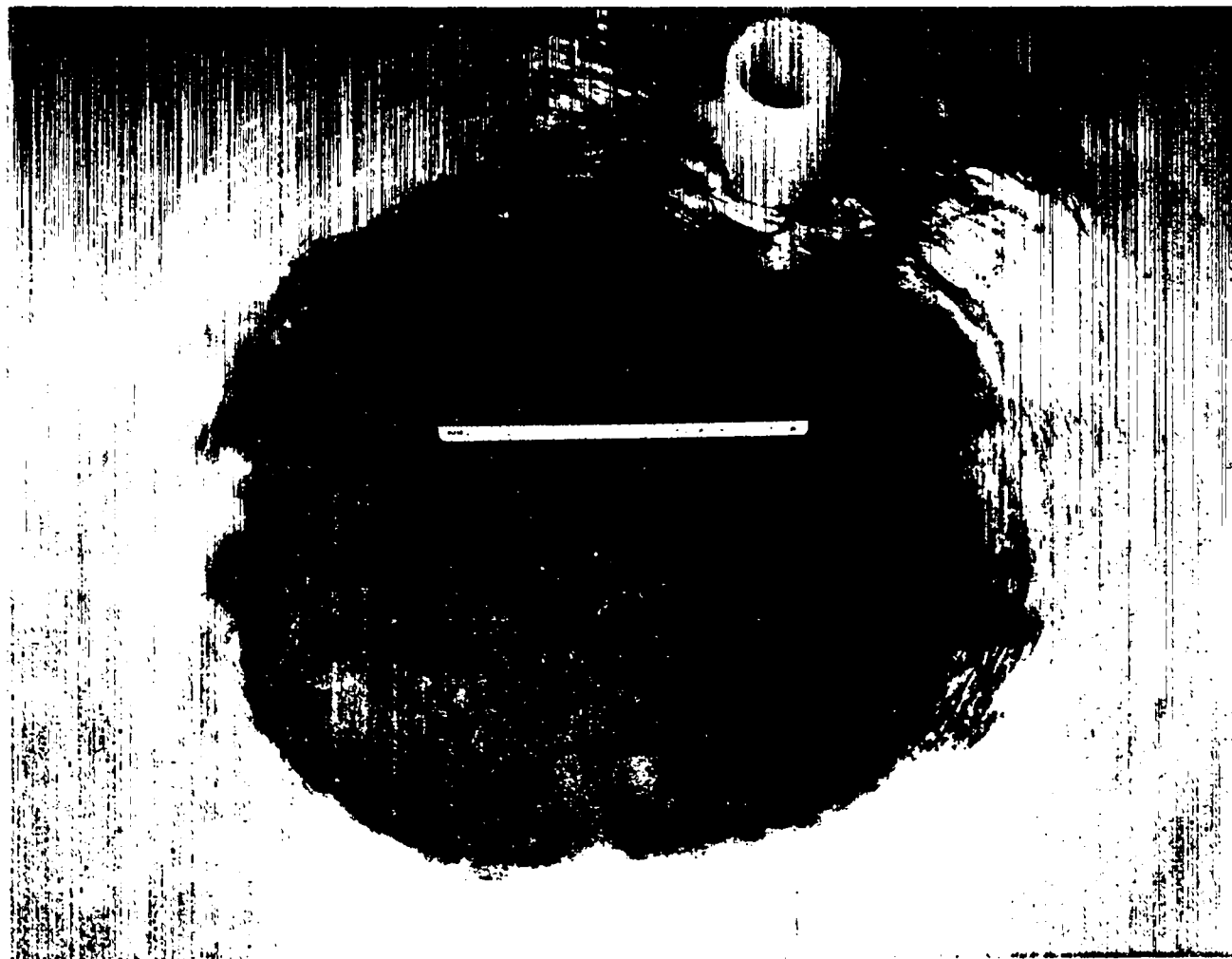dielectric grease to improve the surface insulation properties, reduce

Fig. 49. Damaged collector plate area which resulted from the high-voltage breakdown. The polyethylene insulation is burned away to a diameter of about 30 cm. (The vertical polyethylene cylinder is an insulating hat for the tie-through bolts that bolt the collector plates together.)

the amount of air between the layers, and hold the layers in place during
the installation procedure. In addition, a liberal quantity of grease
was applied in the insulating arrangement around the tie-through bolts.
Prior to the reassembly, extensive electrical tests of Mylar insulation
were carried out in an arrangement which simulated the Scylla IV
conditions. These tests showed that Mylar was suitable for the required
application.

The collector plates were bolted together on the Mylar insulation
with the 150 tie-through bolts torqued to 2000 ft-lb. An actual measurement
of the elongation of the 3.8-cm diameter, high tensile strength bolts
under this torque showed that the bolts are prestressed to 125,000 psi.

Recabling of the Primary Capacitor Bank

The primary capacitor bank has been recabled with an improved RG
17/14 cable. This cable has a polyethylene insulation thickness of 3.5 mm
compared with a 2.2 mm for the old cable. In addition, there are carbonized
conducting layers outside the inner braid and inside the outer braid. The
inductance of the cable has increased to 131 nH per meter from 118 nH/m
for the nominal RG 17/14 type which was used previously. The 1296 primary
bank load cables have an average length of 5.0 m and a total inductance
of 0.5 nH.

Power Crowbar Installation

Three megajoules of the original Zeus capacitor bank have been
connected through 21 vacuum spark gap switches to the Scylla IV collector
plate system. This bank will be used to power crowbar (PCB) the fast
0.5-MJ primary bank. This PCB bank will be switched into the compression
coil before the time of maximum current in the primary bank. Figure 50
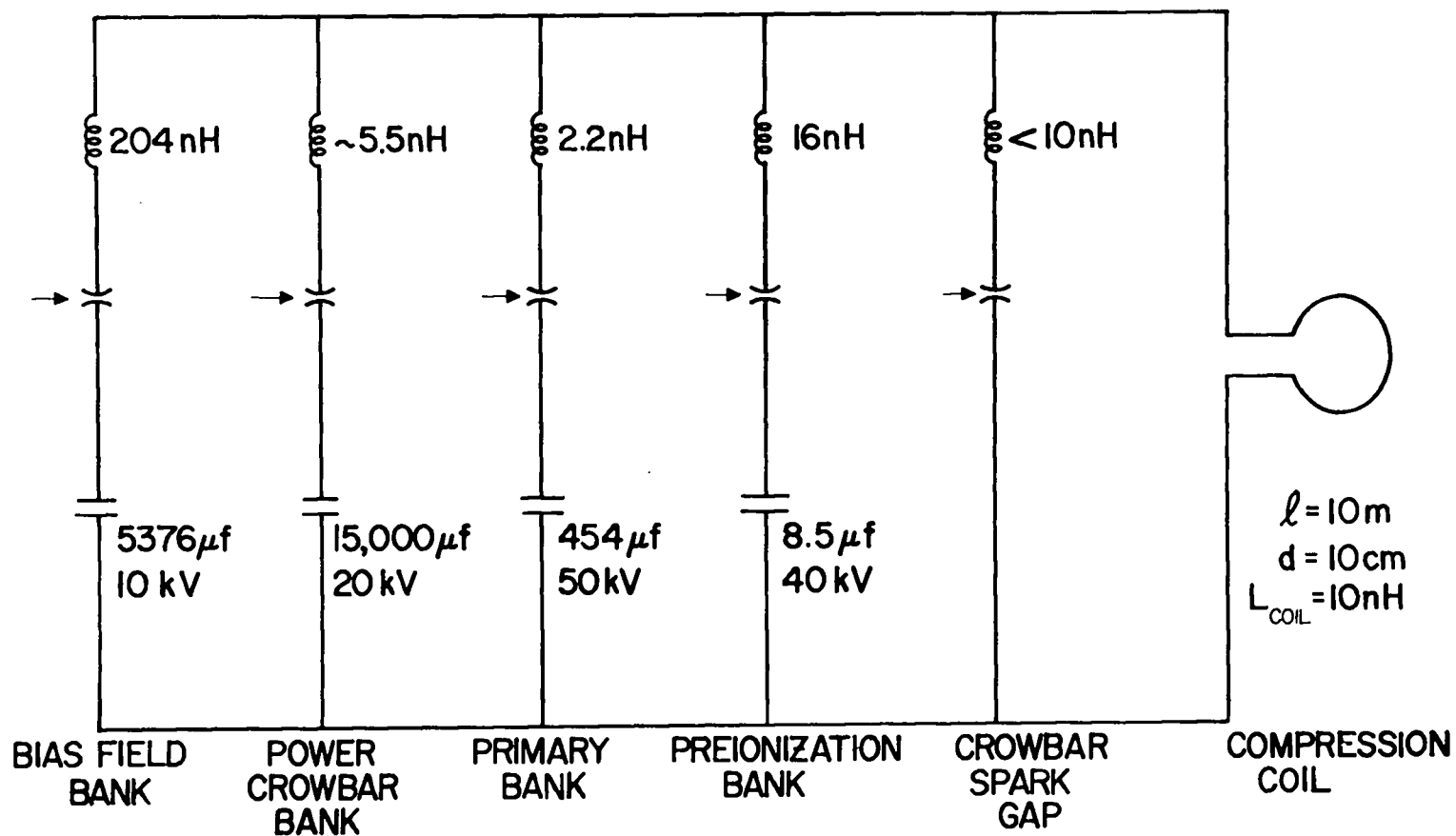shows an electrical schematic of the Scylla IV system with the PCB
bank.

Fig. 50. Electrical schematic diagram of the Scylla IV system
with the power crowbar capacitor bank

The connection of the PCB bank to the Scylla IV system has involved the installation of 21 vacuum spark gap switches (cf. LA(MS)-3085, p. 46) and their associated vacuum systems, the cabling from the bank to the collector plates, and the installation of the trigger, charge, and protect systems. The PCB bank consists of three vertical racks, each of which contains seven shelves of capacitors with an energy storage of 1 MJ at 20 kV. A single vacuum spark gap is used to switch the 140 kJ of each shelf into the collector plate system. Each rack contains a vacuum system which evacuates the gaps through a vertical vacuum manifold. The gap is triggered with a washer gun on the PCB bank side and evacuated on the collector plate side. The entire vacuum system is insulated from ground to withstand the 50-kV pulse of the primary bank. In addition, the gun trigger resides at the dc voltage of the PCB bank.

In order to protect against the deposition of large amounts of energy in an electrical fault in the bank, the following system is employed. Each of the 48 capacitors (15-µf, 20-kV) in a shelf is connected through a single RG-17/14 cable to the spark gap to provide inductive isolation. To protect against electrical faults, a Rowgowski loop is placed around one of the capacitor cables in each shelf to detect any current flow. These cables are connected to a monitor system which upon receipt of a signal triggers the spark gaps. This fires the bank into the low inductance load, eliminating the deposition of large amounts of energy in an electrical fault in the bank.

The trigger system for the vacuum spark gaps consists of the following: (1) A 20-kV, 3-µF capacitor with an ignitron switch drives 21 cables. Each of these cables connects to a coaxial cable isolation transformer, whose secondary drives the spark plug of the washer gun trigger. (2) A 20-kV, 15-µF capacitor with an ignitron switch energizes 21 cables, each of which connects to a coaxial cable isolation transformer. The secondaries of these transformers drive the washer gun triggers.

The installation of the PCB bank has been completed and electrical tests are being started.

E X B PLASMA HEATING IN NONZERO MINIMUM B FIELD CONFIGURATIONS

(L.C. Burkhardt, J.N. DiMarco, H.J. Karr)

E x B in Magnetic Mirror Geometry

Since the preceding semiannual report (LA(MS)-3085), experimental work has been continued to test the feasibility of rotational plasma acceleration in crossed electric and magnetic fields as the means for generation and heating of plasmas in the minimum B systems—the stuffed cusp and caulked stuffed cusp—that are to be investigated as confinement geometries. Most of the experimental effort during the current period has been devoted to E x B plasma generation in conventional mirror geometry to observe the plasma behavior and check out diagnostics before going into the more complicated minimum B geometries. The Mark III cusp (picket fence) machine has been modified for use in these experiments as shown in Fig. 51. The dc field coils supply an axial magnetic field up to $\sim$ 4000 G with an axis mirror ratio of 1.2 for a distance of 140 cm between mirrors. Deuterium gas is injected from a fast valve at the midplane within the axial stuffing conductor.

Figure 52 shows the gas pressure distribution at 350 μsec after gas injection which is approximately the onset time of the radial current which drives the plasma into rotation. The average D_2 density in the midplane is of the order of 10^{14} cm^{-3}. This pressure has been varied by a factor of $\sim$ 20 in the course of the experiment. A radial electric field between the stuffer bar and the coaxial outer electrode is supplied from a 45-μF, 20-kV capacitor bank (Fig. 51). After the plasma reaches maximum rotational velocity in 10 to 20 μsec, as indicated for example by the maximum diamagnetic signal, the voltage is removed by crowbarring the system.

Experimental measurements so far include: (1) current and voltage, (2) diamagnetism due to plasma rotation, (3) recoverable charge after crowbar, (4) electric field distribution within the plasma, (5) visible and ultraviolet light emission, (6) Doppler shift of lines due to rotation
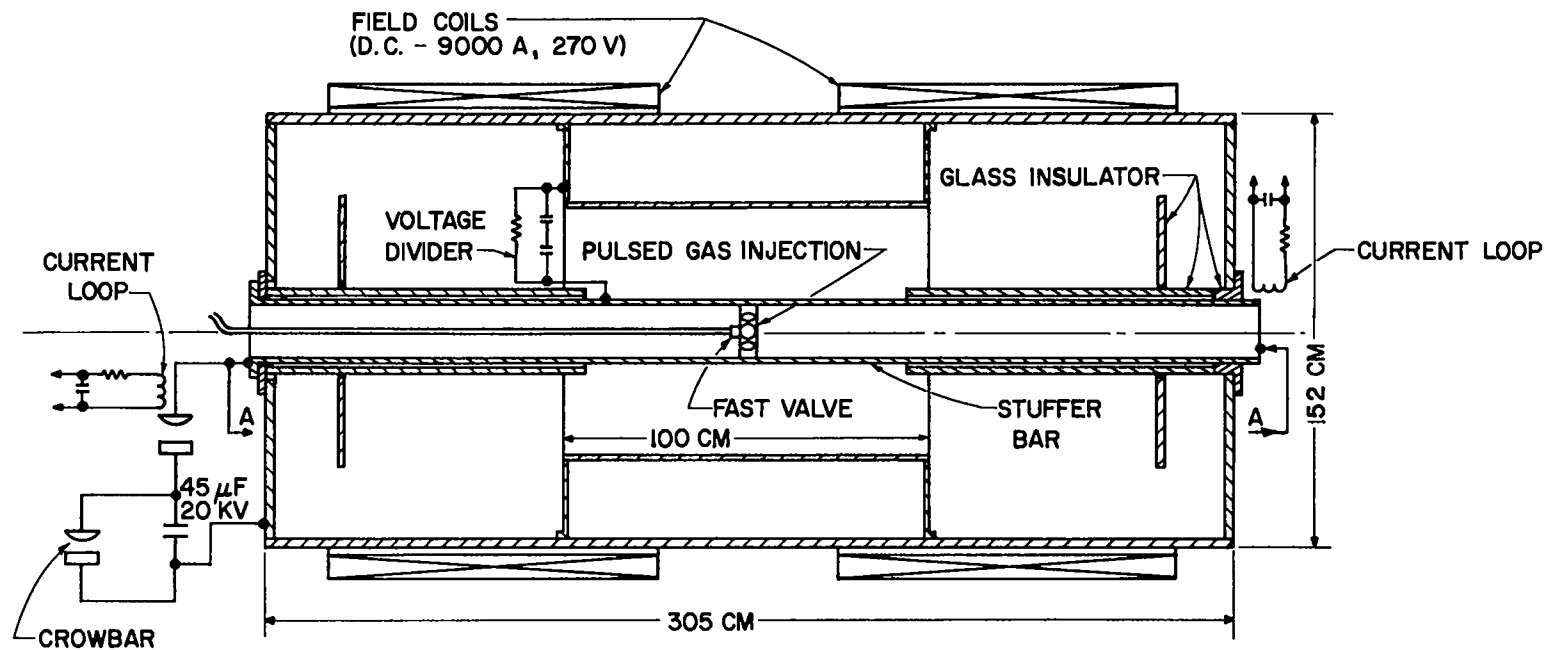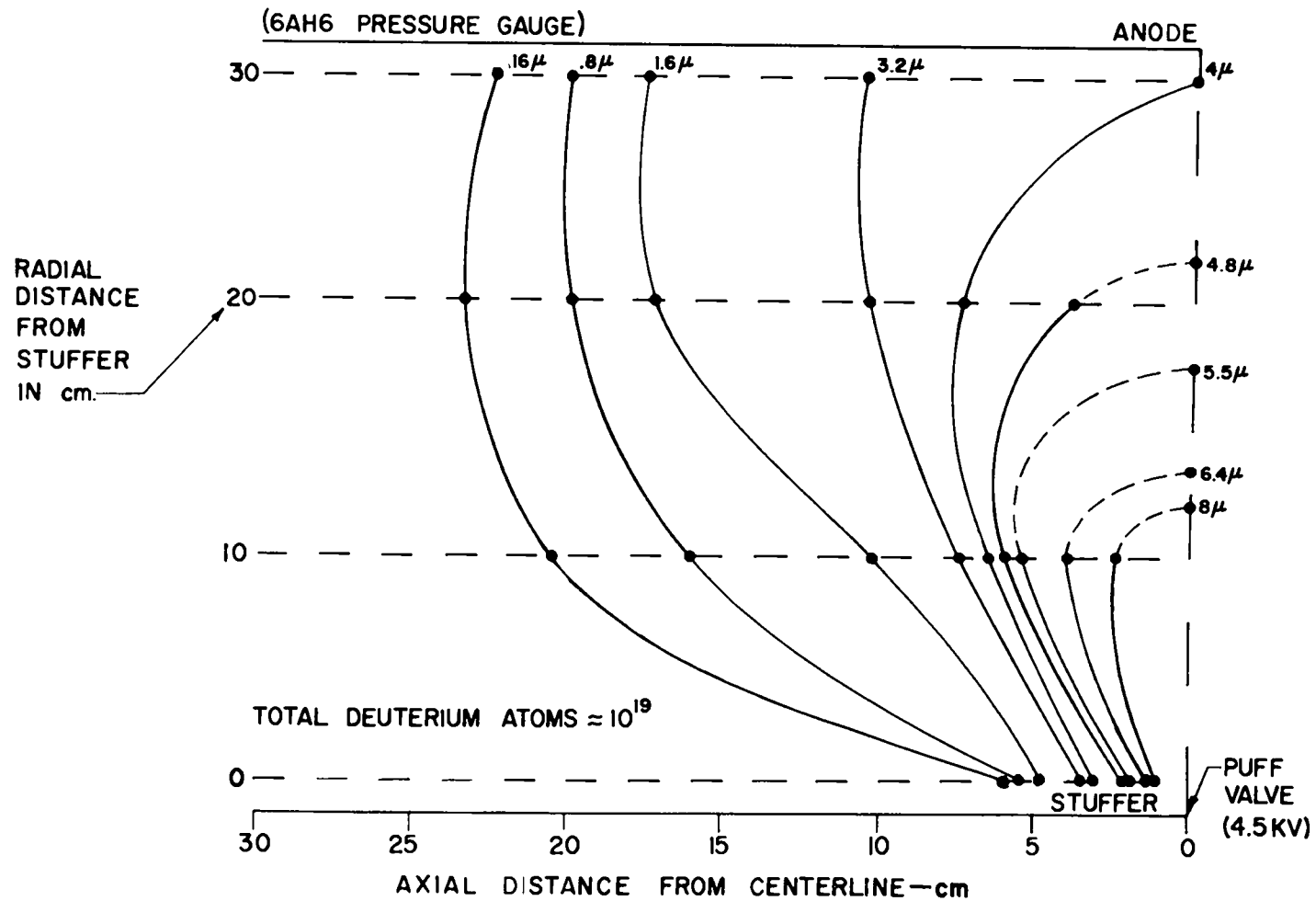
Fig. 51. Modified Mark III cusp (picket fence) machine

Fig. 52. Deuterium gas pressure distribution at 350 μsec after gas injection

and thermal line broadening (He gas injection and He II radiation for this purpose), and (7) image converter camera pictures of the plasma generation process. These measurements have been made over a range of injected gas pressures, applied voltages, and magnetic fields.

The results so far show that the E x B method generates a fully ionized plasma of density $\gtrsim 10^{14}$ cm^{-3}; but impurities, particularly from the electrodes, are prominent. The large diamagnetic signals obtained together with the Doppler shift of spectral lines and the large fraction of recoverable charge after crowbar indicate that plasma rotation of the expected velocity ($\sim 10^7$ cm/sec) does occur. Plasma temperatures have not yet been determined from the Doppler shift and line broadening data. Plasma density is to be investigated using an infrared laser densitometer based on the Ashby-Jephcott technique as modified at LASL (see p. 57).

E x B in Minimum B Geometry

Coils for the caulked stuffed cusp system are under construction. When these are completed, within a month or so, the experimental work will be changed from the magnetic mirror system to the caulked stuffed cusp.

Redesigned Mk III System

The vacuum tank of the redesigned Mk III system has been received. The oil-free, ultrahigh vacuum system estimated delivery date is November 15 and the new, larger coils are expected by the end of the year. The design pumping speed of the new system is $>$ 150,000 l/sec and is expected to lower the base pressure by more than an order of magnitude. The new coils will increase the dc magnetic field to a level of $\sim$ 12 kG.

PARTICLE ORBITS

(H.R. Lewis)

Cusp Field

Non-adiabatic particle orbits in an idealized cusp field have been computed as an attempt to shed light on the results which were obtained in the Picket Fence III experiment with an ion detector (cf. IAMS-3004). In this experiment, all positive ions entering the detector with a momentum greater than some critical momentum were detected and the ion current was measured as a function of time. A striking result is the behavior of the ion current as a function of time. Initially, the current decreases rapidly with time, so that at 100 μsec it has decreased by about a factor of ten, and thereafter it decreases approximately exponentially with a mean life $\gtrsim$ 60 μsec. It may be possible to explain part of this behavior on the basis of single particle motion of heavy ions.

The ion detector was positioned in the mirror section of the cusp field, i.e., at a location where the field is nearly parallel to the axis, and at a distance from the axis which was at most a few times the Larmor radius of the detected ions. The critical momentum selected by the detector was approximately that of 10-keV D ions. For an ion to be detected, its velocity vector must have been approximately perpendicular to a line of force and approximately parallel to a flux surface.

Computations were performed for D's of speed 100 cm/μsec moving in the usual idealized cusp field: $A_\theta \propto rz$ in a cylindrical coordinate system. The wall of the containment vessel was defined to be at $r = 100$ cm and $|z| = 100$ cm. Time was allowed to run backward and thus the initial location of the particle is defined to be the location of the detector. The initial z coordinate was always taken to be 50 cm; at this value of z, near the axis the field is very nearly parallel to the axis and the magnitude of B is only a little dependent on the distance from the axis.

The magnitude of B was chosen such that the Larmor radius of a 100 cm/ μsec deuteron moving perpendicular to a line of force is 3.5 cm. The initial values of r were taken as 3.5, 7.0, and 14.0 cm, i.e., as respectively 1, 2, and 4 times the initial Larmor radius. In Figs. 53-56 these initial values of z and r have been characterized by $\sqrt[3]{c_1}$ = $\sqrt[3]{zr^2}$ evaluated at the initial location, i.e., 8.50, 13.49, and 21.42 cm. In addition to computations for a speed of 100 cm/μsec, calculations were also made for speeds of 50 cm/μsec and 25 cm/μsec.

The choice of initial velocity directions may be described with reference to the following coordinate system. Take the z axis along $\vec{B}$ and the x axis along the outward normal to the flux surface defined by zr^2 = constant; θ and φ are the polar angles, defined in the usual way, of the initial velocity vector in this coordinate system. Values of φ equal to 0, $\pi/2$, π, and $3\pi/2$ were chosen for each value of θ, and equally spaced values of θ were used.

The results in Figs. 53-56 are based on averages over the four values of φ and over the values of θ such that $3\pi/8 \leqslant \theta \leqslant 5\pi/8$. Figure 53 is for the 100 cm/μsec particles at the three initial locations; Figure 54 is the result of an average over the three initial locations of Fig. 53. In Fig. 55, the histogram of Fig. 54 is plotted on a semilogarithmic scale. The e-folding time is determined from the straight line which has been drawn through the points. If the points followed an exponential law exactly, then the e-folding time and the average time would be the same. In Fig. 56, results are given for the two lower speeds. It would appear to be difficult to explain the experimental results on the basis of single particle motion if the particles are D's. However, if they are assumed to be eight or more times heavier than D's, but to have the same momentum as 10-keV D's, then the corresponding average times are close to the experimentally observed mean decay times of the ion detector current.
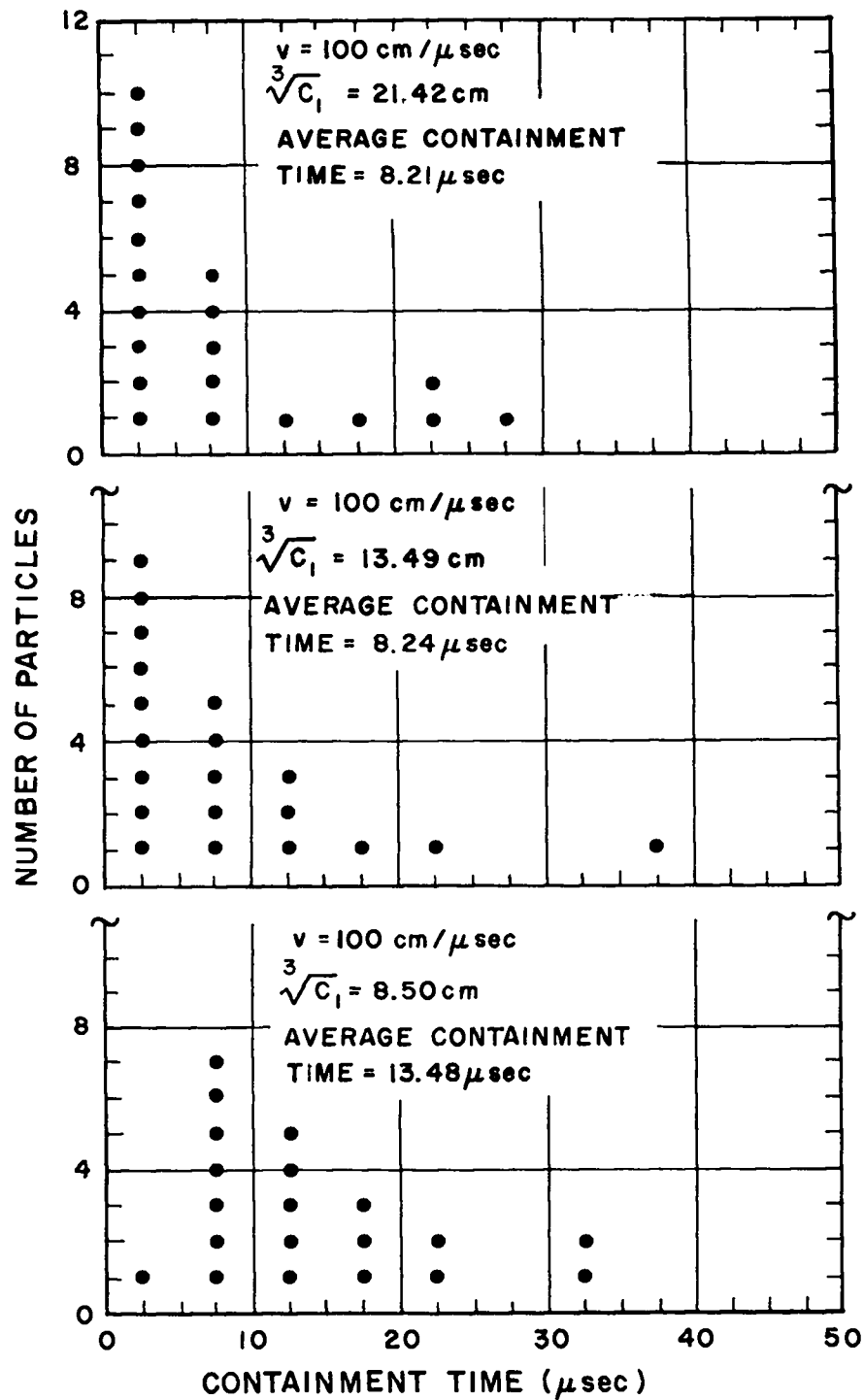
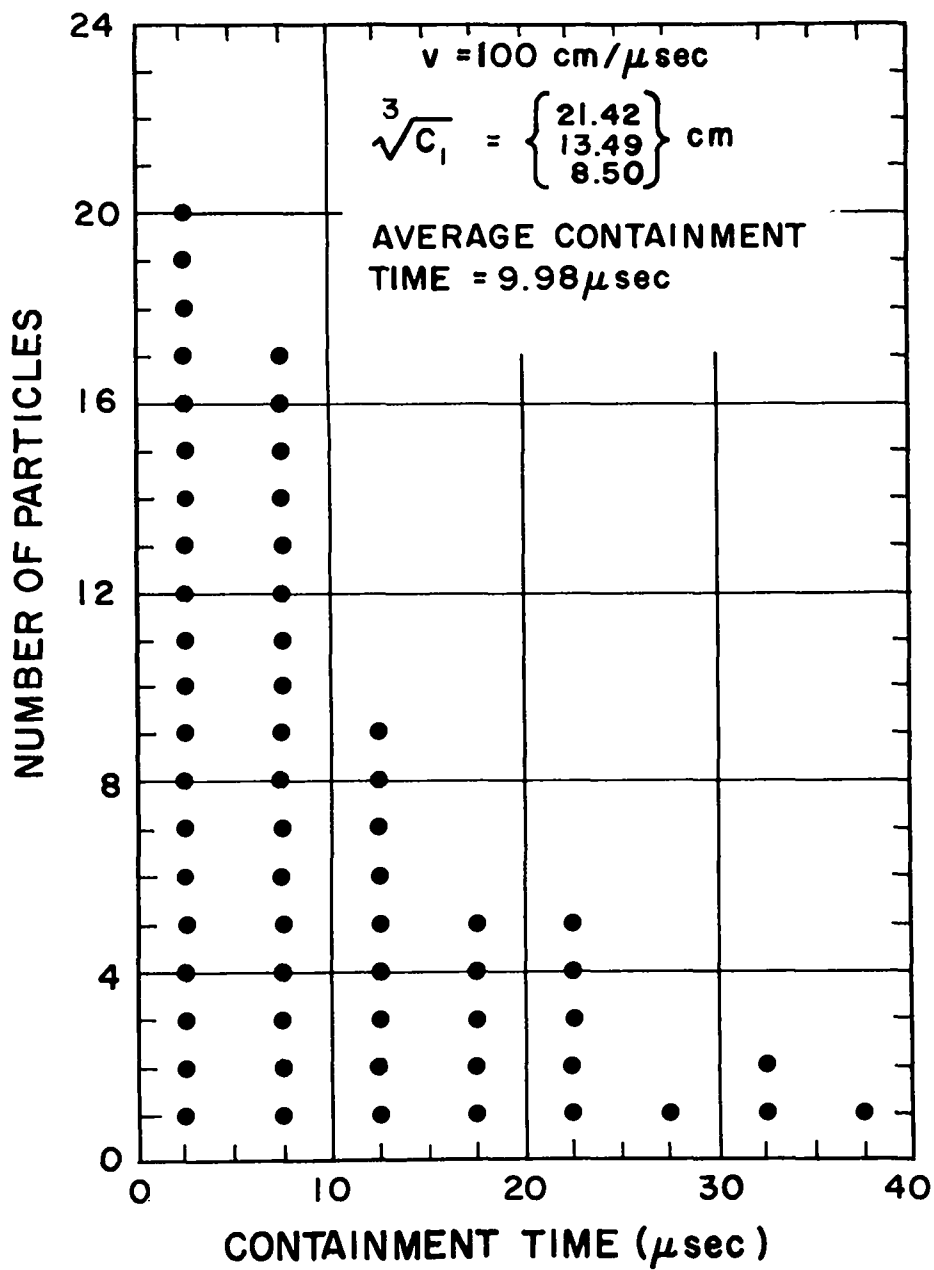Fig. 53. Containment times for various initial
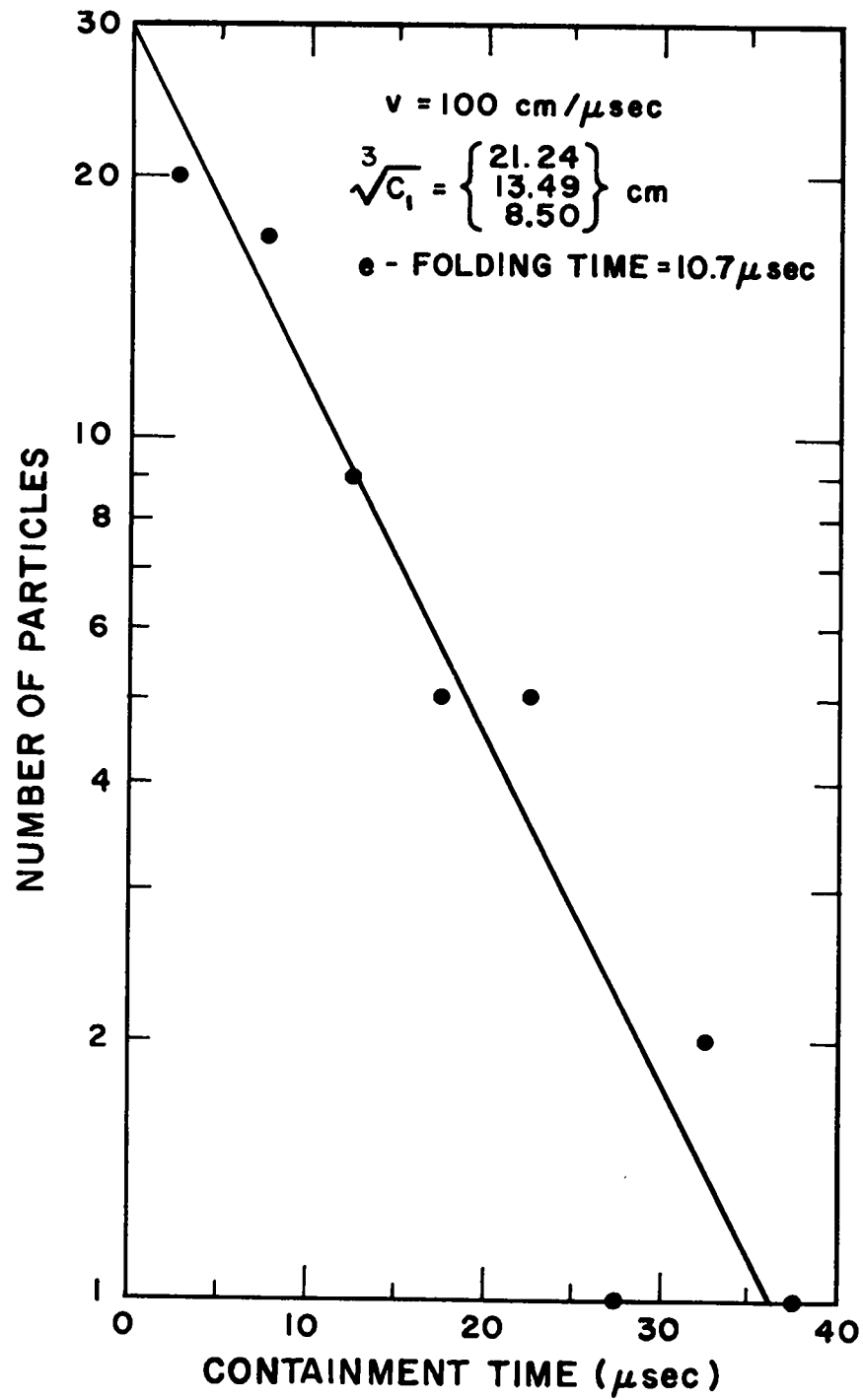locations (speed 100 cm/μsec)

Fig. 54. Averaging of data in Fig. 53

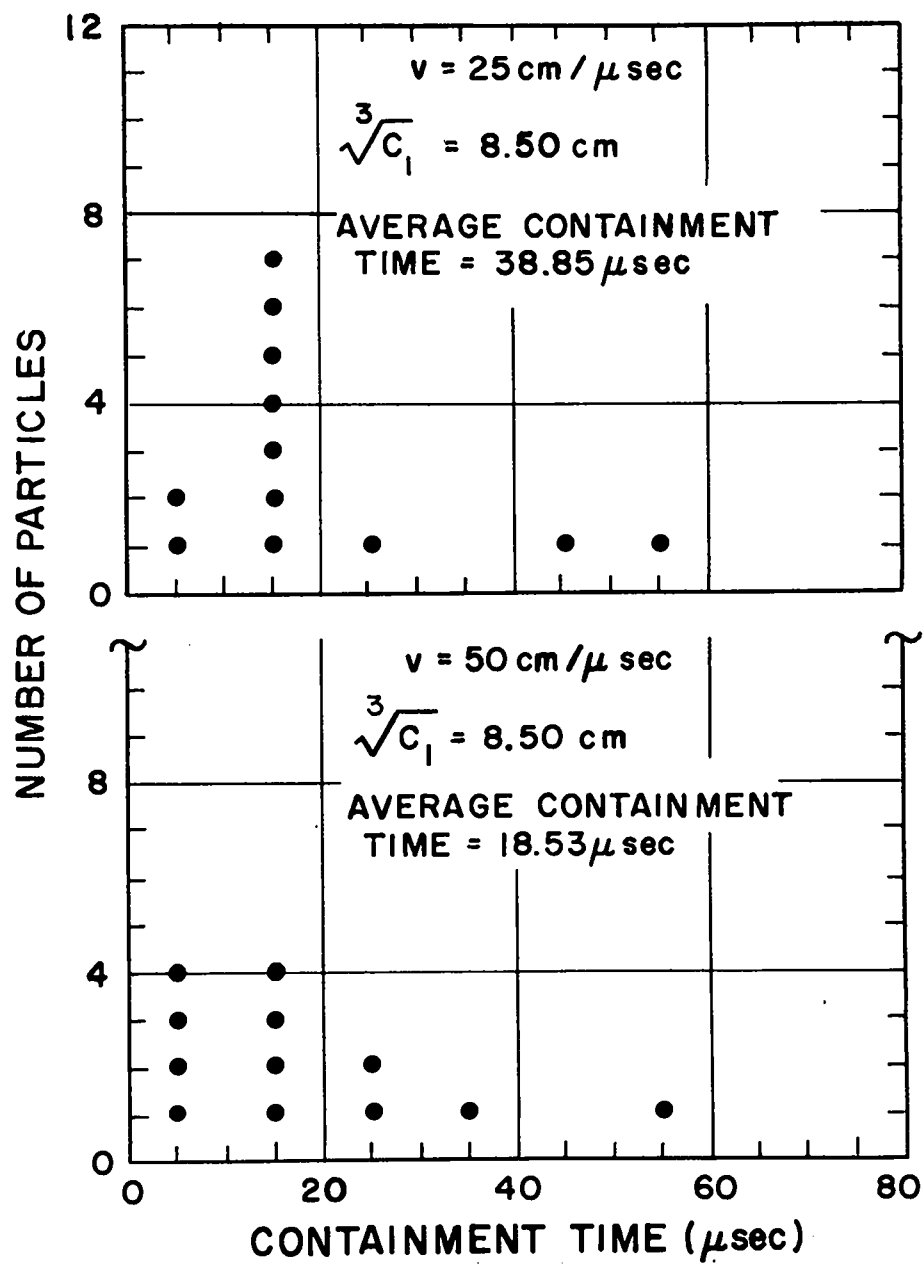Fig. 55. Plot of histogram of Fig. 54 on semilogarithmic scale

Fig. 56. Containment times for speeds of 25 and 50 cm/μsec

Stuffed Cusp Field

Many particle orbits have also been computed for a "stuffed-cusp" field, which is a superposition of the cusp field of the previous section and the field of an axial current. The minimum value of this field occurs off-axis in the median plane of the cusp and is non-zero. The original motivation for beginning these computations was to understand the single particle containment properties of a stuffed-cusp field as they applied to experiments which had been envisioned. In the interim, plans for experiments in stuffed-cusp systems have been modified, and the need for orbits in this particular field configuration is not pressing. The techniques which have been developed for computing, displaying, and understanding particle orbits will continue to be of interest, and some characteristics of the orbits are significant in relation to adiabatic theory. One special feature is the existence of many orbits which appear to represent very adiabatic behavior, i.e., high degree of periodicity, long-term containment, small expansion parameter, but for which the magnetic moment, $\frac{1}{2} \frac{W_\perp}{B}$, oscillates by a large amount. In one such case, the oscillation of the magnetic moment is $\pm$ 22%. It is also of interest that, in this case, addition of the next term in the asymptotic magnetic moment series reduced the fluctuation to $\pm$ 9%. Some further investigation of the behavior of adiabatic invariants is planned.

PULSED MAGNETIC FIELD COMPUTATIONS

(H. R. Lewis)

One of the problems of current interest at LASL is the computation of magnetic and electric fields in cases where the first step is to solve a partial differential equation. An example of this type of problem is finding the magnetic field in a region bounded by conducting surfaces when those surfaces can be considered to be flux surfaces of the field. The vector potential $\vec{A}$ then satisfies Laplace's equation $\nabla^2\vec{A} = 0$. Numerical techniques for solving the pertinent partial differential equations in situations of this sort usually result in values of a potential at the points of a rectangular mesh which covers the range of coordinates of interest. The problem then is to find values of the potential together with its first, and probably second, derivatives at arbitrary points in the region of interest. This problem of interpolating in a two-dimensional table of values of a function to find values of the function and its derivatives at arbitrary points is a common and important one.

D. Harder and T. Jordan (LASL T Division) have developed a computer code with which the analogous one-dimensional interpolation problem can be treated very well. This code generates a so-called "spline fit" to a table of functional values. Important characteristics of the spline fit are that the function and its first two derivatives are everywhere continuous and that, among the class of functions which have continuous first and second derivatives, the spline fit minimizes $\int (dy/dx)^2 dx$. This last condition insures that the fit is smooth and that it does not have overly large curvature.

Recently, T. Jordan has devised a scheme for similarly treating the two-dimensional interpolation problem. The scheme was developed for use with a rectangular mesh which has rectangular boundaries. The problems to which two-dimensional interpolation techniques are applied in the Sherwood group usually involve boundaries which are far from rectangular. It has now been determined that the method of Jordan can be applied to problems with non-rectangular boundaries with very good results by enclosing the region of interest with rectangular boundaries and letting the function in each region of no physical interest equal its value on the boundary of that region. Computer codes have been extended to use the random access capabilities of the drum storage facility of the IBM 7094. With this modification, the code can handle a mesh as large as 200 x 200 points to give interpolated values of the function and its five first and second derivatives, all of which are everywhere continuous. If the size of the array is limited, so that the core memory of the IBM 7094 or 7030 can be used for storage, then the speed of operation is very much increased.

Methods for using two-dimensional spline functions directly in the solution of the partial differential equation are being investigated for possible improvement of flexibility and efficiency in carrying out a relaxation computation.

CONSTANT-CURRENT POWER SUPPLY DEVELOPMENT

(T. M. Sprague)

Introduction

In order to procure reliable, constant-current power supplies for capacitor bank charging, many circuits have been investigated. The use of a saturable reactor in series with a high-voltage transformer-rectifier system holds considerable promise. The simplified schematic diagram of Fig. 57 shows the single-phase case of this type of control. In Sherwood applications, the load impedance Z_L is a high-voltage transformer, rectifier, and associated capacitor bank. The saturable reactor impedance Z_R then not only controls the magnitude of the load current i_L and consequently the capacitor charging current, but it also acts as the on-off control. The "off" condition is about 3% of the maximum current and 3% of the maximum voltage.

Theory of Operation

The saturable reactor in Fig. 57 has two separate cores, A and B, connected in series with a load impedance, Z_L. The saturating winding, N_C, is wound around both cores. A low-impedance dc power supply provides current for the saturating winding. When the saturating current, i_c, is zero the reactor impedance is much greater than the load impedance so there is only a small voltage developed across Z_L. The load current at this time is approximately

$$i_L \approx E \frac{\sin \omega t}{Z_{R \text{ (off)}}} .$$

It will be assumed that winding N_C aids the ampere turns of winding N_A for each positive half-cycle of i_L. When the control current i_c is increased to a given value, core A will saturate at some time during
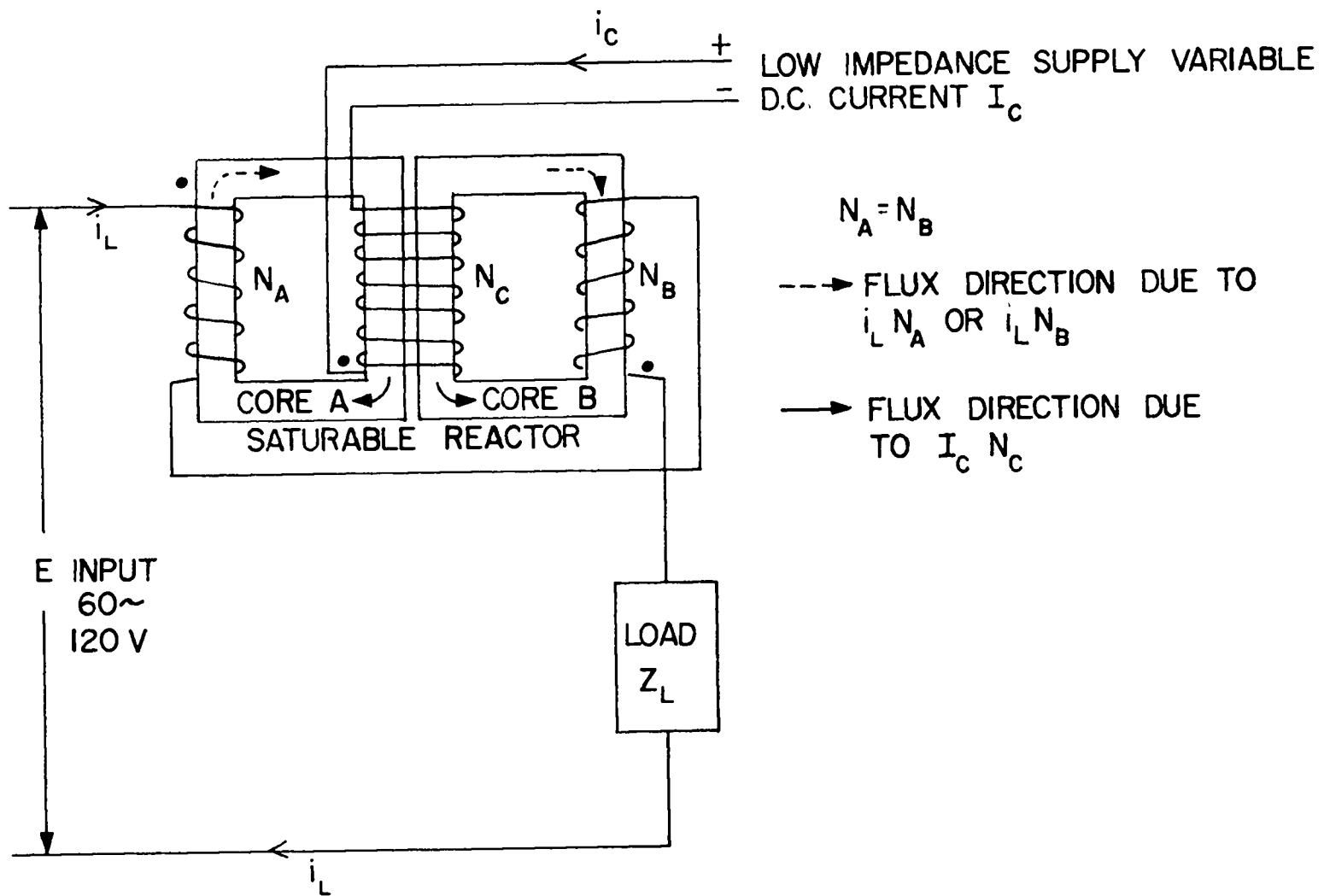
132

Fig. 57. Simplified schematic of use of saturable reactor for current control

the positive half-cycle of i_L. When saturation occurs the impedance of the windings on core A becomes very small. Core B remains unsaturated since the ampere turns in N_C oppose the turns in N_B. At this time, core B may be considered part of a transformer with N_B as the primary and N_C as the secondary. Then the low impedance of the control supply is reflected into the primary N_B as a very low impedance. Thus in saturated condition the impedance of the saturable reactor drops to about 1% of its unsaturated impedance. On the alternate half-cycles the two cores exchange functions in the circuit.

The point on each half-cycle where saturation occurs is determined by the magnitude of i_c. The greater i_c becomes, the longer the saturated time during the half-cycle and the larger the load current within the limitations of E/Z_L. In practice, i_L does not exceed 80% of the maximum because of the finite impedance of the saturable reactor. However, controlling i_c controls i_L through a range of about 50 to 1; this is adequate for power supplies used to charge capacitor banks.

The capability of almost constant current from short circuit (uncharged capacitor bank) to full voltage for a given setting of i_c is shown in Fig. 58. The drop in the current is caused in part by trying to get almost full line voltage to the rectifier transformers and the peak clipping waveform of a capacitor input power supply.

Since the type of charging system described above reduces voltage transients, eliminates overvoltage on open circuit, limits short circuit currents, and is extremely flexible, it will be used in the future for capacitor banks at LASL.
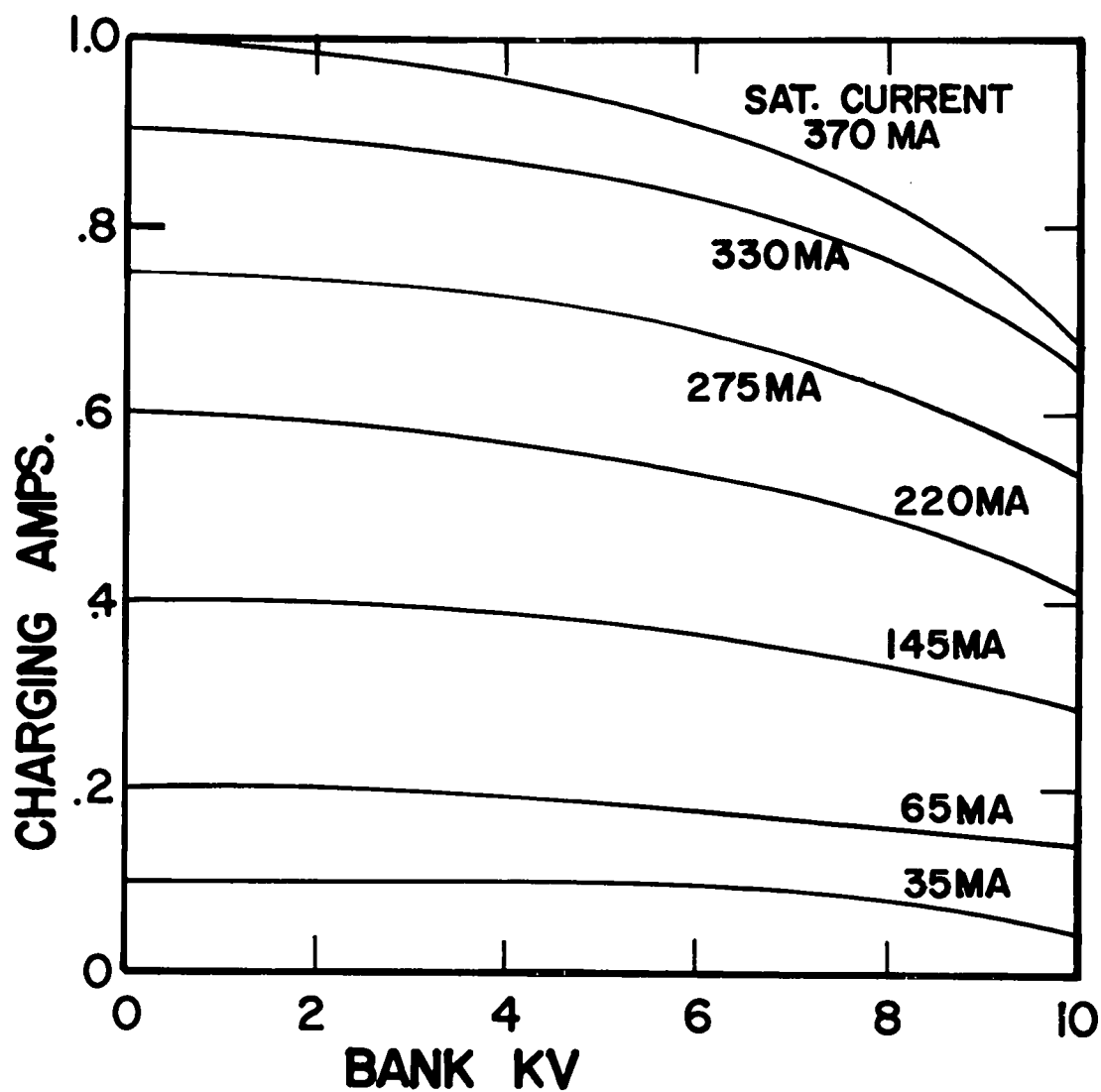
Fig. 58. Charging current for various settings of the saturation current

50-kV IGNITRON DEVELOPMENT

(G. Boicourt and E. Kemp)

Most energy storage capacitor banks for Sherwood experiments operate in the range of 5-50 kV. The lower part of this range (5-25 kV) can be switched by presently available ignitrons. For several reasons, a desire has been expressed for an ignitron that would extend the range to 50 kV.

In selecting a switch for an experiment, there is a choice among three types: an air spark gap, a vacuum spark gap, or an ignitron. As a class, spark gaps require fairly elaborate triggering systems; the air spark gap is unsuitable for many experiments since its firing range is limited to the voltages near its maximum voltage; and the vacuum spark gap requires a rather elaborate vacuum system. On the other hand, the ignitron triggering system is simple; it will fire at any voltage from almost zero to its maximum hold-off limit and it requires no special pumping apparatus. Several years ago some experiments were made connecting two ignitrons in series to obtain higher voltage hold-off. This solution was unsuitable for three reasons: (1) the inductance of the switch became excessive, (2) the triggering systems became more elaborate, and (3) external voltage-grading resistors were necessary.

Another approach was made under a contract with General Electric to develop a better ignitron. This was a cavity grid tube, which has been described previously (IAMS-2416, p. 24), that was rather long and therefore inductive. It also appeared that it would not be capable of carrying the high peak currents required. Further work was dropped on the termination of the contract.

When Scylla IV was built, it was designed to use 3 MJ of the Zeus capacitor bank as a power crowbar. It was then decided to investigate ignitrons as a possible crowbar switch. In this application the tube must withstand the 50-kV voltage pulse produced by the primary bank of

Scylla IV and then discharge Zeus at a very low voltage across the ignitron. The progress of this development has been described in earlier progress reports (LAMS-2754, LAMS-2816, LAMS-2874, LAMS-2916, LAMS-3004, and LA(MS)-3085).

In summary, the aim was to develop a low-inductance, high-voltage ignitron suitable for power crowbar application. Flux plots were made of a proposed configuration in order to avoid high field concentrations. General Electric has submitted six tubes representing three generations of development. The tests have been encouraging but the tubes failed to meet the qualifications for the Scylla IV-Zeus crowbar tubes. It is felt that this failure was mainly due to General Electric's inability to hold the internal dimensional specifications of the tube.

During the present report period, two 50-kV tubes (NL-1040) were received from National Electronics. During preliminary hypot testing it was discovered that the lower section of the tube was shorted. An x-ray showed that the inner shielding structure of the lower section was approximately 1/4 in. lower than it should be. It appears that a misunderstanding of the blueprints had resulted in the shield being welded to the wrong side of the gradient grid support ring. National Electronics has agreed to replace the faulty tubes.

10-kV HIGH-DENSITY, LOW-COST CAPACITOR DEVELOPMENT

(G. Boicourt and E. Kemp)

Units from four capacitor manufacturers have been received and testing has begun. The following tests will be used for evaluation: (1) a test to assure satisfactory peak current capability, (2) an electrification t est to assure satisfactory ability to withstand the long time on charge anticipated for very large banks, and (3) a simulated-use test.

The first test consists of a heavily damped discharge switched by an ignitron. The capacitor is subjected to a peak current of approximately 33 kA. The test is carried out well below the rated voltage of the c apacitor and thus any failure should be due to current. At present, three capacitors each from four manufacturers have been evaluated; only one capacitor has failed.

In the electrification test the capacitor is R-C charged to 10 kV in 4-3/4 min. It thus spends over 2-1/2 min at 90% or more of rated voltage before it is discharged through a large resistor; then the cycle is repeated. Two capacitors have completed 5000 charges in this mode. In order to speed testing, a second mode is being tried on these two capacitors. The capacitor is R-C charged to 11.6 kV instead of 10 kV. Using the 5th power law, this makes one charge of mode two equivalent to two charges under mode one. One capacitor has completed 5000 charges under both mode one and two, and a second unit is now undergoing the mode two test. If it completes this test successfully, all future testing will be done at the higher voltage.

The simulated-use test will evaluate ten capacitors at a time in a crowbarred bank. Such a bank, consisting of thirty 65-μF, 10-kV capacitors, has been set up to check the power supply and control systems,

th: switching tubes, the voltage reversal on the capacitors, and the capacitor fuses. A check of the voltage reversal has shown it to be about 20%. This rather high value is attributed to two causes, namely, the late firing of the crowbar tube and the high arc drop in the crowbar ignitron. Two special types of size D ignitrons have been ordered to determine if the voltage reversal can be reduced. One type will be shorter and have no internal baffles. The other design will be a standard unit without baffles.

Some difficulty has been experienced in obtaining a suitable fuse, but samples from Franklin Engineering Co. are now showing signs of promise. Since the noise from the firing of a fuse is unbearable, a second bank will be built in a semi-soundproof room. This bank will be primarily used to test the capacitors. The existing capacitor bank will be used to evaluate arc drop and firing of ignitrons, and possibly also as a power source for certain inductive storage experiments.

MISCELLANEOUS EQUIPMENT DEVELOPMENT

(G. Boicourt and E. Kemp)

A continuing program of capacitor testing is being carried on; the purpose is to evaluate new designs and to check the quality of re-ordered old designs. Recently a spot quality check caused two orders of 100 capacitors each to be returned to the manufacturer for replacement.

Ignitor wetting in metal anode tubes continues to be a problem. Several tests have been carried out of tubes submitted by General Electric.

Coaxial cable is being used increasingly in Sherwood capacitor bank transmission systems. During the report period, several cable evaluations have been made; these involve checks of the resistance and inductance, and often also of the high-voltage capabilities of the cable.